CELLULOSE NANOCRYSTAL/POLYMER NANOCOMPOSITES: PROCESSING STRATEGIES, STRUCTURE VARIATION AND EXPLORED APPLICATIONS

A Dissertation
Presented to
The Academic Faculty

by

Ke Qiu

In Partial Fulfillment
of the Requirements for the Degree
Doctor of Philosophy in the
School of Material Science and Engineering

Georgia Institute of Technology
August 2019

CELLULOSE NANOCRYSTAL/POLYMER NANOCOMPOSITES: PROCESSING STRATEGIES, STRUCTURE VARIATION AND EXPLORED APPLICATIONS

Approved by:

Dr. Karl Jacob, Advisor
School of Materials Science and Engineering
Georgia Institute of Technology

Dr. Preet Singh
School of Materials Science and Engineering
Georgia Institute of Technology

Dr. Hamid Garmestani
School of Materials Science and Engineering
Georgia Institute of Technology

Dr. Kyriaki Kalaitzidou
G.W. Woodruff School of Mechanical Engineering
Georgia Institute of Technology

Dr. Donggang Yao
School of Materials Science and Engineering
Georgia Institute of Technology

Date Approved: May 20, 2019

Dedicated to my family, friends for their endless love, support, and inspiration

ACKNOWLEDGEMENTS

I would like to express my sincere gratitude to my advisors, Prof. Karl Jacob for his invaluable guidance and support of my Ph.D. work and teaching me how to face challenges in my life. I truly appreciate the opportunity to work with him, and grateful to him for giving me the freedom to select my research topics and allowed me to develop and think independently.

Beside my professor, I would like to thank the members of the dissertation committee, Dr. Hamid Garmestani, Dr. Kyriaki Kalaitzidou, Dr. Donggang Yao and Dr. Preet Singh for their kind acceptance and providing me valuable insights and guidance on my research. I would like to sincerely extend my appreciation to Dr. Rina Tannenbaum for her remote discussions on polymer composites and helped me to initiate my work.

I would like to thank the present and past members of the Jacob, Russo, Kumar and Shofner research groups: Dr. Xin Dong, Dr. Huibin Chang, Dr. Jeffery Luo, Dr. Matthew Orr, Dr. Emily Fitzharris, Dr. Xujun Zhang, Luc Le, Cameron Irvin, Mingxuan Lu, for sharing your friendship, knowledge and lab equipment with me. I truly enjoyed the time we collaborate in the labs and brainstorms in my office. Their help and effort were invaluable to the completion of this research. A very special thanks to Dr. Paul Kohl and his team, especially Garrett Huang, for their tremendous help on the electrochemical study.

I would like to thank my funding source, the Renewable Bioproducts Institute for funding provided through the Paper Science and Engineering Fellowship. I thoroughly enjoyed being a member of TAPPI student chapter as well as the CN@GT group.

Lastly but certainly not least, I would like to thank my family and friends, who have shared their companionship with me throughout this chapter of life. I am truly grateful for your amazing friendship and the special moments that we have shared. Thanks to my mom and dad for their support, taught, and unconditionally loved me for 28 years. Its been almost nine years since I was studying in other countries and three years away from home. Even though I could not be there with you for such a long time, I could still constantly receive your love and guidance that helped me to move along this journey. Thank you for believing in me and giving me the strength to pursue my dream.

Table of Contents

LIST OF TABLES

LIST OF FIGURES

SUMMARY

Interest in the most ubiquitous and abundant organic compound—cellulose, harvested from the forest product, has increased notably over recent decades. This bio-based material has been used essentially in bio-composites or in the paper industry; mainly due to its high mechanical reinforcement ability or barrier property respectively. Its nano-scale dimensions and its capacity to form a strong entangled nanoporous network have encouraged the emergence of new high-value applications. The principle reason to utilize cellulose nanocrystals (CNCs) and cellulose nanofibrils (CNFs) as a reinforcing material is that we can potentially exploit the high crystal modulus of cellulose as well as the ability to chemically modify their surface structure. Its high stiffness arises from the hydrogen bond networks formed on the glucose residues from one chain with oxygen molecules on another chain. By selecting the appropriate polymer of choice, the polymer matrix will be bonded strongly with cellulose.

From our first design, CNC was used as reinforcement fillers in a two-part epoxy system. The epoxy film containing various CNC loading was prepared through the solvent-assisted dispersion of CNC, followed by different solution processing method. It was found sample prepared by the dropwise mixing protocols showed better mechanical performance than the samples prepared by bulk mixing. The solvent played an important effect at the final stage of mixing to lower the viscosity of the composite mixture thus led to the more homogeneous distribution of CNC/crosslinker into the epoxy matrix. But the solvent would also plasticize the matrix that causes a decrease in crosslinking density and lower the

thermal/mechanical performance of the composite. The solvent effect was highly depending on the initial degree of crosslinking density (crosslinker selection).

From our second design, a much more compatible polymer matrix-polyvinyl alcohol (PVA) with CNC was used. Composite films were produced with up to 70 wt% CNC content through water-based solution processing. Composite sample with up to 20wt/% CNC loading was fabricated without significant CNC agglomeration. The good interface interactions between cellulose and PVA surface improved the thermo-mechanical properties of the composite film by forming intense hydrogen bonding networks.

Since the PVA/CNC composite could be potentially used for fuel cell applications, a chemically modified proton conducting membrane with PVA/CNC backbone was fabricated and tested. Sulfosuccinic acid (SSA) was used as both the crosslinking agent and proton conductor. Water uptake, ionic conductivity and thermal properties of the crosslinked PVA/CNC/SSA membrane with various amount of crosslinking agent were explored. The composite membrane fabricated showed comparable proton conductivity with much lower methanol permeability compares to the commercially available Nafion® membrane.

The goal of this research is to optimize the processing methods to prepare cellulose-based composite films in different polymer systems. The compatibility of CNC in those polymer matrices will strongly affect its reinforcing properties. A low cost, eco-friendly polyelectrolyte membrane with promising potential in green power generation was fabricated.

Chapter 1. INTRODUCTION

Along with the enhancing awareness of environmental protection, there is increased pressure for decreasing petroleum products because they are non-renewable and do not undergo biodegradation after its useful life cycle. Current oil consumption in the US is around 7 billion barrels per year, but DOE estimated that up to 20% of the petroleum consumption would be replaced by biomass by 2030. Thus, an increasing emphasis on products from renewable, sustainable resources researchers to consider renewable materials and to study their processing-structure-property relationship so that such materials could be used for various applications. This increased awareness of sustainability creates an opportunity for most ubiquitous and abundant natural cellulose-based materials (wood, non-wood lignocellulose, agricultural residue/by-products, *etc.*) to find new applications of utilizing this environmentally benign bio-based materials [1-5]. The hierarchical and multilevel design within the plant fibers has been exploited to be processed into cellulosic fibers that span nanoscale to microscale dimension. Owing to their high surface area to volume ratio by high aspect ratio, a high degree of crystallinity and superior thermo-mechanical properties, cellulosic fibers are commonly used as reinforcing fillers for various polymer systems. The plant-based fillers are much "greener" than the conventional inorganic filler (metal oxide, clay, graphene, carbon nanotube, *etc.*), especially in terms of health risks and safety problems caused by using the traditional reinforcing particles [2].

Cellulosic materials have been thoroughly investigated and reviewed over the last two decades to modify their surface for various applications. Nanoscale fillers made from the

plant have been shown to be a more effective reinforcing agent than macro/microfibers due to the high crystallinity from removing structural defects like lignin, hemicellulose and other labile constituents. The rigid cellulose nanoparticles (CNs) are more thermo-mechanically stable and could be used as the building block for new types of bio-composite. There are two primary forms of nanocellulose sources: cellulose nanocrystals (CNCs) and cellulose nanofibrils (CNFs). Both of them are incorporated into a variety of thermoplastic and thermosetting polymers including polyethylene [6, 7], polyvinyl chloride [8, 9], polylactic acid [10, 11], polyvinyl alcohol [12-16], and polyurethanes [17, 18].

Several novel processing techniques have been reported to make cellulose nanoparticles reinforced polymer matrix composites; With the attempts to form fine CN dispersions with percolation structure while minimizing the large-scale agglomeration problems. Adequate processing generally leads to maximum CN-matrix interfacial interaction that minimizes agglomeration. Three commonly used processing strategies to make cellulose nanocomposite are solution casting [19-23], impregnation of porous nanofiber network [24-26] and partial dissolutions [27-29].

Solution casting involves dispersing CNs within a given medium, typically water, but some organic solvent or co-solvent have also been used in case the polymer matrix is immiscible with water [30, 31]. Polymer solution will be added to the CN dispersion and mixed using either mechanical or magnetic stirring under heating. After that, the nanocomposite solution will be cast into mold or petri-dish followed by evaporating the solvent.

Alternatively, impregnation is another possible processing techniques when a high fraction of cellulose nanoparticle is involved. This composite is formed by starting with 100%

cellulose material (usually by solution casting or vacuum infiltration), and the prepared porous nanofiber network can be infiltrated with a low viscosity polymer resin, with or without applied vacuum.

The partial dissolution process is usually used when preparing all-cellulose composites. Two distinct strategies in the literature are summarized. First of these methods involves preparing a solution of dissolved cellulose which is used to impregnate cellulose film as mentioned above. A surface selection dissolution method involves the partial dissolution of the surface fibers from the cellulose film then regenerated in situ to form a matrix around the undissolved portion [32].

This project mainly used the solution casting process and some impregnation technique for later works. Therefore, the solvent selection was crucial across the scope of this research. As originated from the hydrophilic nature of CNs, their utilization is restricted to applications involving hydrophilic or polar media limits their applications. The CNs are incompatible with the hydrophobic matrix, which leads to phase separation and agglomeration of CN in the polymer matrix during mixing as well as in the casting process. Agglomeration causes two issues, it reduces the uniform distribution of fillers in the matrix and results in larger fillers resulting in inferior mechanical and thermal properties. Several solutions have been offered for better distribution of CN in polymer matrices. 1) solvent-assisted dispersion: Cellulose nanoparticles are either dispersed in organic solvents like DMSO, DMF, or co-solvent or dispersed in water first followed by adding/replacing the desired solvent and allows the mixture to evaporate and eliminate water. The solvent is usually removed during casting or molding [19, 22]. 2) surfactant-assisted dispersion: there are two types of surfactants that can be chosen, non-ionic or ionic surfactant. For nonionic

surfactant, the hydrophilic head group of the surfactant adsorbs on the cellulose surface whereas its hydrophobic tails find proper solvency conditions in the polymer matrix [33]. As for ionic surfactant, negatively charged cellulose nanocrystals will actively interact with cationic surfactant via electrostatic interactions, leading to the formation of hemi and micelles structures, as well as flocculation phases [34]. 3) Surface modification of CNs: as benefited from a large number of hydroxyl groups exposed on CN surfaces, which can be functionalized via chemical reactions. The type of surface modification usually depends on the polymer matrix of interest and are based on reducing surface energy. Thus, the reduced intermolecular affinity between CNs prevents agglomeration, as well as increase its compatibility with hydrophobic matrices.

The objective of this research is to threefold: In the first design, CNC was used as reinforcement fillers in a two-part epoxy system. Epoxy films containing various CNC loading were prepared through solvent-assisted dispersion of CNC, followed by different solution processing method. A co-solvent system which is miscible for both CNC and epoxy was identified. The role of residual solvent and the compatibility between the epoxy matrix and CNC was analyzed through mechanical, thermal and optical characterizations. The first objective was to find the optimized dispersion methods and processing strategies for cellulose nanocrystal in epoxy resins and aliphatic diamine curing agents with different polyether backbone (propylene oxide, ethylene oxide) length. This could test the compatibility of the CNC with both hydrophobic epoxy monomers and hydrophilic diamine functionalized crosslinker. In particular, optimization for the synthesis of such nanocomposites in order to maximize properties was investigated. Through this research, an increased understanding of the processing-structure-property relationships of

CNC/polymer nanocomposite is achieved that provides useful insight for designing the CNC/epoxy formulation.

In the second design, a much more compatible polymer matrix-polyvinyl alcohol (PVA) with CNC was selected. Composite films with up to 70 wt.% CNC content were produced through water-based solution processing. The effect of various CNC loading on the optical, thermal and mechanical properties of the nanocomposite films was studied. Renewable and eco-friendly films can be formulated for different applications.

Finally, the fuel cell application possibility of the nanocellulose-based membrane was evaluated. After deciding the optimum CNC content in the PVA matrix, sulfosuccinic acid (SSA) was used as both the crosslinking agent and proton conductor. The composite films prepared had a proton conductivity in the same magnitude with much lower methanol permeability compared to a commercial perfluorinated membrane such as Nafion®. The optimum composition provided membrane was six times higher in selectivity than the corresponding value for Nafion®. Also, the convenient preparation method, low cost, thermal stability, and recycling potential demonstrated the enormous potential of CNC-based ionomer membrane in the field of DMFC applications.

The goal of this research was to optimize the processing methods to prepare cellulose-based composite films in different polymer systems. The compatibility of CNC in those polymer matrices was found strongly affect its reinforcing properties. A low cost, bio-based polyelectrolyte membrane with promising potential in green power generation was fabricated in replacement of petroleum-based counterpart.

Chapter 2. LITERATURE REVIEW

Cellulose is the most abundant natural polymer resource on earth. This carbohydrate-based material is a well-known biopolymer for its renewable, biodegradable and sustainable properties. It is the major constituent of the cell walls of the plant that provides structural integrity. Cellulose can be obtained from various sources (wood, hemp, kenaf, cotton, sugar cane, crop straw, tunicate, etc.), but the concentration varies significantly between different plants and animals. It is preferable to extract cellulose from pure cellulose sources such as wood pulp (40-50% cellulose) or cotton (90% cellulose). The general physical and chemical properties of cellulose fibers made from wood and non-wood resources are summarized in **Table 2.1**. Cellulose has been widely used by humankind for thousands of years, particularly in industrial forest product like papers. In many early societies such as the European, Egyptian, and Chinese, the paper was traditionally made from non-wood materials, mainly from textile waste products and fiber crops (hemp, flax, rags, etc.). Hemp is probably one of the oldest plants cultivated for fiber. The first paper ever made was by Ts'ai Lun of China in 105 A.D., who used hemp as raw material followed by retting and cooking of the fiber before withdrawing the first sheet of paper from a silk screen mold. Papermaking using cotton and linen fibers spread to Europe in the 13th century. In those days, the paper was a relatively expensive commodity.

Table 2.1 Comparison of physical and chemical properties of non-wood fibers with those of wood raw materials [35]

Properties	Kenaf	Straw	Bagasse	Bamboo[d]	Eucalyptus[d]	Birch[d]	Spruce[d]
Physical:							
Fiber length, mm	1.3[a]	1.3	1.7	2.3	1.0	1.0	3.6
Fiber width, um	27[a]	12.9	20	14.4	18	25	35
Felting factor[b]	49[a]	102	85	161	51	58	101
Chemical:[c]							
Cellulose, %	43.9	54	49.9	57.1	56	41	44
Hemicellulose, %	32.6	24.1	27.9	19.5	18	40	27
Lignin, %	16.2	18.4	20.8	23.4	26	19	29
Extractive, %	7.3	3.5	1.4	0	0	0	0

[a] Dimensions for whole stem kneaf from bast and core in the ratio of 35% and 65%, respectively.
[b] The ratio of fiber length to fiber width
[c] Expressed on dry matter
[d] Extractive free basis

In general, cellulose is a linear syndiotactic polysaccharide made up of carbon, oxygen, and hydrogen. The repeat units of two ringed anhydroglucose units (AGU) is given in *Figure 2.1*, which are linked together through oxygen covalently bonded to the C1 of on glucose ring and C4 of the adjoining ring. Importantly, each AGU unit bears three hydroxyls (-OH) groups, which point laterally along the cellulose chain. One primary hydroxyl group is belonging to C6 and two secondary hydroxyl groups attached to C2 and C3. The hydroxyl groups of cellulose can provide the inherent chemical reactivity, means they can be partially or fully react with various chemicals to provide derivatives with useful properties. It is found that the hydroxyl group at the 6 position can react ten times faster than the other OH groups during esterification while the other two groups are more reactive to etherification [36].

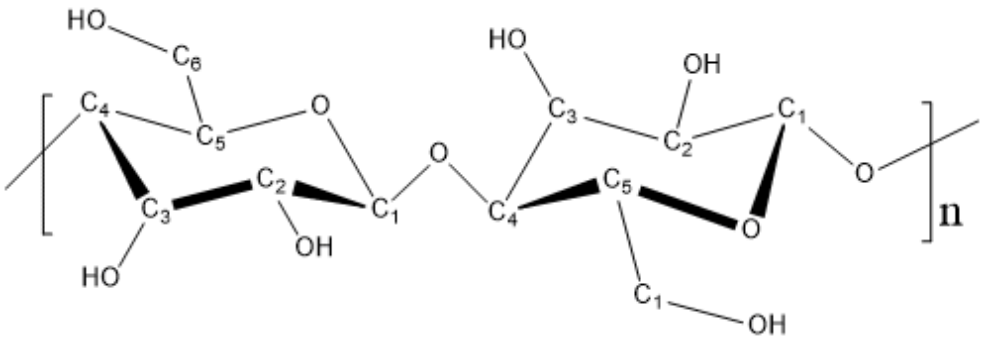

Figure 2.1 Chemical structure of cellulose

These hydroxyl groups along with oxygen moieties of adjoining ring molecules enable the cellulose chain to readily form inter/intra-molecular hydrogen bonding to stabilize the linkage and form linear chain configuration with relatively high axial stiffness and rigidity. 30-100 individual cellulose chains could merge into elementary fibrils by parallel stacking, which can be further packed into larger microfibrillated cellulose with diameters up to several tens of nanometers and with lengths of several microns [3]. As presented in Figure 2.2, each elementary fibril consists of a long strand of cellulose crystals linked with disordered amorphous domains. Bundles of microfibrillated cellulose further combined with non-cellulosic matrix contain hemicellulose, lignin, and other extractives, assembling into the individual cellulosic fiber.

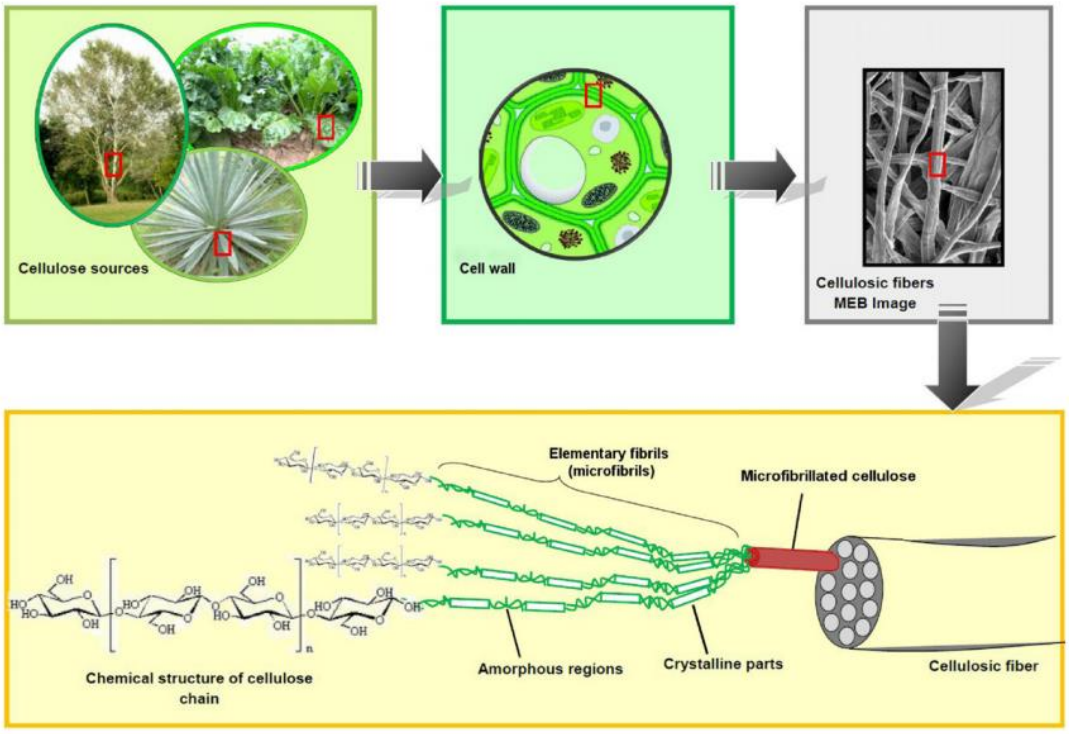

Figure 2.2 Schematics of cellulosic fiber structure with emphasis on the microfibrils [37]

2.1 Cellulose Nanoparticles

The first successful isolation of cellulose microfibrils (MFC) was reported 30 years ago by Turbak et al. and Herrick et al. [38, 39] using a Gaulin laboratory homogenizer with high shear force to individualize cellulose microfibrils. Scientists have demonstrated the significant commercial potential in a variety of applications and tried to further reduce MFC into cellulose nanoparticles known as cellulose nanocrystals (CNCs) and cellulose nanofibrils (CNFs). Nanofibrillated cellulose is typically created by some combination of chemical, enzymatic, and mechanical treatments of lignocellulosic materials, such as wood [40, 41]. They have a nanoscale diameter (usually less than 100 nm) and length up to a few micrometers. CNFs contain both amorphous and crystalline regions of cellulose and have

a large aspect ratio with the high surface area. There are two main pretreatments that can be applied to cellulose fibers to produce NFC with significant energy consumption reduction, enzymatic pretreatment or (2,2,6,6-Tetramethylpiperidin-1-yl)oxyl/TEMPO-mediated oxidation. The energy required to individualizes cellulose nanofibrils were reduced from 30MWh/ton with untreated fibers to less than 1MWh/ton after pretreatment [42]. These processes aim to limit interactions between microfibrils. TEMPO process can selectively oxidize the surface of cellulose fiber under aqueous and mild conditions.

As mentioned in Figure 2.2, MFC contains bundles of amorphous regions, which are susceptible to attack by acid. Therefore, CNCs can be obtained via acid hydrolysis of MFC. Sulfuric acid is most commonly used as it converts surface hydroxyl groups on the particles into the negatively charged sulfate ester group, which contribute to their stability in aqueous suspensions. Other acids including hydrochloric [13, 31], maleic [43], phosphoric [44] and nitric acid [13, 44] have also been used to make CNC. The geometry and surface functionality of the resulting CNCs vary depending on the source of cellulose and the hydrolysis conditions. CNCs typically have a rod-like or whisker-shaped structure, ranging from 5-20 nm width and 50 to 500 nm length. CNCs have a high aspect ratio and with highly crystalline (54-88%), due to the removal of amorphous parts during hydrolysis [3]. From theoretical evaluations and experimental measurement, the elastic modulus of individual CNC in axial and transverse direction has been estimated to lie between 120-220 GPa and 5-50 GPa, with tensile strength up to 10 GPa [3, 4, 37]. The nanocellulose paper prepared from enzymatic hydrolysis gives relatively lower properties compare to the theoretical values. With Young's modulus of 13.2 GPa and tensile strength of 214 MPa [45]. Due to low densities of CNCs, the specific module and strength of crystalline

cellulose are comparable to those of engineering reinforcements such as Kevlar, glass, clay and carbon fiber. With the aforementioned extraordinary mechanical properties, as well as low density, low coefficient of thermal expansion, high optical transparency, high surface area-to-volume ratio, engineered surface chemistry, and most attractively, biocompatibility and renewability. Composite community is attracted to CNCs and have a broad range of applications.

2.2 CNC/Polymer Nanocomposite

2.2.1 Epoxies

Epoxy resins are one of the largest class of thermoset polymers used extensively in structural and composite applications. It was first produced in Europe and the United States simultaneously around the 1940s by Pierre Castan of Switzerland and S.O. Greenlee of the US who investigated the reaction of bisphenol-A with epichlorohydrin [46]. Epoxies are commonly used as adhesives and coatings because of their excellent wetting characteristics with a high degree of adhesion to almost all substrates, unique balance of chemical-mechanical-thermal properties combined with extreme processing versatility. There are three crucial components of an epoxy resin that needs to be considered when deciding the formulation that will yield the desired application characteristics and end-use properties: base resin (epoxy monomer), curatives (crosslinker or hardener), and the modifier (organic or inorganic fillers). The first and most common commercial base resin is the diglycidyl ether of bisphenol-A (DGEBA) which is also used in this work. It contains two epoxy or oxirane ring separated by phenolic glycidyl ethers backbones. Depending on the molecular

weight of this backbone, DGEBA can be both solid and liquid forms. The viscosity of liquid DGEBA is range from 5000-20000 cP at 25 ºC. The epoxy equivalent weight (EEW) is defined as the weight of the resin per epoxide group and will be around 174-200 for liquid resin and over 500 for solid resin. Other classes of epoxides include phenol and cresol novolacs (phenolic glycidyl ethers), glycidyl amines and cycloaliphatics. Different classes of resins will have different viscosities, curing rates for processing, and their cured form will have versatile properties (glass transition temperature, chemical-mechanical-thermal performance).

Epoxy resins can react with a variety of curative or hardeners such as amines, amine derivatives, anhydrides, and thiols with considerable strength and flexibility. Curing can be classified based on the curing temperature [47]. Most amines and amides can be cured safely at room temperature due to their high reactivity. BF_3 complexes and imidazoles can be cured at room temperature or elevated temperature and often used as accelerators in conjunction with other hardeners. Aromatic amines and anhydrides need to be cured about 100 ºC with postcures temperatures ranging to 200 ºC. Some resin formula can be cured with nonthermal radiation sources like ultraviolet, infrared and electron beam at a higher cost. In this work, polyetheramines (PEA) was used as curatives. They are also known by the trade name Jeffamine®, with polyether backbone. They are of general interest because of low viscosity, flexible backbone, controllable reactivity and most importantly, good health and safety record [48]. Polyetheramines with different polyether backbone lengths were used to evaluate their compatibility with CNC, and the molecular structures of the hardeners are listed in Table 2.2. Both hardeners have low viscosity, which makes them ideal for blending with high viscosity filler solution like CNC. The methyl group adjacent

to the nitrogen allows for a relatively long pot life, important in leveling when casting films. They are completely miscible with a wide variety of solvents, where ED600 is completely water-soluble liquid, thus should be more compatible with CNC than D230. Meanwhile, the long polyethylene glycol chain in ED 600 impart the flexibility of the cured products, as well as lowering crosslink density. As a result, when the crosslink density decreases, the glass transition temperature T_g decrease due to enhanced mobility of polymer chains. As reported in the literature [49-51], the value of T_g for DGEBA/ED600 type epoxy networks is about 13-25 ºC, whereas DGEBA/D230 type show T_g value of 88 ºC. Curing with D230 is commonly found in surface coating, flooring, potting and reinforced composite formulations. ED600, however, is weaker in mechanical performance. Hence may not be used as a sole curing agent for the above applications, but usually blended with other PEA to improve low-temperature flexibility and to reduce plasticizer migration in high-temperature molding operations.

Table 2.2 Chemical composition and molecular weight of Jeffamines

Name	Chemical composition	Approx. molecular weight
D230	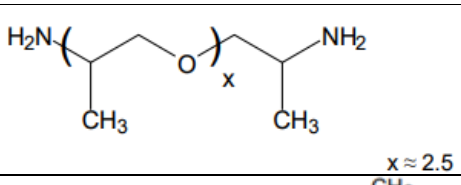	230
ED600	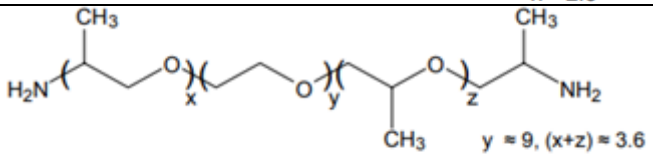	600

As mentioned above, as a result of the hydrophilic nature of CNs, their utilization is restricted to applications involving hydrophilic or polar media and is incompatible with hydrophobic matrices such as epoxy. However, the hydrogen bonding between hydroxyl

groups of CNs and epoxy groups of epoxy resin allows the formation of filler/polymer network in a cured system. The incorporation of cellulose nanofillers into epoxy resins have been studied in the last decade[1, 20-26, 52-68]. Several methods are introduced to disperse CN in the epoxy matrix without large-scale agglomeration. 1) Infiltration of porous CN preform: This requires producing a three-dimensional scaffolding or aerogels of cellulose nanoparticles. Either by freeze drying or vacuum filtration of diluted CN suspensions followed by impregnation or infiltration of low-viscosity epoxy resin [24, 26, 57]. 2) Surfactant-assisted dispersion: surfactant can be used to tailor the hydrophilic surface of CNs with the hydrophobic epoxy matrix. Chemists had formulated waterborne epoxy resin with surfactants, which would disperse these hydrophobic resins in water. The epoxy resins can be in liquid, solid or mixed forms. The aqueous CNC can be directly mixed with waterborne epoxy without further treatment [23]. Meanwhile, the ionic or non-ionic surfactant can also be added into CNC suspension before mixing with epoxy resins [58]. 3) Surface modification of CN: By utilizing cellulose's hydroxyl surface chemistry, scientists can modify their hygroscopic properties by introducing new functionality. Acetylation is one of the simple modification methods with a relatively high degree of substitution (DS) [1, 21]. Hygroscopicity of modified cellulose nanoparticles could be controlled by varying the length of the aliphatic side chains. Esterification reaction using organic acid chloride aliphatic chains is also reported [6]. However, to favor ester formation, an excess of reagent and catalyst will be required and is usually at a loss of raw material during the process. Silane coupling agent treatment of cellulose can also be categorized as surface modification approach [69, 70]. 4) solvent-assisted dispersion: cellulose nanocrystals with negatively charged sulfate ions prepared by acid hydrolysis

process were seen to be stable in polar aprotic media such as dimethylformamide (DMF), dimethyl sulfoxide (DMSO), and N-methyl pyrrolidine (NMP) due to the high dielectric constant of the solvent. Nanocomposites are then accessible by mixing organic CNC solution with a polymer of choice soluble in the same organic solvent. Dispersion of CNC in organic solvent was done by either solvent exchange or solvent mixture. For example, Tang *et al.* [20, 22] and *Peng et al.* [23] prepared cellulose whisker organo-gels via a sol-gel process. Acetone was added to the aqueous CNC solution. The top acetone layer was replaced with fresh acetone 1-2 times daily until the bottom layer forms a mechanically coherent CNC-acetone gel. The solvent exchange process takes a long period of time (3-7 days) and uses abundant organic solvents. This leads to environmental concerns on the emission of organic solvent to the atmosphere as well as human exposure to volatile organic compounds (VOC). For solvent mixing, an aqueous CNC solution is usually mixed with a solvent compatible with the matrix, and a small amount of water is necessary for stable dispersion in organic solvents [30]. Chang *et al.* [71] studied the effect of water on the dispensability of CNCs in organic solvents. 25-75 volume H_2O/DMF co-solvent shows the lowest hydrodynamic radius after 24h of bath sonication. They suggest that the strong water-DMF interactions can effectively alleviate the H-bond formation between CNCs, thus more accessible to individualized CNC in the co-solvent. The solubility of epoxy resin and CNC in various common solvents are summarized in Table 2.3.

Table 2.3 Solubility or epoxy resin and CNC in various solvents

Solvents	Epoxy Resin[a]	CNC[b]
Water	0	1
Methanol	0	1
Ethanol	0	1
2-propanol	0	1
Acetone	1	0
Tetrahydrofuran (THF)	1	0
Acetonitrile	1	0
Dimethylformamide (DMF)	1	1
Dimethyl sulfoxide (DMSO)	1	1
Chloroform	1	0
Hexane	0	0

[a] Solubility is determined by the Hansen solubility parameters (HSP) method [72]. [b]dispersion of HCl-treated cellulose nanocrystals is investigated by cross-polar images [31] "1" and "0" stand for the good and bad solvent, respectively.

DMF/water co-solvent mixture is selected to disperse CNC and later to mix with epoxy monomer and hardeners. However, the residual solvent could influence curing behavior and network structure by plasticizing the epoxy matrices. Coelho *et al.* [59] and Hong *et al.* [60] studied the effect of residual acetone, which caused a decrease in T_g and brought detrimental effect on the mechanical properties of the composite [73, 74]. Sun *et al.* [75] stated the positive effect of residual DMF on mechanical properties on Epoxy-CNT composite. The decrease of crosslinking density and T_g due to the plasticized matrix was confirmed from the dynamic mechanical analysis. They suggest that the DMF was decomposed into aliphatic amine during high-temperature curing (240 °C), acting like excess hardeners as well as a terminating agent, increasing chain packing and improving Van der Waal's interaction.

In this study, the influence of both processing routes and solvent effect on thermal and mechanical properties of CNC/epoxy nanocomposites was studied. CNCs are first dispersed in the DMF/water co-solvent mixture to form a 3wt% solution. The CNC solution

was first combined with hardeners to make a homogeneous, well-dispersed CNC/hardener mixture before mixing with epoxy monomer. The objectives of this study were: (a) to fabricate CNC/epoxy nanocomposite by using bulk and dropwise mixing method; (b) to understand the curing behavior of the residual solvent in nanocomposites; which is done by preparing solvent removal (SR) samples following the same procedure except the co-solvent is removed from CNC/hardener mixture before mixing with epoxy monomer. (c) to evaluate the role of two types of polyether diamines hardener in the resulting nanocomposite structure and properties.

2.2.2 Polyvinyl alcohol

Polyvinyl alcohol (PVA) is a water-soluble, semi-crystalline, non-toxic, biodegradable and biocompatible polymer. The vast number of hydroxyl groups on the hydrocarbon backbone allows the formation of intermolecular hydrogen bonding. PVA is one of the most commonly used synthetic polymer which is easily obtained with low cost of productions. It has the good film-forming ability, easy processability, high optical clarity, and high tensile strength and flexibility, and is used in a variety of industries including biomedical, filters, packaging and paper industry [76, 77]. CNC film is very brittle and breaks easily when handling the film, and its high price compared to conventional polymers hinder its use. Therefore, it is a promising strategy to blend PVA and CNC to obtain the combined properties of both polymers. PVA is compatible with CNC due to the formation of hydrogen bonds between the hydrophilic surfaces, and this leads to the formation of a new biocompatible film via a solution casting method.

Since both fiber and matrix are hydrophilic with similar surface energies, incorporation of nanocellulose into PVA is greatly facilitated by the simple mixing in aqueous solution. However, PVA becomes solubilized in water at a temperature higher than 80°C, whereas CNC will start to gelation above the same temperature, which is attributed to desulfation of CNC surface, resulting in a destabilization of CNCs in suspension [78]. Thus, PVA needs to be suspended in water first and cool down before mixing with an aqueous CNC solution. The PVA-CNC mixture can be cast on to a plastic disc and wait water evaporates. The homogeneity of the nanocomposite suspension will depend on the CNC concentration, the matrix material and preparation conditions. Lee *et al.* [79] compared neat PVA films (E=1.1 GPa, σ=49 MPa) to a series of composite hydrobromic acid treated CNC/PVA films (0 to 5 wt.%). The tensile strength of nanocellulose reinforced PVA film showed the highest value (σ=79 MPa) at the loading of 1 wt.% and diminished with higher CNC loading, with the increased modulus (40-80%) as compared to the neat PVA film. The addition of CNC to PVA also showed a significant effect on the thermal stability of CNC reinforced films due to the dense hydrogen bonding network form between the hydroxyl group of CNC and PVA matrix.

Apart from solution casting, an aqueous dispersion of PVA and CNC can also be used to prepare nanofibers by electrospinning. Peresin *et al.* [80] prepared electrospun fiber webs of neat PVA and PVA loaded with 0-15 wt.% CNC with maximum diameters of about 290 nm. They reported the increased crystallinity and melting temperature as being the result of the interaction of PVA matrix and CNC phases with the improved alignment of CNCs along the fiber length by high shear stresses during electrospinning. The resulting composites exhibited improved storage modulus in the rubbery region of the dynamic

viscoelastic curve at all concentration, with the 3-fold increase for 15 wt.% CNC reinforced fibers compared with neat PVA fiber. The strengthening mechanism was attributed to the effective stress transfer at CNC-matrix interface.

In the current study, PVA/CNC films were prepared with loading up to 70 wt.% CNC through the solution casting method, and the chemical, optical, mechanical, and thermal properties were investigated. The resultant film with the optimum performance was selected for further modifications to fabricate ionomer membrane for fuel cells applications.

2.3 Nanocellulose in Fuel Cells

Fuel cell technology as a promising power generator attracted a tremendous level of attraction in recent years. It is an electrochemical device that converts the chemical energy of a fuel directly into electrical energy as long as the fuels are continuously supplied to the cell [81-86]. Different types of fuel cells can be characterized by their electrolyte material with different operation temperature varieties [87]. Figure 2.3 summarizes the different fuel cell technology and illustrates the prominent feature in each type.

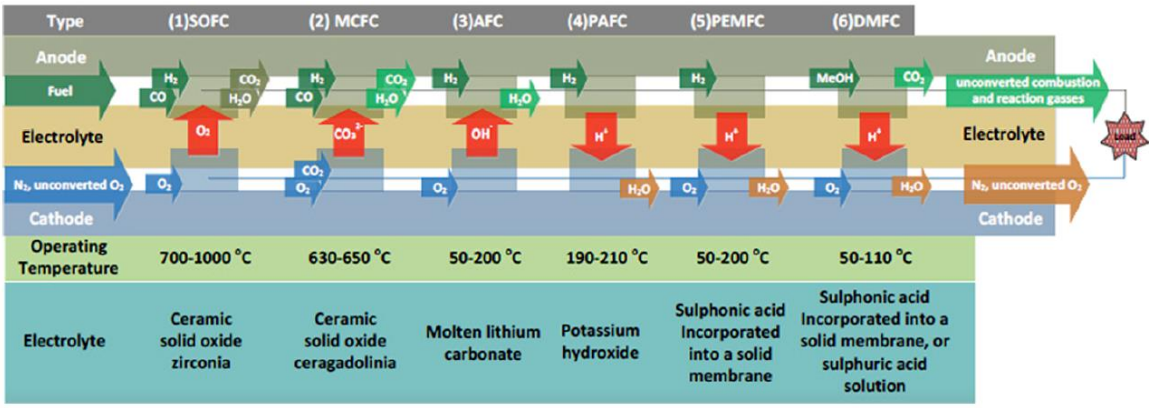

Figure 2.3 Schematic of six different fuel cell technologies [88]

In this work, direct methanol fuel cells (DMFCs) was investigated. The DMFC is developed as a power source for portable electronic devices such as notebook, laptop, and cellular phones [86, 89]. Ion exchange membranes consist of polymer backbones with ion exchange sites as pendant groups and mobile counter-ions. The ion exchange groups are usually covalently bonded to the polymer backbone and will dissociate with sufficient water. Depending on the type of ionic groups, the membranes can be categorized into cation exchange membrane/proton exchange membrane (PEMs) and anion exchange membranes (AEMs). Sulfonic acid, phosphoric acid, and carboxylic acid groups are mostly presented in PEMs, whereas quaternary ammonium and imidazole cations are generally found in AEMs [90]. Proton exchange membrane is one of the most determinant factors in overall fuel cell performance. The configuration of a typical DMFC fuel cell is shown in Figure 2.4. Typical the liquid feed DMFC is operated at a temperature from 80 to 100 ^{o}C. Liquid methanol fuel is fed into the anode and penetrate the diffusion layer (DL) and arrive the catalyst layer (CL). The protons are conducted from the catalyst layer migrate through the proton exchange membrane, and the electrons travel through the electronic circuits. The CO_2 produced in the catalyst layer will move back to the flow channel and forced out of the system. At the cathode, oxygen or air pass over the cathode. The protons will react catalytically with oxygen and electrons to produce water. The anode, cathode, and overall cell reactions are shown below:

$$\text{Overall: } CH_3OH + 3/2O_2 \rightarrow CO_2 + 2H_2O \quad E=1.186V$$

$$\text{Cathode: } 3/2O_2 + 6H + 6e^- \rightarrow 3H_2O$$

$$\text{Anode: } CH_3OH + H_2O \rightarrow CO_2 + 6H + 6e^-$$

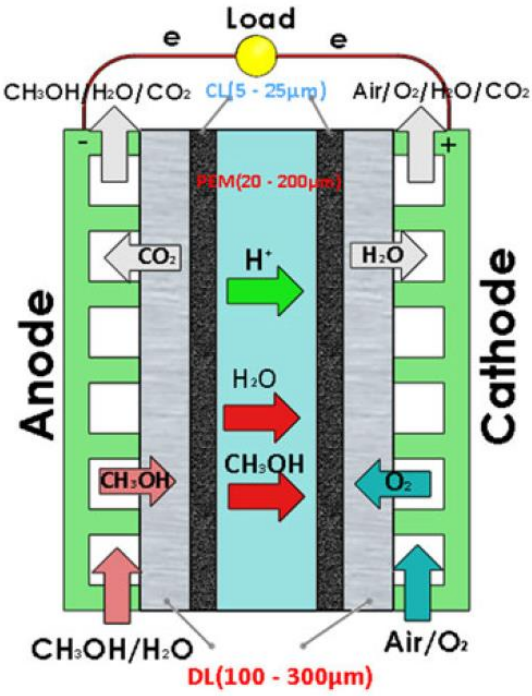

Figure 2.4 Schematic representation of the direct methanol fuel cell (DMFC) [89]

There are various commercially available proton conducting membranes on the market, and the most popular ever used is Nafion® (E.I. DuPont de Nemours & Co., Inc.). It consists of a polytetrafluoroethylene (PTFE) backbone with a perfluorosulfonate side chain that is terminated with a sulfonic acid group. The hydrophobic PTFE backbone and hydrophilic pendant sulfonated moieties create a nanoscopic phase separation in the hydrated state [86]. These nanochannels are permeable to cations or protons but reject anions. However, even Nafion® has several deficiencies, especially high methanol crossover and poor conductive performance at elevated temperature. Due to the chemical similarity of water and methanol, the methanol has a considerable solubility in the polymer membrane, leading to a significant crossover. The methanol crossover is closely relative to the methanol permeability of the membrane, membrane thickness and the cell operating condition (temperature and methanol feed concentration), and strongly affect the cell performance.

Methanol reached to the cathode will react with cathode catalyst (Pt), resulting in mixed potential without generation of electricity. Methanol will be oxidized with the consumption of O_2, and the intermediate product (CO) will poisoning the cathode catalyst. Also, water produced by methanol oxidation will lead to serious water accumulation, which will reduce the effectiveness of oxygen reach cathode catalyst sites [91, 92].

Although fuel crossover is the most pressing problem associated with DMFC, dehydration at elevated temperature will also decrease the conductivity, with loss of mechanical stability caused by film shrinkage. Sometimes, the changes of membrane microstructure are irreversible when the membrane becomes dehydrated. Therefore, the research to modify Nafion® or development of alternative PEM is highly active. With the rapid growth in nanoscience, the use of nanofillers has become an approachable development direction. Nanofillers are introduced to regulate and control the ionic channels formed within the polymer structure. Some researchers have incorporated organic/inorganic nanoparticles in PEM in order to suppress methanol crossover by creating tortuous pathways by using additives, for example, clay, alumina oxide, graphene oxide, titania nanotubes, multi-walled carbon nanotubes and PVA nanofiber [93-96]. However, this may also lead to depression of proton conductivity due to the interference with proton transport nanochannels and decrease in proton conduction sites density. Hence, functionalization of incorporated particles has been investigated to compensate for the loss in proton conductivity [86, 97, 98].

The desired properties of PEM membrane materials include high ionic conductivity, low electronic conductivity, low permeability to gas or liquid fuels, adequate mechanical and chemical properties with dimensional stability in the operating environment. Additional

aspects like simple fabrication with lower cost and ecological compatibility should also be considered in membrane material research. Some promising materials like polybenzimidazole (PBI), sulfonated polyetheretherketone (SPEEK), sulfonated polyimides (SPI) and composite polymer materials were used to fabricate electrolyte. However, Nafion® still outperforms most of these alternative electrolytes in PEMFC applications, especially regarding ionic conductivity and durability.

Proton conductivity is an intrinsic property of membranes. In general, polymer-based electrolyte membranes utilize acid group as proton carrier and hydrogen bonding networks as proton migration channels [99-101]. The presumptive illustration of the proton transport mechanisms in PEM is shown in Figure 2.5. Because proton cannot exist alone in aqueous solution, it is usually carried by water molecules. Two of the basic proton conduction mechanisms are related to the proximity of water to the acid groups (hydration level of the electrolyte). Proton transport in the bulk-like water can be explained by the Grotthuss mechanism, which involves proton hops between water molecules by forming hydrogen bonds (proton hopping), followed by cleavage of hydrogen bond and the proton reorients to another water molecule (reorientation). Cleavage of hydrogen bonds is generally the rate-determining step in proton conduction, the activation energy for such steps should be around 10.6 kJ/mol [102]. The second transport mechanism is the vehicle mechanism, where a proton combines with solvent molecules, producing a proton vehicle like H_3O^+ (hydronium) $H_5O_2^+$ (Zundel) and $H_9O_4^+$ (Eigen) cation with several water molecules per proton, and diffuse through the membrane while a counter diffusion of unprotonated water occurs [101, 103]. Therefore, water management is crucial to the PEM. If there is not enough water in the membrane, the shortage of proton conductive pathways will cause a

decrease in proton conductivity. This problem is more prominent at lower relative humidity, and an alternative proton conduction mechanism likely occurs if a relatively large number of acid groups present in the membrane. This last mechanism is caused by proton hopping along with dissociated acid groups on the pore surface. When the acid concentration is low, and the distance between acid groups is too far, hydronium ions are required to bridge the conductive pathway. Takaya et al. [100] proposed a packed-acid mechanism for materials containing highly concentrated acids. The acid-acid interaction could eliminate the pseudo-shuttling (proton trapped between the proton donor and acceptor) and weakening the hydrogen bond network that facilitates proton conduction.

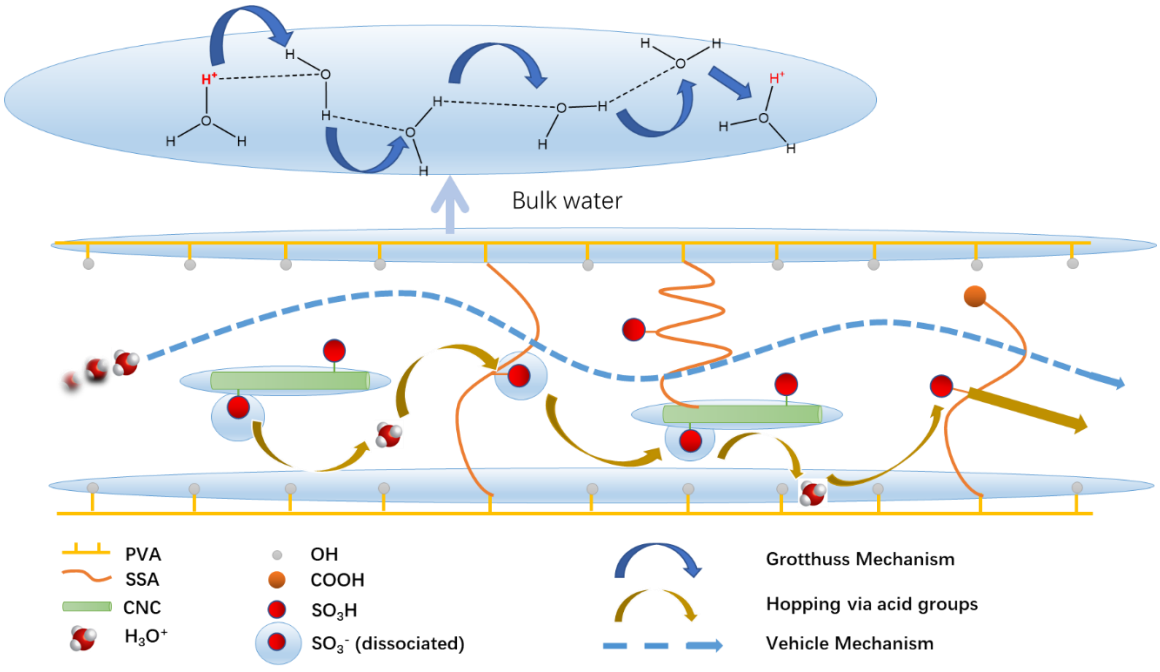

Figure 2.5 Presumptive illustration of proton transfer mechanism in PEM

Nanocellulose has been extensively used to prepare fuel cell membranes due to the good gas barrier properties, high aspect ratio, and outstanding mechanical and thermal properties. Furthermore, the sulfuric acid hydrolyzed cellulose nanocrystals contain sulfate ester

groups that could potentially help proton conduction, and the enormous hydroxyl groups on CNC has a high capacity to absorb and retain water. Also, the presence of hydroxyl groups on the cellulose backbone facilitates the grafting of cations for enhanced ion exchange capacity and provides a high potential for its modification into sophisticate nanoparticles. Cellulose has been investigated in composites with Nafion®. Hasani-Sadrabadi *et al.* [104] reported the potential of acid-hydrolyzed cellulose nanocrystals as a nano-additive for Nafion® membranes. They showed that the inclusion of 5 wt.% CNCs could considerably increase the proton conductivity across the full range of temperature and humidity of investigation (25-120 ºC) through regulating the ionomers microstructure. The excellent affinity of CNC to Nafion® matrix made the membrane more resistance against dehydration, which retained its proton conductivity at the elevated temperature up to 120 ºC (~0.17S/cm) whereas the recast Nafion® membranes had negative conductivity-temperature dependency above 90 ºC because of the loss of water. Methanol permeability of the composite membrane (2.33×10^{-7} cm^2 s^{-1}) was one order of magnitude lower than Nafion® 117 (2.0×10^{-6} cm^2 s^{-1}) and recast Nafion® membrane (2.09×10^{-6} cm^2 s^{-1}). Nanocomposite membranes showed higher overall efficiency of 21% at 1M and 15% at 5M methanol concentration, compared to other types of Nafion® membranes, attributed to the reduced methanol crossover.

Recently, paper membranes fabricated by pure unadulterated cellulose resource have been investigated [101]. In their research, nanocellulose paper was prepared using cellulose nanofibrils (CNFs) and cellulose nanocrystals (CNCs). The CNC and CNF dispersion were vacuum-filtered to form a hydrated membrane. The filtrated CNC membrane can be peeled off filter directly whereas CNF membrane was hot-pressed to form a dense film before can

be peeled off the filter. The nanocellulose papers were targeted for PEFC-type hydrogen fuel cells applications. Hydrogen permeability of both CNC and CNF membrane were three orders of magnitude lower than that of Nafion®. The proton conductivity of the CNC membrane increased with temperature up to 120 ºC whereas the CNF membrane shows a drop in conductivity above 100 ºC. The maximum conductivity of CNF paper (5×10^{-5} S/cm at 100 ºC) was much lower compared with CNC (4.6×10^{-3} S/cm at 120 ºC), which was attributed to the acid hydrolysis treatment of CNC. The sulfate ester group attached to the side will not only provide more proton conduction paths but also increase the hydrophilicity of the CNC membrane to retain water at high temperature. However, the author stated that the CNC membrane was very brittle and fully dissolves in water due to its high hydrophilicity. The achieved proton conductivities were still two orders of magnitude lower than that of Nafion®-based PEM. Thus, it only provided an insight into how nanocellulose paper could be utilized as a promising material for environmental-friendly, low cost, and bio-based membrane in next-generation fuel cells.

In order to suit the nanocellulose membrane in DMFC application. Two distinct methods were considered in this research. One approach to improving the handleability of CNC with polymers to prepare a free-standing and flexible film. PVA is one of the best candidates, owing to its high selectivity of water over methanol or alcohols, which can function as an excellent methanol barrier and this polymer is fully compatible with CNC phases as discussed previously. Since both PVA and CNC are soluble in water and have a high degree of swelling, the hydrophilicity of the composite film needs to be controlled. Lu *et al.* [105] prepared CNC based PEM with PVA and silica gel hybrid. The Composite film with 40% hydrophobic binder exhibited both high water uptake (80%) and superior dimensional

stability with enhanced self-supporting ability. Covalent crosslinking is another approach to increase the hydrostability of the film. The next approach is to increase the proton conductivity of both CNF paper and CNC/PVA film by chemical modification with polymer contains negatively charged ions (carboxylic and/or sulfonic acid group), such as poly (styrene sulfonic acid-co-maleic acid) (PSSA-MA), and sulfosuccinic acid (SSA) [77, 106-111]. PSSA-MA and SSA acted as both the cross-linking agent and proton conductor. Rhim *et al.* [106] prepared crosslinked PVA membrane with the various amount (5-30 wt.%) of SSA and also with different crosslinking temperature (120-130 ºC) to achieve desirable proton conductive properties. They suggest that the PVA/SSA membrane was partially crosslinked at 120 ºC and the unreacted carboxylic acid can act as proton conducting sites. For membrane crosslinked at 125 and 130 ºC, water uptake, proton conductivity, and methanol permeability decreased until the amount of SSA reached to 17 wt.%. Meaning the water retention in the polymer matrix had a dominant effect on proton and methanol transport. However, different results have been showed for cellulose-based crosslinked membrane by SSA [109]. The result showed that the water uptake and proton conductivity increased with SSA loading and the mechanical properties were enhanced with SSA concentration up to 15 wt.%. The difference may cause by the different nature of matrices used. The effect of crosslinking may play a more dominant role in PVA than in cellulose as the PVA has higher hydroxyl group density. These studies point to a critical need to control and optimize the amount of SSA and the crosslinking conditions for CNC/PVA based membrane for DMFC application.

2.4 Thesis Overview

This thesis aims to help CNC-based product become commercialize in the market space. The first part of this thesis is to compare different processing strategies to overcome the critical challenge of use CNC in composite, which is related to their homogeneous dispersion within a polymer matrix. Different solvent-assisted routes to improve CNC dispersion in the epoxy-based composite were assessed. The optical, thermal, mechanical properties of the epoxy resin with different hardener structure were investigated. It was found the compatibility of CNC in polymer matrices will strongly affect its reinforcing properties.

The second part of this thesis is exploring new applications for CNCs, which is one of the significant efforts required in the Agenda 2020 nanocellulose roadmap. A low cost, bio-based polyelectrolyte membrane with promising potential in green power generation was fabricated using the nanocellulose based nanocomposite. A highly compatible polymer matrix PVA was used to produce nanocomposite with high CNC loading. The PVA/CNC based film was chemically modified to fabricate polyelectrolyte membrane. The hydration, electrochemical and barrier performance of the crosslinked membrane were conducted to develop an understanding of the novel low dimensional proton conductor as fuel cell electrolyte for the direct methanol fuel cell application.

Chapter 3. EFFECT OF PROCESSING TECHNIQUES AND RESIDUAL SOLVENT ON THE THERMAL/MECHANICAL PROPERTIES OF EPOXY-CELLULOSE NANOCRYSTAL NANOCOMPOSITES

3.1 Overview

In this study, nanocomposites with 0-5 wt.% of cellulose nanocrystals (CNC) were fabricated by the solution casting method. The CNCs was first dispersed in hardener solution using DMF/water co-solvent. After that, the CNC/hardener mixture and epoxy monomer were mixed using two different protocols: bulk mixing and dropwise mixing. The distribution and dispersion state of CNC within the epoxy matrix achieved by these two mixing protocols will affect the CNC's reinforcing efficiency.

As a result of the hydrophilic nature of cellulose nanofibers (CNs), their utilization is restricted to applications involving hydrophilic or polar media and is incompatible with a hydrophobic matrix such as epoxy. However, the hydrogen bonding between hydroxyl groups of CNs and epoxy groups of epoxy resin allows the formation of filler/polymer network in a cured system. The selection of hardeners could also impart the hygroscopic properties of the epoxy system. The incorporation of cellulose nanofillers into epoxy resins have been studied in the last decade [1, 20, 21, 23, 55]. However, there has not been a study that explores the effect of processing strategies on the dispersion and final properties of the epoxy nanocomposite. In addition, the residual solvent could influence curing behavior and

network structure by plasticizing the epoxy matrices [74, 75]. When and how to remove the solvents will also impact the composite's performance.

In this study, solution casting protocol was used, and the solvent selection was crucial. DMF was chosen because both epoxy resin, and CNC showed good solubility in DMF. Chang *et al.* [71] studied the effect of water on the dispensability of CNCs in an organic solvent. The 25-75 volume percent of H_2O/DMF co-solvent showed the lowest hydrodynamic radius after 24h of bath sonication. They suggest that the strong water-DMF interactions can effectively alleviate the H-bond formation between CNCs, thus more accessible to individualized CNC in the co-solvent. Therefore, the 25-75 volume percent of H2O/DMF co-solvent was used here.

In this work, the influence of both processing routes and solvent effect on thermal and mechanical properties of CNC/epoxy nanocomposites were studied. The hardener used here was completely water soluble with low viscosity. Therefore, CNC solution was first combined with hardeners to make a homogeneous, well-dispersed CNC/hardener mixture before mixing with the epoxy monomer. The objectives of this study were: (a) to fabricate CNC/epoxy nanocomposite by using bulk and dropwise mixing method; (b) to understand the role of residual solvent in the cured nanocomposite.

3.2 Experimental

3.2.1 Materials

The epoxy resin used in this work was monomeric Diglycidyl Ether of Bisphenol A (DGEBA, DER-332, supplied by Dow Chemical, epoxy equivalent weight (EEW) = 178) cured with amine-terminated Poly (propylene/ethylene glycol)s (Jeffamine ED600,

supplied by Huntsman, amine hydrogen equivalent weight (AHEW) = 132). The Jeffamine ED600 was used at the stoichiometric mixing ration of 73 parts per hundred parts of resin (phr). Freeze dried CNC was purchased from the University of Maine, produced by the U.S.D.A Forest Products Laboratory. The dimensions of these CNCs were determined to be 5-20 nm in diameter and 150-200 nm in length as provided by the supplier. Dimethylformamide (DMF) was obtained from Sigma-Aldrich Co. and was used as received without further purification. Millipore-processed (Darmstadt, Germany) deionized (DI) water was used with a resistivity of 18.2 MΩ-cm.

3.2.2 Preparation of Epoxy/CNC nanocomposite film

For solvent-assisted dispersion samples. The 3% CNC solution was prepared by dispersing 3g of freeze-dried CNC in 100 ml of DMF/H_2O co-solvent (75-25 volume percent) by a bath sonicator (Crest CP500D, 120W, 42 kHz) for 24 h until a transparent suspension was achieved. The amine hardener was added to the desired amount of CNC solution (0-5 wt.%) and was magnetically stirred for 1-3 h depending on CNC loading. The DGEBA epoxide monomer was preheated at 60 °C for 1 h in a vacuum oven to melt any crystals present and to remove air bubbles.

The liquid nanocomposite mixture was produced by two methods. In the first method, DGBEA was adding into CNC/hardener suspension and magnetically stirred, referred to as bulk mixing. In the second method, both DGEBA and CNC/hardener suspension was added to a new glassware dropwisely while the magnetic bar in stirring, referred to as dropwise mixing. The adding speed was controlled to allow both epoxide monomer and

CNC/hardener suspension to be used up in the same period. The nanocomposite mixture was mixed at 40 °C for 0.5-1 h depending CNC concentration.

The solvent-removal (SR) specimens were prepared by removing most of residual DMF/H_2O in CNC/hardener suspension using a rotary evaporator (Buchi R-200 Rotavapor) at 40 °C for 10-20 mins, prior to DGEBA addition using both mixing methods. The specimens prepared without solvent-removal step are designated as regular (R) specimens.

For direct mixing (D) samples, freeze-dried CNCs were directly dispersed in hardener without solvent, using a probe sonicator (Qsonica Q500) at 25% amplitude and 10s/5s on/off cycles until a good dispersion was achieved. Then, the DGEBA monomer was added to the CNC/hardener mixture with bulk mixing method.

The well-mixed nanocomposite solutions were degassed under vacuum to remove the air bubbles and was cast into a polytetrafluoroethylene (PTFE) mold. The mold was precured in a fume hood at room temperature for 72 h, while the solvent was evaporated. All samples were cured at 80 °C for 2 h, and 125 °C for 3 h. Neat epoxy films were prepared using the same procedure for both bulk and dropwise mixing methods. Neat CNC film was made by solution casting into a polystyrene petri-dish and dried at 60 °C for 24 h.

3.2.3 Polarized light microscopy (POM)

The cured composite samples were observed using an Olympus BX51 microscope to qualitatively analyze the level of CNC dispersion in the matrix by the different processing methods mentioned above. The images were taken with the samples between two crossed polarizers in transition mode using 5X magnification and at full extinction.

3.2.4 Fourier-transform infrared spectroscopy (FTIR-ATR)

Attenuated total reflection (ATR) FTIR analysis was performed on a Nicolet iS50 FTIR (Thermo Scientific) to study the chemical structure of cured films as well as to qualitatively analyze the amount of solvent left in the composite before and after curing by the different processing method. The spectra were collected in the range of 4000-500 cm^{-1} with a resolution of 1 cm^{-1} and a total of 32 scans. It was assumed that the benzene ring in the DGEBA monomer does not participate in the curing reaction, which could be used as an internal standard. Aromatic rings absorb in the 1620-1580 cm^{-1} region with a unique absorption peak at 1608 cm^{-1} [112].

3.2.5 Tensile Testing

Uniaxial tensile testing was performed using an Instron 5842 equipped with a 100 N load cell. Tensile specimens were prepared by die cutting the film into dog-bone samples following ASTM standard D638 Type V with the preset width and gauge length. The thickness of each specimen was measured with a digital micrometer in three different areas. The experiments were conducted at a strain rate of 5mm/min. At least five samples were tested for each type of specimen, and the average values were reported.

3.2.6 Scanning electron microscopy (SEM)

The morphology of broken tensile specimen fracture surfaces was examined with a Phenom G2 Pro Desktop SEM (Phenom-World BV). The samples were sputter coated with gold and imaged at 5 kV.

3.2.7 Differential Scanning calorimetry (DSC)

The glass transition temperature (T_g) for neat epoxy and nanocomposite specimens were conducted on TA Q200 (TA Instruments). 7-10 mg of samples were sealed in standard aluminum pans, and DSC tests were run under a nitrogen atmosphere. Samples were first heat to 150 °C at a rate of 10 °C /min and held for 5 mins to remove thermal history. Then, cooled to -30 °C, and subsequently heated to 200 °C at a rate of 10 °C /min. The value of T_g was calculated from the second heating ramp.

3.2.8 Thermogravimetric analysis (TGA)

Water absorption, thermal stability, and degradation behavior were investigated with thermogravimetric analysis (TGA) with TA Q50 (TA Instruments). Samples were tested under a flowing nitrogen atmosphere with the sample size 5-7 mg. Samples were first heating from room temperature to 120 °C at a rate of 10 °C /min and held for 20 mins to monitor the weight loss due to water uptake. Then, samples were heated to 600 °C at a rate of 10 °C /min. The onset degradation temperature was determined with TA Universal Analysis software.

3.3 Results and discussions

3.3.1 Processing concept for CNC/Epoxy nanocomposite

Mixing methods

Bulk mixing or pot pouring is the conventional, simple, and widely used method to mix the two-component epoxy. In this work, the cellulose nanocrystals were first dispersed in

DMF/water co-solvent. Then CNC solution was mixed with hardeners to create a stable suspension. ED-600 hardener had low viscosity and completely miscible with a wide variety of solvents, which makes them ideal for blending with high viscosity filler solution like CNC. The co-solvent helped to maintain the suspension at low viscosity and prevent potential CNC aggregations. Stoichiometry amount of epoxy monomers were then added into the CNC/co-solvent/hardener suspensions.

Instead of pouring epoxy monomers into the CNC/co-solvent/hardener suspensions. Both components were added dropwisely into a new beaker, as a continuous flow setup; where two pipets carrying the phases converge to mix at the nozzle, followed by intensive mixing in the beaker. By doing simultaneous dropwise mixing, CNC could be further homogeneously distributed and dispersed within the epoxy matrix.

Effect of residual solvent

Residual solvent could influence curing behavior and network structure by plasticizing the epoxy matrices. Coelho *et al.* [59] and Hong *et al.* [60] studied the effect of residual acetone, which caused decreases in T_g and brought detrimental effect on the mechanical properties of the composite [73, 74]. Sun *et al.* [75] stated the positive effect of residual DMF on mechanical properties on neat epoxy and lignin epoxy composite. The residual DMF causes a decrease of crosslinking density and T_g due to the plasticized matrix was confirmed from the dynamic mechanical analysis. However, enhanced mechanical performances were observed, and they suggest that the DMF was decomposed into aliphatic amine during high-temperature curing (240 °C), acting like excess hardeners as well as a terminating agent, increasing the chain packing and improving the Van der Waal's interaction. In order to evaluate the impact of DMF/water on the nanocomposite system. Three nanocomposite

solutions with different amount of residual solvents before curing were prepared. Regular sample (R) without solvent removal have the highest solvent content during final composite mixing. As for solvent-removal (SR) specimens, a majority of the co-solvent was removed from the CNC/co-solvent/hardener suspensions. The amount of solvent removed was controlled by rotary evaporation time and was determined gravimetrically to be ~80, 70 and 60 % for CNC loading of 1, 3 and 5 wt.% respectively. A critical amount of solvent is necessary for a flowable suspension when mixing with the epoxy monomer. Direct mixing (D) sample using no solvent at all, therefore, higher sonication power is required to help CNC to disperse in the hardener. However, sedimentation of CNC was observed and formed a continuous layer at the bottom of the suspension after standing overnight. Although ED600 can be used as a protic solvent that could form hydrogen bonding with CNC and the amine group can be protonated into cationic moieties that can form ionic interaction with the negatively charged sulfate groups. Lack of electrostatic repulsion in an apolar organic solvent significantly reduce suspension stability [30, 31, 113]. Optical, chemical, thermal, and mechanical properties of CNC/epoxy nanocomposites and their corresponding R, SR and D specimens were analyzed below, using both bulk and dropwise mixing procedures.

3.3.2 Optical properties

The epoxy composites with addition of up to 5 wt.% CNC were produced, and all films retained a similar level of transparency to the neat epoxy, indicating good dispersion state of CNC in the matrix. Each film was around 1mm in thickness and looks homogeneous at the macro level. However, the color of the specimen becomes more yellowish as CNC

content increase. To estimate the dispersion level of the CNC at the microscale. Polarized optical microscopy images were collected and illustrated in Figure 3.1. A 530 nm retardation plate was used, giving an otherwise black image a magenta hue background, and birefringent domains due to agglomerated CNC had a yellow-green color. The neat epoxy film showed limited birefringence, and there were isolated regions with birefringence in films prepared by solvent-assisted methods (R and SR). The films prepared by direct mixing showed extensive birefringence at all CNC loading, and the coloration was more prominent at higher CNC loading. This confirmed CNCs were not well dispersed in ED600 hardener matrix even using high sonication power.

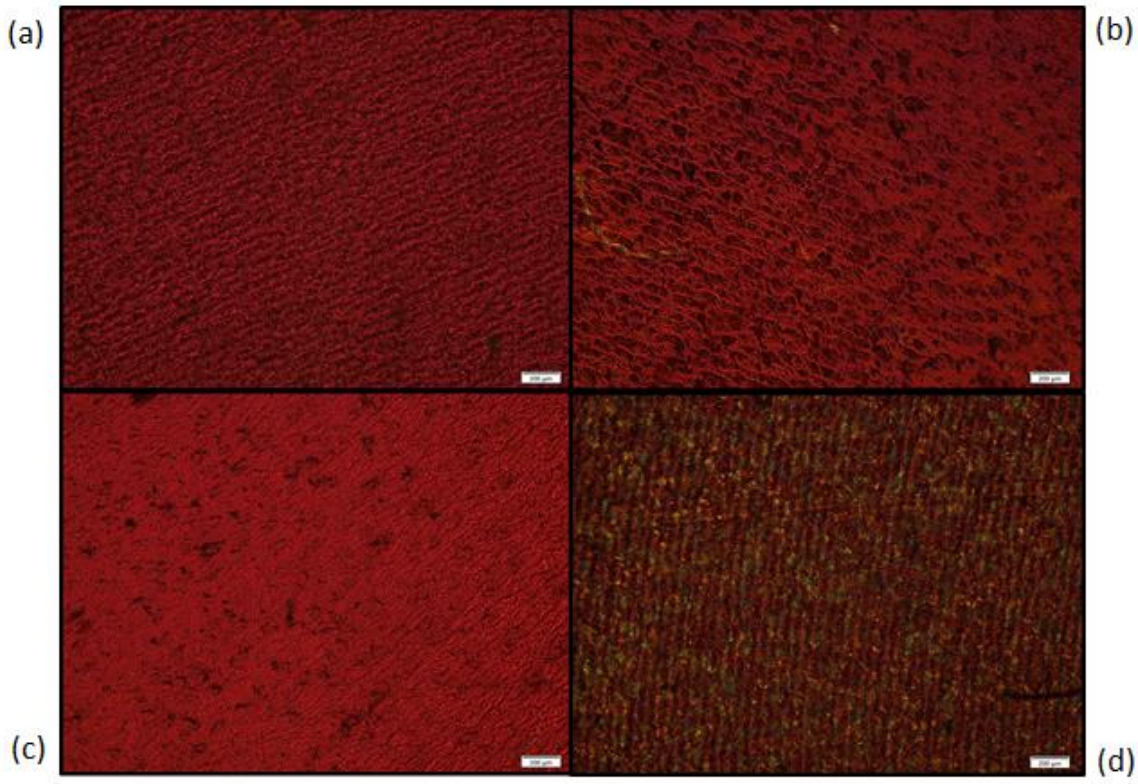

Figure 3.1 Polarized microscopy images of neat epoxy (a) and epoxy nanocomposite with 1CNC prepared by regular (b), solvent removal (c), and direct mixing (d) methods. All samples were bulk mixed. The scale bar is 200 µm.

The fracture surfaces of neat epoxy and CNC/epoxy nanocomposite were also investigated by SEM as shown in Figure 3.2. Due to the low contrast between CNC and epoxy matrix, individual CNC could not be identified. The surface of neat epoxy was very smooth and showed a homogenous fracture surface. The fracture surfaces of CNC/epoxy samples were rougher and showed ripples running across the smooth fracture surface, indicating matrix shear yielding/plastic deformation and shear banding, which led to crack deflection and helped energy dissipation as suggested by previous epoxy studies [114, 115]. A good dispersion of CNC in polymer matrices was observed in all solvent-assisted film regardless of processing method. However, CNC aggregates present in the form of micro-sized flakes were found in direct mixing samples, due to the poor interfacial interaction between hydrophilic CNC and hydrophobic matrix [116].

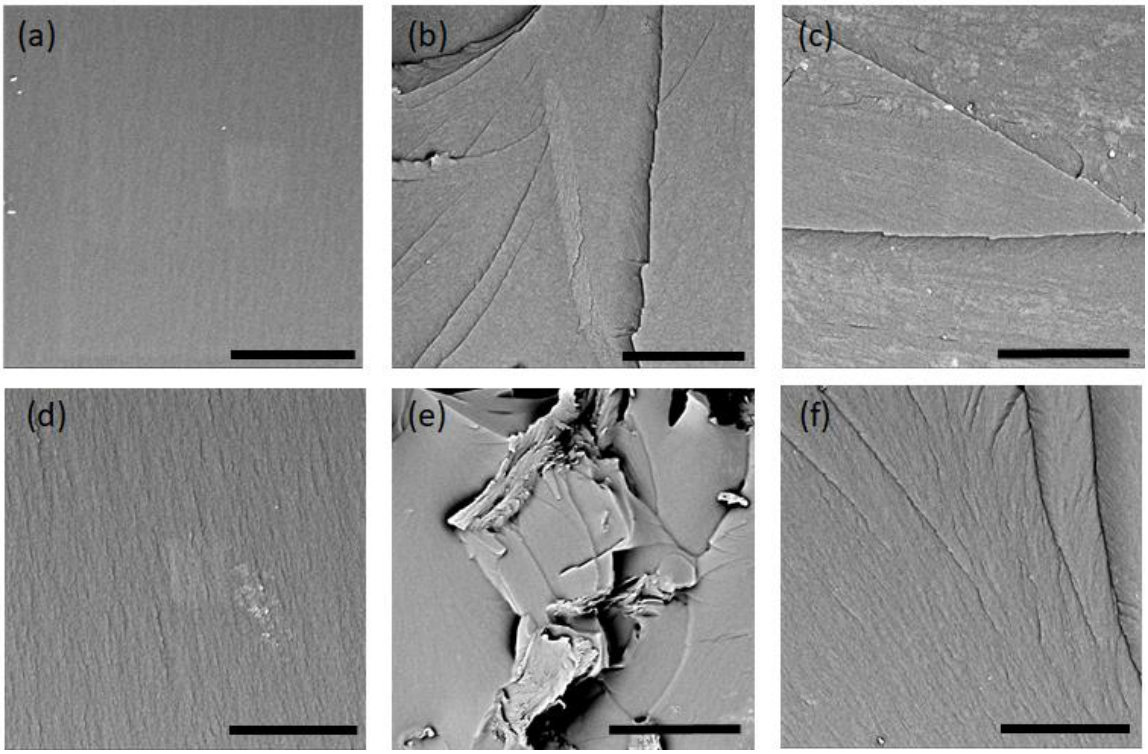

Figure 3.2 SEM images of fracture surfaces of films after tensile testing neat epoxy (a) and epoxy nanocomposites with 1 CNC (b,) 5 CNC (c-f). Where (a-e) were prepared by bulk mixing without (a-c) and with (d) solvent-removal, (e) direct mixing, and (f) dropwise mixing without solvent-removal. Scale bar is 20 µm.

3.3.3 Chemical analysis

To understand the chemical structure of the nanocomposite and to qualitatively analyze the amount of solvent left in the composite before and after curing with different solution processing method, FTIR spectra were measured for nanocomposite solutions and films. From Figure 3.3, the band at 915 cm^{-1} is the characteristic peak of epoxy group, and its disappearance in cured films indicated complete curing. The 1620-1690 cm^{-1} band is a characteristic band of the carbonyl group in DMF, and the peaks at 1600-1620 cm^{-1} belong to the benzene ring in the DGEBA monomer, which does not participate in the curing reaction and can be used as an internal standard to determine DMF content. The extent of

DMF in the system was calculated by the ratio of $H_{C=O}/H_{benzene,}$ which is the intensity of carbonyl and benzene ring respectively. The ratio was 5.55 to 3.62 for the regular and solvent removed composite solution before curing as shown in Figure 3.3b. It confirmed that less DMF was left in the solvent removed samples compared with the regular samples. However, the ratios were identical after curing, meaning most of the DMF was removed during the curing process. CNC has the characteristics peaks at 3600-3200 cm^{-1} due to hydroxyl groups, 2900 cm^{-1} belongs to CH groups, and 1250-1000 cm^{-1} belongs to C-O or C-O-C (ether) groups [19, 23, 55]. All these bands were found in the neat epoxy spectrum. Thus there was no observable interaction between CNC and epoxy from FTIR. However, an increased intensity was observed in the 3600-3200 cm^{-1} region and was shifted to a higher wavenumber with increase CNC addition. This indicates that there is more hydrogen bonding formed between the surface hydroxyls of CNC and epoxy matrix. The reduction in peak intensities of C-O stretching vibration at 1250-1000 cm^{-1} was also due to the formation of hydrogen bonds and was commonly found in PVA/CNC composite [14, 15, 117].

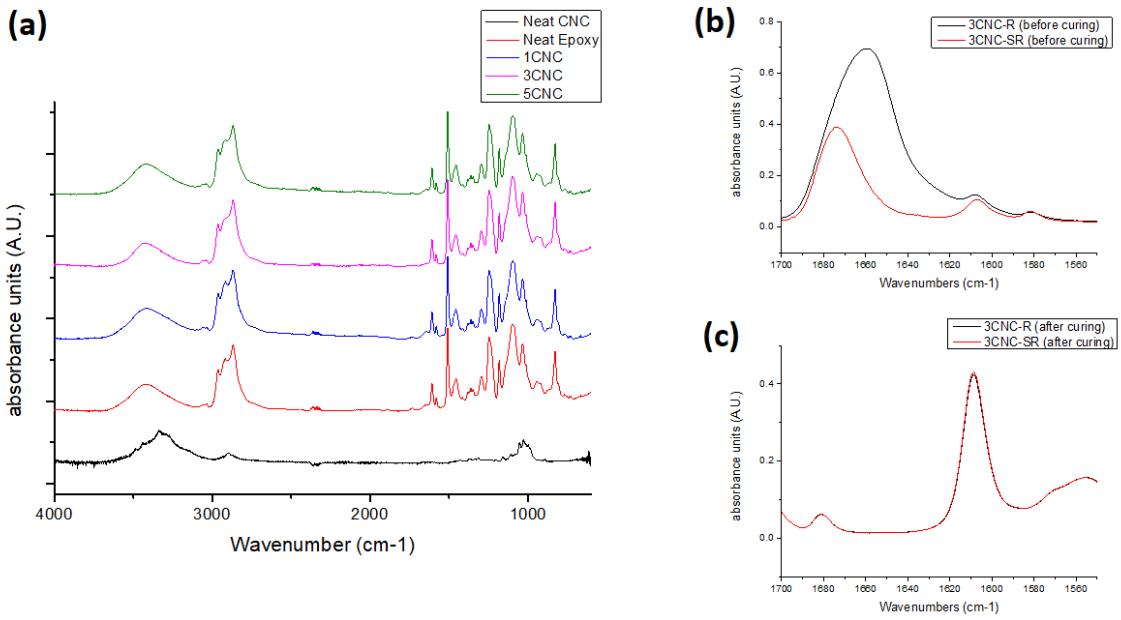

Figure 3.3 (a) ATR-FTIR spectra of films prepared by bulk mixing with increase CNC loading. (b,c) FTIR spectrum to quantify the extent of DMF residual (b) before and (c) after curing.

3.3.4 Mechanical properties

To evaluate the mechanical performance, uniaxial tensile tests were carried out. Neat epoxy and nanocomposite prepared with bulk and dropwise mixing were reported separately. The impact of residual solvent on the nanocomposite system was also analyzed, by controlling the amount of solvent left in the system using regular (R), solvent removal (SR) and direct mixing (D) methods. One thing to notice is that the tensile modulus measured in this thesis is the apparent modulus of elasticity, which is defined as the ratio of stress to strain within the elastic deformation region.

Bulk Mixing

The tensile testing results for all bulk mixing samples were given in Figure 3.4. ED 600 is a bifunctional hardener with long polyether backbone. Therefore, the neat epoxy was a ductile polymer with high failure strain. There was a trend of increase tensile strength and elastic modulus with increase CNC loading for solvent-assisted samples, with higher improvement found in the solvent removal samples. For direct mixing specimens, there was no significant improvement in tensile strength, but a positive trend of modulus was observed at CNC loading higher than 1 wt.%. Also, a trend of decreasing failure strain and work of fracture was found with direct mixing samples, which was associated with the breaking of agglomerated CNC flakes, as supported in SEM and POM results. Solvents must be introduced to achieve a good dispersion of un-modified CNCs in the hydrophobic epoxy matrix. To determine the influence of residual solvent, 5CNC-R and SR specimens were assessed. When 5wt.% of CNC was incorporated with the assistance of solvent removal, they have the better increment in tensile strength, failure strain and work of fracture than that of regular sample (89.6%, 25.2% and 171% vs 63.1%, -6.2% and 36.9%

respectively), in comparison with neat epoxy. One possible explanation for this difference is that the higher dosage of solvent would lower the viscosity of the composite mixture. Therefore, CNCs in low viscosity mixture may have time to condense at the bottom of the solution or even cause reaggolmeration [118]. Another explanation is due to the plasticizing effect of DMF or water at curing stages, which lower the crosslink density and change the network structure. Meanwhile, Hong *et al.* reported that the absorption of heat by residual solvent could change the curing behavior, and affect the mechanical properties of the resultant epoxy composite [119].

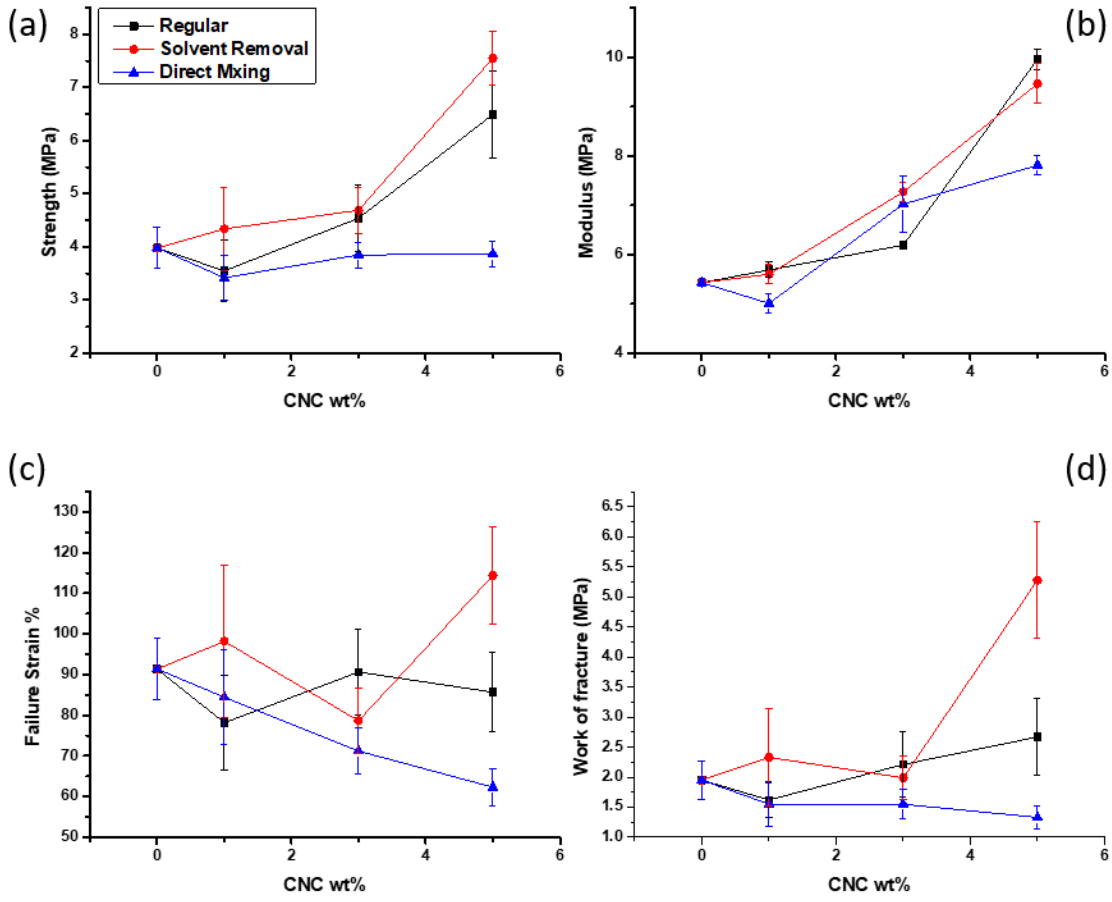

Figure 3.4 Mechanical properties of CNC/epoxy nanocomposite prepared by bulk mixing: (a) tensile strength, (b) tensile modulus, (c) failure strain, and (d) work of fracture.

Dropwise Mixing

The tensile testing results for all dropwise mixing samples were given in Figure 3.5. The purpose of dropwise mixing was to increase the level of dispersion and distribution of both CNC and hardeners in the epoxy matrix. The tensile properties of neat epoxy prepared by dropwise mixing were similar to that of the neat epoxy prepared by bulk mixing. The composites prepared by solvent removal method shows a significant improvement in mechanical properties when 1 wt.% sample compared with neat epoxy. However, further increase of CNC loading showed the elastic modulus had reached a plateau, while the tensile strength, failure strain and work of fracture showed a statistically significant decrease. This could attribute to the high viscosity of the solvent-removed CNC/hardener mixture, which hindered the well dispersed CNC solution to be homogeneously distributed into the epoxy matrix, and subsequently led to an inhomogeneous reaction of ED600 with the epoxy resin. The mechanical properties of regular samples showed a progressive increase from 1 to 5 wt.% CNC loading. Introduction of 5wt.% of CNC into epoxy matrix led to a 2.5, 2.3 and 3 folds enhancement of tensile strength, modulus, and work of fracture of the nanocomposites respectively, in comparison with neat epoxy.

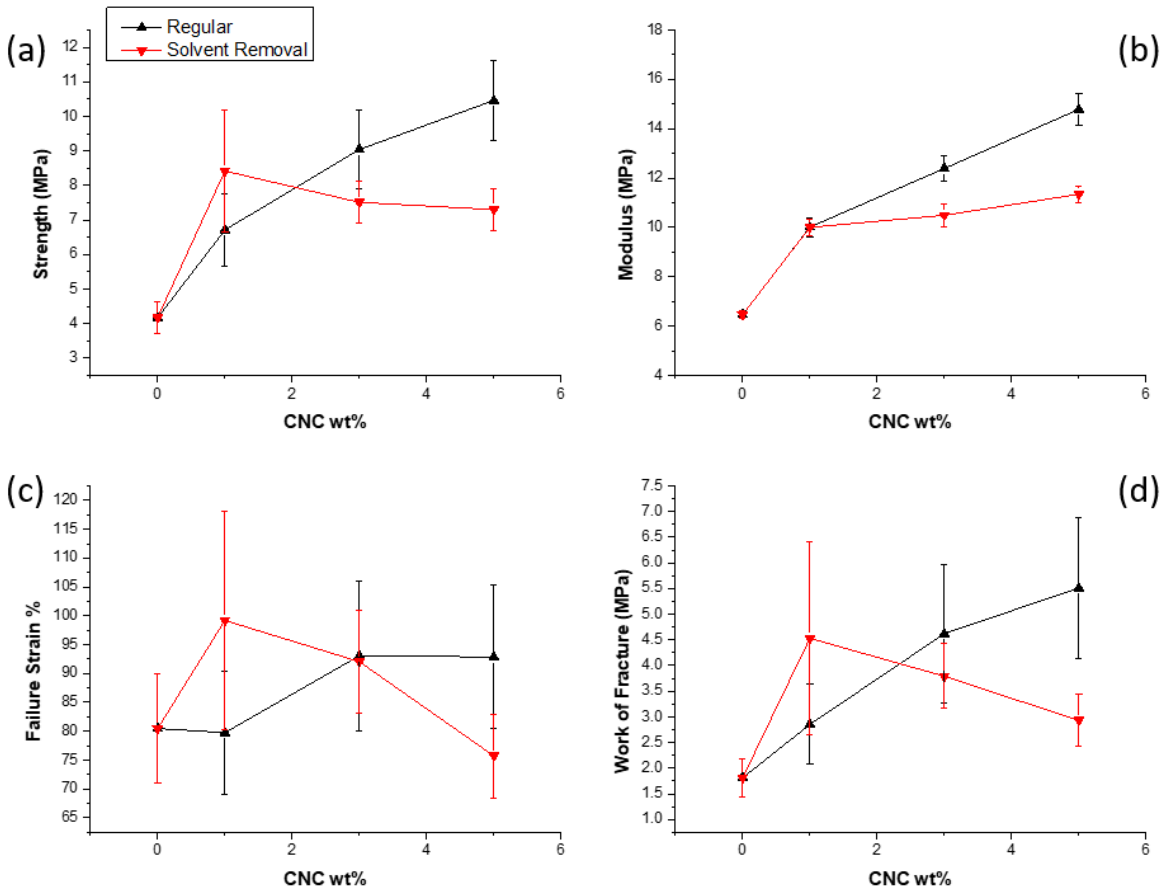

Figure 3.5 Mechanical properties of CNC/epoxy nanocomposite prepared by dropwise mixing: (a) tensile strength, (b) tensile modulus, (c) failure strain, and (d) work of fracture.

The effect of processing was much more evident when comparing the tensile strength and modulus data of the regular specimens prepared by both mixing methods. As shown in Figure 3.6, neat epoxy made by both mixing methods has similar values for the tensile strength and slightly higher modulus with the dropwise mixing. These suggest that the processing methods were not found to affect the properties of neat epoxy. The considerable difference observed in composite samples could be mainly resulted from a different level of CNC dispersion and CNC/hardener distribution in the epoxy matrix. As mentioned before, there were two effects upon the introduction of solvents. First was lower the

viscosity of the composite solution to allow better mixing. The other is related to the plasticizing effect of the solvent which generally led to a decrease in crosslinking density. In this experiment, the significant improvement in mechanical properties of solvent-assisted nanocomposite samples suggested that the CNC reversed the plasticizing effect through its superior mechanical reinforcing efforts, and dropwise mixing process led to the better dispersion compared with the bulk mixing process. The high aspect ratio CNCs could form a percolation network and acts as a stress transferring component in polymer matrices. It is worth noticing that the ED 600 hardener used in this study has a relatively long hydrophilic backbone, and the epoxy composite cured with it already have a flexible network with low crosslink density. Therefore, the detrimental effect of residual solvent may be trivial, meaning the filler effect is more significant than the solvent effect in this case.

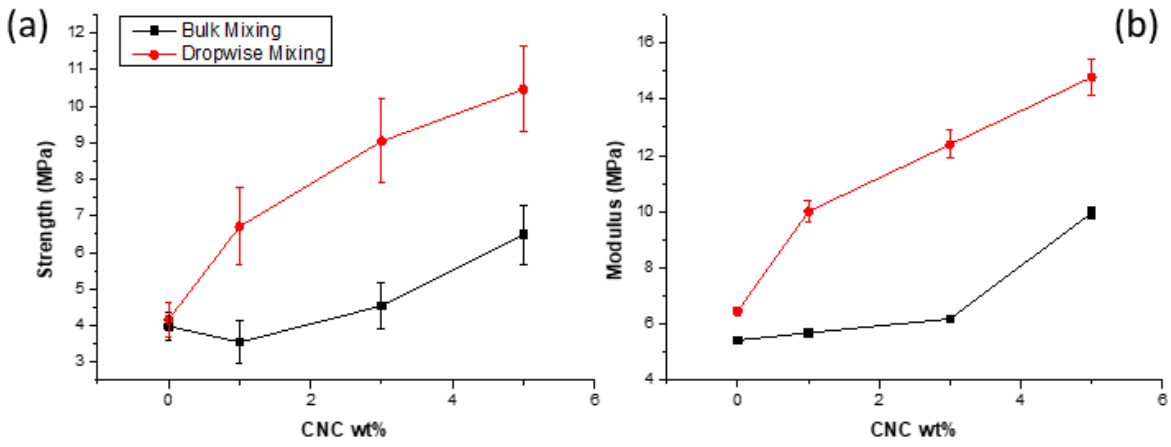

Figure 3.6 (a) Tensile strength and (b) Modulus for CNC/Epoxy nanocomposites made by bulk and dropwise mixing

3.3.5 Thermal properties

DSC was used to determine the solvent effect on the values of glass transition temperature (T_g) of the nanocomposite films prepared by bulk mixing protocol, and the results were shown in Table 3.1. As expected, the solvent left in the regular samples caused the decrease of T_g as CNC loading increase (higher solvent dosage). This was due to the plasticizing effect of DMF or water at curing stages, which lower the crosslink density and change the network structure. Samples prepared by solvent removal or direct mixing methods showed the CNC content did not significantly affect the T_g of the composite samples. Meanwhile, SR and D samples prepared at higher CNC concentration (5 wt.%) led to slightly higher T_g compared with the T_g of neat epoxy. The increase may be the result of CNC interactions with the matrix, and the rigid CNC formed a percolation network, which restricts the mobility of the polymer chains.

Table 3.1 Glass transition temperature (°C) values with varied CNC loading and residual solvent content

Sample ID	Regular	Solvent Removal	Direct Mixing
Neat Epoxy	13.9±0.8		
1 CNC	13.1±1.1	14.5±0.2	11.1±0.5
3 CNC	12.4±0.6	13.3±0.5	14.0±0.4
5 CNC	5.5±2.1	14.7±1.5	14.4±1.0

Table 3.2 compares the T_g of composite films made from two different processing method. For neat epoxy, the film prepared by dropwise mixing showed a slightly higher Tg than that of the film prepared by bulk mixing. This shift of T_g to higher temperature could be attributed to higher homogeneity of hardener in the monomer matrix when using dropwise mixing technique, thus increasing crosslink density of the cured film. Increase in T_g was found for both regular and solvent removal sample with 5 wt.% CNC content prepared by

dropwise mixing, which suggested that the rigid percolation network effectively suppressed the movement of the polymer chain, and the filler effect outperformed the plasticizing effect caused by the residual solvent.

Table 3.2 Glass transition temperature (°C) with different processing method

Sample ID	Bulk Mixing		Dropwise Mixing	
	Regular	Solvent Removal	Regular	Solvent Removal
Neat Epoxy	13.9±0.8		14.7±0.6	
5CNC	5.5±2.1	14.7±1.5	15.0±2.0	14.9±0.3

Thermal stability and water adsorption on the composites were conducted using TGA, and the results were shown in Figure 3.7. The TGA curves were similar for neat epoxy and composites, with a single weight-loss event around 400 °C. Neat CNC film had much lower thermal stability compared with neat epoxy film and decomposed around 230 °C. This suggests that CNC decomposes at a much higher temperature in the epoxy matrix, which was attributed to the good interfacial interaction between the CNCs and the matrix. Although the onset temperature and temperature at maximum decomposition rate was reduced with increasing CNC concentration, given in

Table 3.3. It was found that the onset temperature for the composite following rule of mixtures.

Table **3.3** also showed that the amount of water absorbed by the films did not change much with CNC loading, and 3 CNC and 5 CNC-D even show a lower water content than neat epoxy film. Due to the hydrophilic nature, the neat CNC film had a higher water uptake. Nanocomposite films cured with different residual solvent content was not found to affect the water absorption and thermal degradation behavior.

Table 3.3 Water content, onset temperature, and temperature at maximum thermogravimetric decomposition peak for TGA data

	Neat Epoxy	1 CNC	3 CNC	5 CNC	5CNC-SR	5CNC-D	Neat CNC
Water content (%)	1.9	2.0	1.8	2.3	2.1	1.5	6.4
T_{onset} (°C)	371	370	368	365	368	367	235
T_{max} (°C)	386	386	385	384	384	386	244

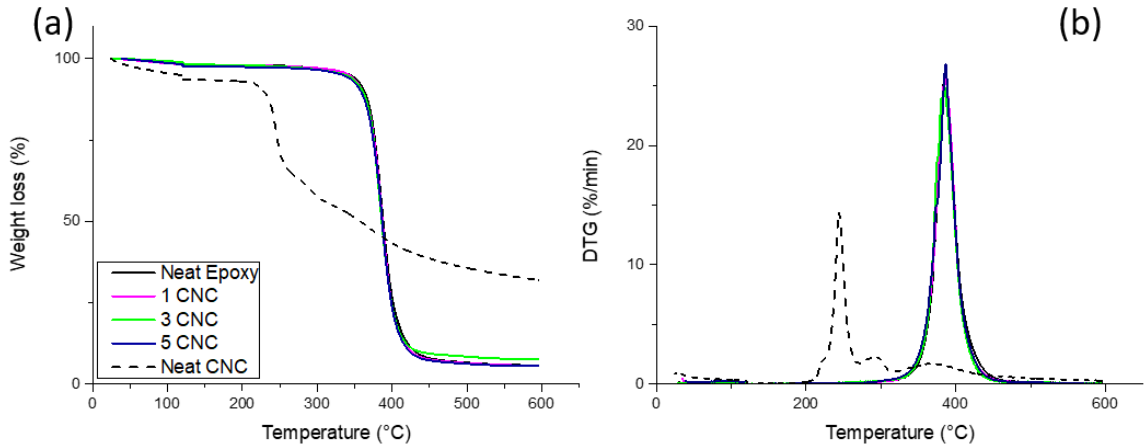

Figure 3.7 (a) Thermogravimetric and (b) differential thermogravimetric curves for neat epoxy, neat CNC and composites films

Table 3.3 showed that the similar water content (2-2.6%) was found in all pure epoxy and nanocomposite with 5 wt.% CNC, regardless of processing method. Interestingly, unlike the thermal depression on T_{onset} and T_{max} observed in bulk mixed 5CNC and 5CNC-SR samples. A slight increase in thermal transition temperatures was found in both regular and solvent removal samples when 5wt.% CNC films were prepared using dropwise mixing method. This could be attributed to the good interactions between CNCs and the matrix when using this processing technique, such that the nanocomposites are more thermally stable than pure epoxy. This increase in thermal stability was not commonly found when using epoxy as the polymer matrix, considering the epoxy decompose at a much higher temperature than the CNCs (370°C vs 235°C).

Table 3.4 TGA data with different processing methods

	Bulk Mixing			Dropwise Mixing		
	Neat Epoxy	5CNC	5CNC-SR	Neat Epoxy	5CNC	5CNC-SR
Water content (%)	1.9	2.3	2.1	2.1	2.4	2.6
T_{onset} (°C)	371	365	368	370	370	372
T_{max} (°C)	386	384	384	387	389	389

3.4 Conclusion

In this chapter, two processing strategies to prepare CNC/epoxy composites were compared. Improved distribution of CNC/hardener premix in epoxy precursor was achieved by a dropwise mixing protocol, which the CNC/hardener mixture and epoxy monomers were mixed dropwisely in a glass reactor. Tensile results revealed that better improvement of the mechanical properties of the composites was achieved when samples prepared by the dropwise mixing process. This suggests that CNCs and hardener could be more homogeneously distributed and dispersed within the epoxy matrix. The solvent effect had also been studied to compare two solvent assisted composites (R and SR) and direct mixing (D) of CNC into hardener without solvent. Our original hypothesis was that the hydrophilic amine hardener could be used as a protic solvent for CNC was found to be invalid as CNC aggregates present in the form of micro-sized flakes, observed in POM and SEM results. The regular sample without solvent removal showed a greater extent of residual DMF in FTIR when compared with solvent removal sample before curing. However, there was no difference after the samples were cured. The depression of T_g in bulk mixed regular samples was found as the CNC loading increases, which was due to the plasticization effect of water or DMF, lower the crosslink density. However, residual solvents assisted the dispersion of hardener and CNC in the epoxy resin by decreasing the

viscosity. The regular sample prepared by dropwise mixing showed the highest reinforcement effect with a 2.5, 2.3 and 3 folds enhancement of tensile strength, modulus, and work of fracture, respectively, at a 5 wt.% CNC addition compared with neat epoxy. Overall, it was found that the filler effect was more significant than the solvent effect in this hardener system.

Chapter 4. COMPATIBILITY OF CNC WITH DIFFERENT CROSSLINKER SYSTEM

4.1 Introduction and Objective

As mentioned in Chapter 1, epoxy is one of the most commercially used thermosetting resin with various applications in the fields of construction, automobile, aerospace, and many other high-performance applications. The numerous end applications for epoxy is attributed to its complex formulation, especially with a wide variety of chemical curing agents with amine, anhydrides, and thiols active groups. Due to the limited thermal stability of cellulose nanocrystals, prior studies mainly used amine functionalized crosslinker with either aromatic or aliphatic backbones [20-24, 26, 55, 60]. The results of these studies showed that addition of nanocellulose fillers to epoxy enhanced the mechanical properties of polymers when the percolation threshold was reached. The dynamic mechanical analysis also showed enhancement of the storage module in both glass and rubbery region. Improvement in the dynamic module could be attributed to the synergism effect of homogeneous dispersion and reinforcing effect of nanocellulose materials. Nanocellulose with high stiffness could effectively transfer load through the physical interaction, which forms a hydrogen bonding network between surface hydroxyl groups of NCs filler and polar groups of the epoxy matrix. The percolated NCs network may also constrain the movement of epoxy polymeric chains and led to an increase in glass transition temperature.

Understand the solvent effect on cure kinetic and resulting epoxy properties is very important, especially when solvent must be introduced to assist the additional fillers [73, 75, 120, 121]. From our previous study, it was shown that DMF/water may affect the

mixing mechanism of CNC into the epoxy matrix and alter the degree of crosslinking. The comparison of the solvent effect of DMF/water on the dispersion level and mechanical properties of CNC filled epoxy composites were reported. The previous result showed that the CNC reinforcing effects outperformed the plasticizing effect caused by the residual solvent. It was suggested that the amplitude of the depression in mechanical properties with residual solvents depends on the initial crosslinking densities of epoxy studied. Since the crosslinked network of cured epoxies is dependent on the hardener selected, it is important to differentiate the CNC reinforcing mechanisms from the different epoxy/hardener systems as well as the solvent effects. Only one study has been conducted to evaluate the compatibility of CNCs with different hardener systems with different functionality and backbone structure (aliphatic vs aromatic) [20]. To date, there are no reports that have compared the composites formed from CNC reinforced epoxy with different hardener backbone chemistry.

From my previous work, an optimized dispersion method for cellulose nanocrystal in epoxy resins was identified, involving adding the CNC/hardener and epoxy monomer together and dropwisely during final mixing. The dropwise mixing process alters the distribution state of CNCs within the epoxy matrix significantly. The aim of this work was to evaluate the CNC reinforcing effect in epoxy systems with different crosslinking densities. Using aliphatic diamine curing agents with different polyether backbone length. In addition, the compatibility of CNC and hardeners with similar viscosity but different hygroscopic properties were evaluated. The mechanical and thermal properties were analyzed and compared with the CNC/epoxy samples in Chapter 3 using the same sample preparation method.

4.2 Experimental

4.2.1 Materials

The resin used in this work was an epoxy resin (DER-332, supplied by Dow Chemical) cured with amine-terminated poly(propylene glycol)s (Jeffamine D230, supplied by Huntsman). The Jeffamine D230 was used at the stoichiometric mixing ration of 33.2 parts per hundred parts of resin (phr). Other materials used in this work are identical to those used in Chapter 2. Specifically, freeze-dried CNC was purchased from the University of Maine, produced by the U.S.D.A Forest Products Laboratory. Dimethylformamide (DMF) was obtained from Sigma-Aldrich Co. and was used as received without further purification. Millipore-processed (Darmstadt, Germany) deionized (DI) water was used with a resistivity of 18.2 MΩ-cm.

4.2.2 Sample Preparation

All of the composite samples are prepared with solvent assisted dispersion. The 3% CNC solution was prepared by dispersing 3g of freeze-dried CNC in 100 ml of DMF/H2O co-solvent (75-25 volume percent) by a bath sonicator (Crest CP500D, 120W, 42 kHz) for 24 h until a transparent suspension was achieved. Then, the amine hardener and CNC solution were combined and magnetically stirred for 1-3 h depending on CNC loading. Finally, a stoichiometric amount of epoxy monomer and CNC/hardener suspensions was added to a new glassware dropwisely, and mixing was carried out at 40 °C for 0.5-1 h depending CNC concentration. The sample prepared are named as xCNC-R where x indicates the weight percentage of CNC content and R means regular sample.

The solvent-removal (xCNC-SR) specimens were prepared by removing most of residual DMF/H2O in CNC/hardener suspension using a rotary evaporator (Buchi R-200 Rotavapor) at 40 °C for 10-20 mins, prior to DGEBA addition.

The nanocomposite mixtures were degassed under vacuum and were cast into a polytetrafluoroethylene (PTFE) mold. The mold was placed in a convection oven and cured at 80 °C for 2 h, and 125 °C for 3 h. The same method is used to fabricate pure epoxy films without any fillers. All samples are kept in a sealed desiccator until experiments were performed.

4.2.3 Polarized light microscopy (POM)

The level of CNC dispersion in the polymer matrix was investigated using an optical microscope (Olympus BX51) equipped with two polarizers (Olympus U-AN360P) in a transition mode at full extinction.

4.2.4 Fourier-transform infrared spectroscopy (FTIR-ATR)

To study the cure kinetic, residual solvent content and chemical structure of the cured film, FTIR analysis was performed on a Nicolet iS50 FTIR (Thermo Scientific) with an attenuated total reflection (ATR) module. The spectra were recorded in the range of 4000-500 $cm^{-}1$ using 32 scans at a resolution of 1 cm^{-1}.

4.2.5 Tensile Testing

The tensile properties were measured on Instron 5842 equipped with a 100 N load cell. Dog bone samples were prepared by die cutting following ASTM standard D638 Type V.

samples were tested in tensile mode at a strain rate of 5mm/min. The values reported here are averaged over a minimum of five samples.

4.2.6 Scanning electron microscopy (SEM)

The fracture surface tensile specimens were imaged with Phenom G2 Pro Desktop SEM (Phenom-World BV) at 10 kV, after a thin layer of gold was sputter-coated on the sample.

4.2.7 Dynamic Mechanical Analysis (DMA)

DMA was executed to determine the storage modulus of CNC/epoxy nanocomposites as a function of temperature. Samples were cut with a razor blade into rectangular strips with 15-20 mm long and 3 mm wide. DMA test was performed using DMA Q800 (TA Instruments), operating in a tension mode in the linear viscoelastic regime for the materials at an oscillation frequency of 1 Hz under strain amplitude of 0.05%. the temperature was ramped from 30 to 150 ºC at a heating rate of 3 ºC/min.

4.2.8 Differential Scanning calorimetry (DSC)

Differential scanning calorimetry (DSC) was carried out by DSC Q200 (TA Instruments) with aluminum sample pan under a nitrogen atmosphere. Samples were first heated from 30 to 250 ºC, then cooled back to 30 ºC, and finally heated to 250 ºC at 10 ºC/min. Data from the second heating step were used to obtain the T_g of samples.

4.2.9 Thermogravimetric analysis (TGA)

The thermal stability of CNC/epoxy nanocomposites was assessed with TGA with TA Q50 (TA Instruments), under nitrogen atmosphere. The weight of the samples varied

from 5-7 mg and scanned from room temperature to 600 °C, and the heating rate was 10 °C/min.

4.3 Result and Discussion

4.3.1 Nanocomposite Morphology and Chemical Structure

It was interesting to analyze the CNC reinforced composite samples prepared with D230 hardener compared with previous studies using ED600 hardener. The representative structures of both diamine hardeners are listed in Figure 4.1.

Name	Chemical composition	Approx. molecular weight
D230	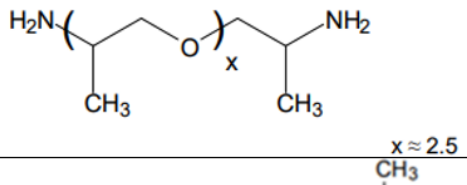	230
ED600	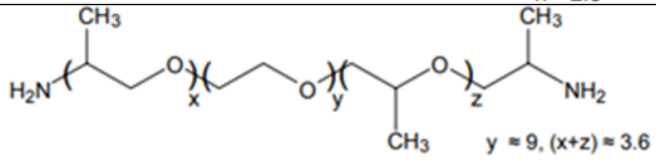	600

Figure 4.1 Chemical structure and molecular weight of hardeners used in this research

Composites with up to 5 wt.% CNC were produced and for all the samples with or without solvent removal steps, the films retained a similar level of transparency and color to the pure epoxy. This indicates a good dispersion of CNC in the epoxy matrix. One thing interesting to mention is that when preparing the final composite blend by mixing CNC/hardener suspension and epoxy monomer, the composite blend with for 5 wt.% CNC content becomes cloudy initially, but then turns back to a clear solution after extensive

mixing. This observation was found in both R and SR samples and was mainly attributed to the higher water dosage in the CNC/hardener mixture. However, such effect was not observed in the previous study.

The discrepancy of these two studies could be due to the difference in their hardeners' backbone structure. ED600 had a triblock copolymer backbone composed of a central hydrophilic chain of PEO flanked by two hydrophobic chains of PPO. The predominantly PEO backbone that imparts complete water solubility and is miscible with DGEBA. It was found that the surface free energies of epoxy blend increased upon addition of amphiphilic block copolymer (PEO-b-PPO-b-PEO), thus increasing the hydrophilicity of the blends [122-124]. Moreover, the large PEO blocks could anchor the PPO domains, ensures maximum interface exposure between epoxy and PEO blocks. D230 hardener, however, has only hydrophobic PPO block in its backbone. Therefore, the emulsion observed was due to the fact that the epoxy monomer and PPO block formed a separated microphase at relatively higher water dosage. After extensive mixing, DMF could be rearranged to tailor the water and epoxy interfaces, and the blend could undergo microphase separation on a nanoscale, making the particle so small that light does not scatter, thus solution becomes transparent.

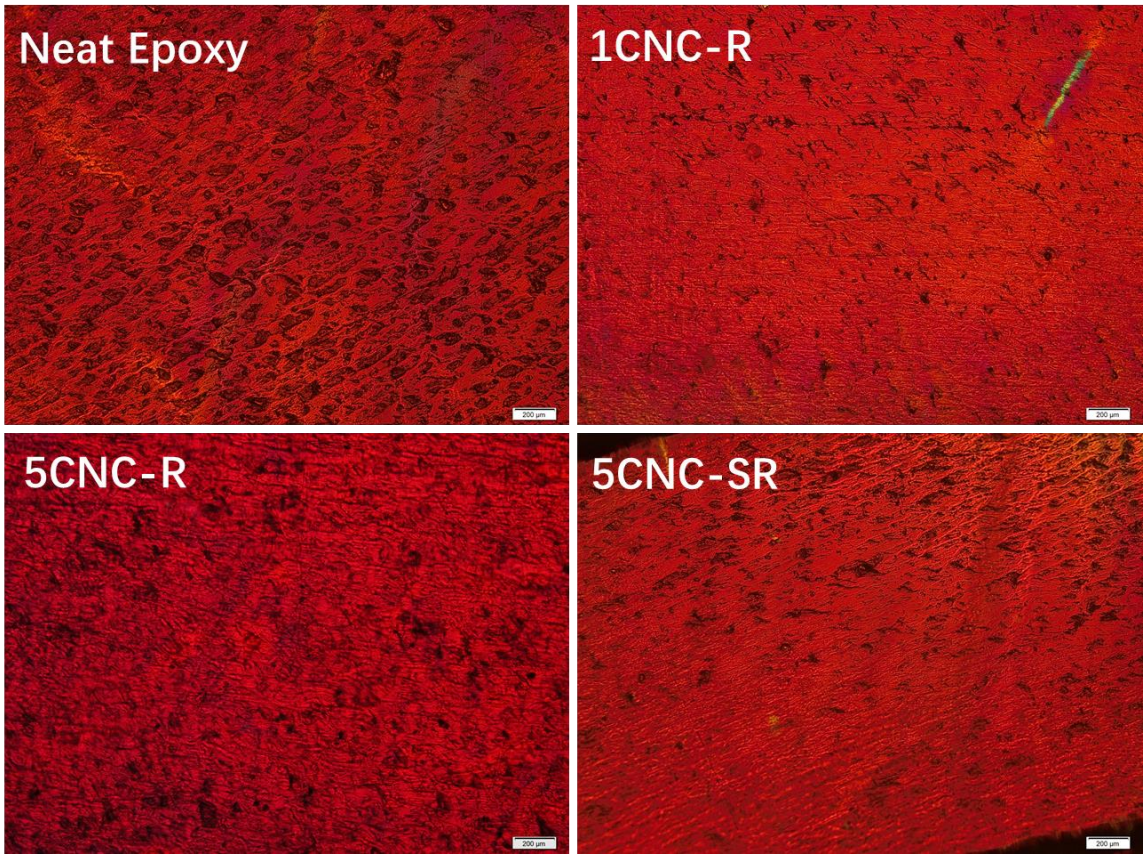

Figure 4.2 Polarized light microscopy images of CNC/epoxy nanocomposite cured with D230. Scale bar is 200µm

Although the addition of nanocellulose did not change the transparency of the film, and all films look homogenous at the macroscale. The dispersion state of CNCs within the cured epoxy was evaluated using an optical microscope under polarized light and was shown in Figure 2. Both neat epoxy and nanocomposite samples showed a similar level of a red background due to the retardation plate inserted, and there were inconspicuous birefringence regions noticed. Therefore, it was suggested that the CNC/Epoxy composite films had a low degree of microscale CNC agglomeration. To confirm that, fracture surfaces of tensile samples were investigated with SEM, and results are given in Figure 4.3.

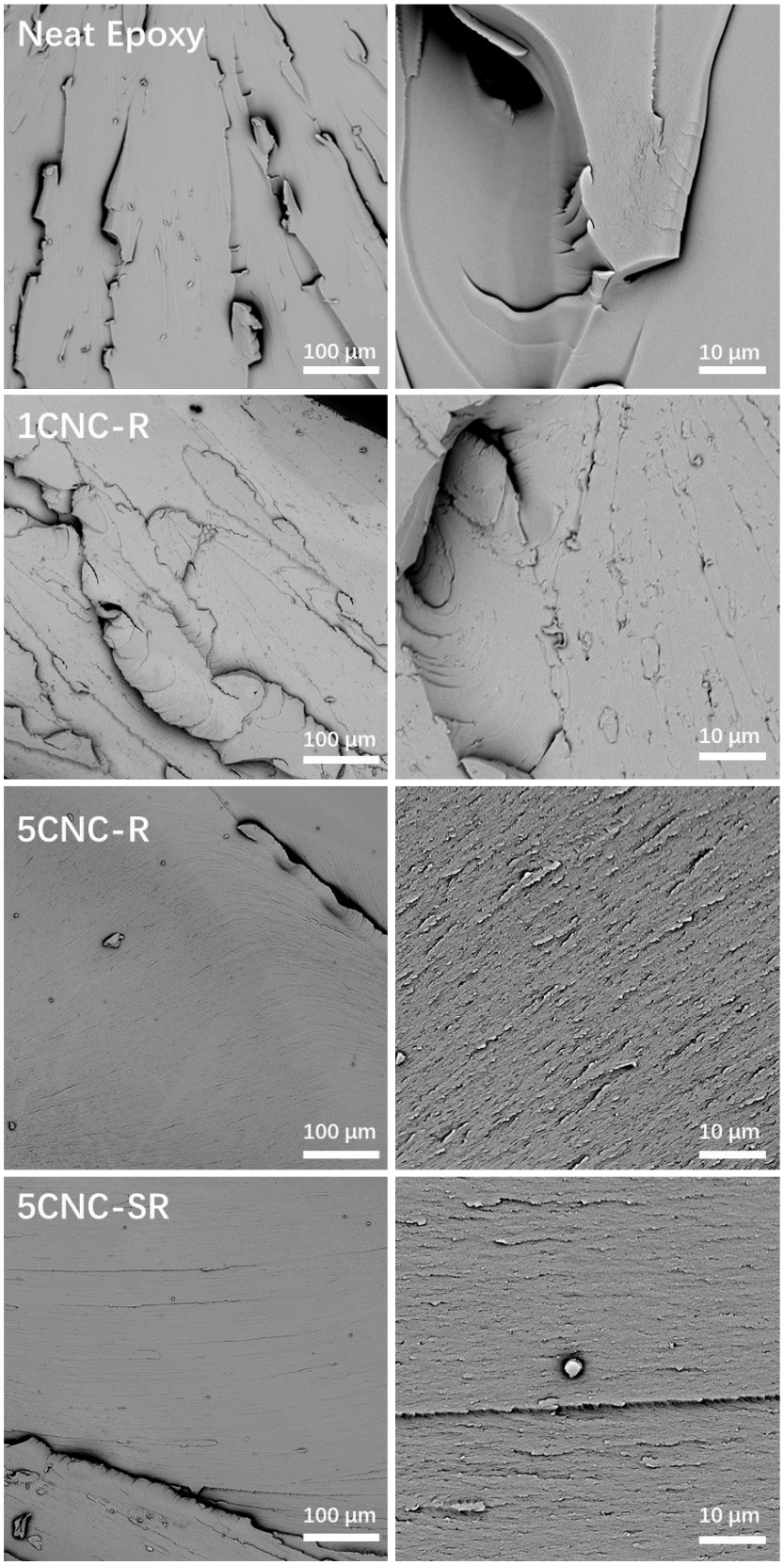

Figure 4.3 SEM images of the fracture surfaces of films after tensile testing

The SEM imaging indicates that neat epoxy had a very smooth and homogeneous fracture surface, which represented a brittle failure with limited crack growth resistance. With 1 wt.% CNC loaded, the specimen had a similar pattern as neat epoxy at low magnification. The interface of the composite appeared rougher and have many thorn-like cracks and void on the surface when viewed at higher magnification, indicating a tougher fracture with possible crack deflection, fiber/matrix debonding, matrix shear yielding/crazing and micro-void formation that helps to dissipate stress and to interrupt the crack propagation through the matrix. However, at higher CNC loading, the rougher fracture surface of the 5 CNC-R and 5CNC-SR show more ductile deformation. We hypothesized that the solvent required to disperse a large amount of CNC in epoxy matrix plasticized the epoxy matrix and led to this significant morphology change, and even the solvent removal step could not alleviate this problem. These energy-absorbing plastic deformations were confirmed with the results tensile test. In addition, no visible CNC aggregation was observed for all nanocomposite sample, which reflects good dispersion of the nanocrystals in the epoxy matrix.

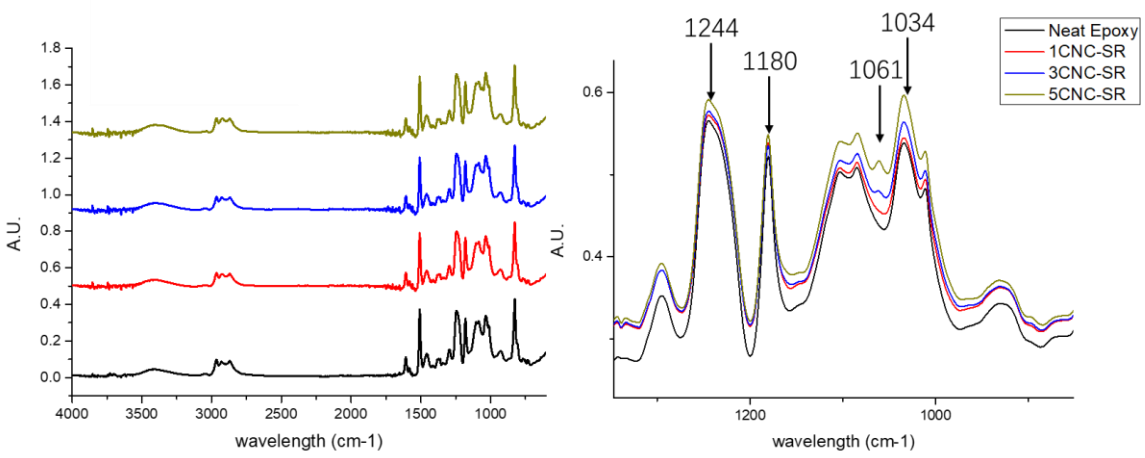

Figure 4.4 ATR-FTIR spectra of cured films with different CNC content

The representative FT-IR spectra of cured neat epoxy and composite with different percentages of CNC were shown in Figure 4.4. The 915 cm^{-1} bands associated with unreacted epoxide group disappeared, indicated that all epoxy groups were consumed, and all samples were fully cured. Also, the characteristic band of the carbonyl group from DMF around 1680 cm^{-1} was not shown in all cured sample. Thus, there was no trace of DMF left in the nanocomposite. Increase in intensities were observed in a few peaks 1244, 1180, 1084 and 1034 cm^{-1} with increase CNC loading. These bands are associated with C-O or C-O-C stretching. A new peak appeared at 1061 cm^{-1}, which was related to the sulfonic acid group that could be presented in acid-hydrolyzed CNC and the intensity of this band gradually increase with CNC loading.

4.3.2 Mechanical Property of Nanocomposites

D230 is also a diamine hardener as ED600 that are commonly used in the epoxy formulation. D230 has shorter backbone length with higher amine content than ED600 and such it could from higher crosslinking density networks than ED600 as well as potentially more intense hydrogen bonding network with CNCs.

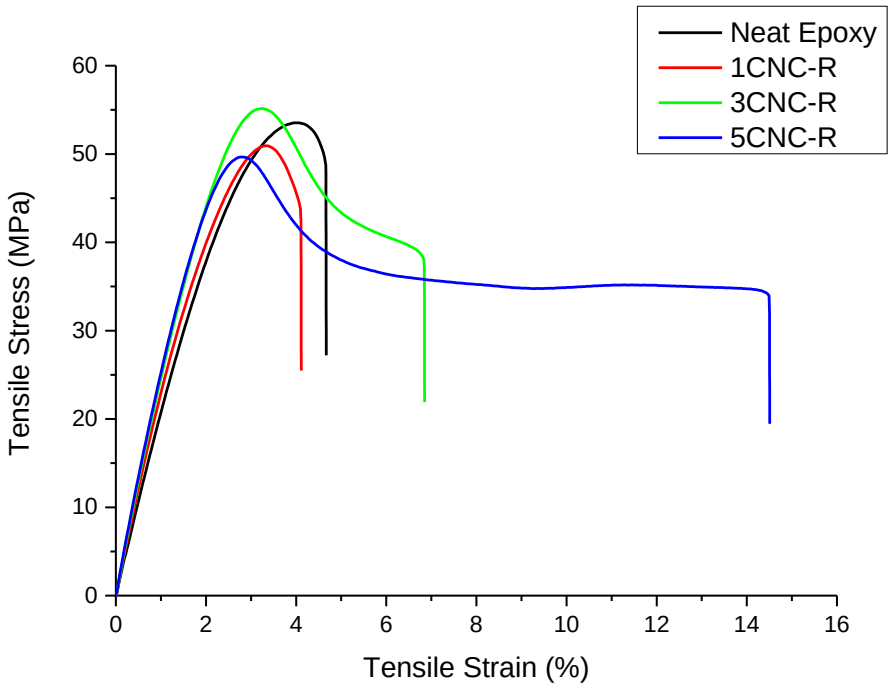

Figure 4.5 Representative stress-strain curve in uniaxial tension of Epoxy-CNC composite obtained from the regular sample with different nanofiller content

The stress-strain curves from tensile tests were presented in Figure 4.5. The mechanical properties of CNC/epoxy nanocomposite cured with D230 were evaluated using a uniaxial tensile test and the results were shown in Figure 4.6. For Young's modulus, a considerable enhancement was found in both regular and solvent removal nanocomposites samples whose filler was up to 3 wt.%. This could be due to the formation of a rigid CNC percolation network within the epoxy matrix that provides the stiffening effect on the nanocomposite. However, for solvent removal samples, a further increase in nanocellulose concentration led to a decrease in tensile modulus. The change in tensile performance could be due to the aggregation of CNCs, but no evidence was found on its fracture surface in Figure 4.3. The tensile strength, strain at failure and work of fracture for D230 cured specimens showed similar trends. There were no significant differences between neat epoxy and nanocomposite specimens with up to 3 wt.% CNC loaded. At 5 wt.% CNC, a

significant drop in tensile strength and a notable increase in strain at failure and work of fracture were found in both R and SR specimens. The magnitude of change in these tensile properties was more prominent in SR samples. This could be a result of the presence of residual solvent (DMF and water) before curing stages. As mentioned in Chapter 2, introducing the co-solvent to make CNC/epoxy composite was crucial, which the co-solvent helped to lower the solution viscosity and to form a homogenized and well dispersed CNC filler in the composite mixture. However, it was known that even a small amount of solvent left in the epoxy mixture during the course of curing would significantly influence the rate of epoxide conversion, leading to different curing state of the final product [120]. From the strain-stress curve, a clean brittle to ductile transition was found with increase CNC loading, with 5CNC-R sample shows a pronounced necking behavior. These indicated a dramatic change of the epoxy network when cured with residual solvent, and was commonly seen in most solvent casted epoxy composite [20, 75]. Also, the larger standard deviation in strength and modulus of SR samples were observed compared to Regular Samples, which indicates a diverse sample profile across all SR samples that link to the less homogeneous CNC-hardener-epoxy mixing due to its high viscosity.

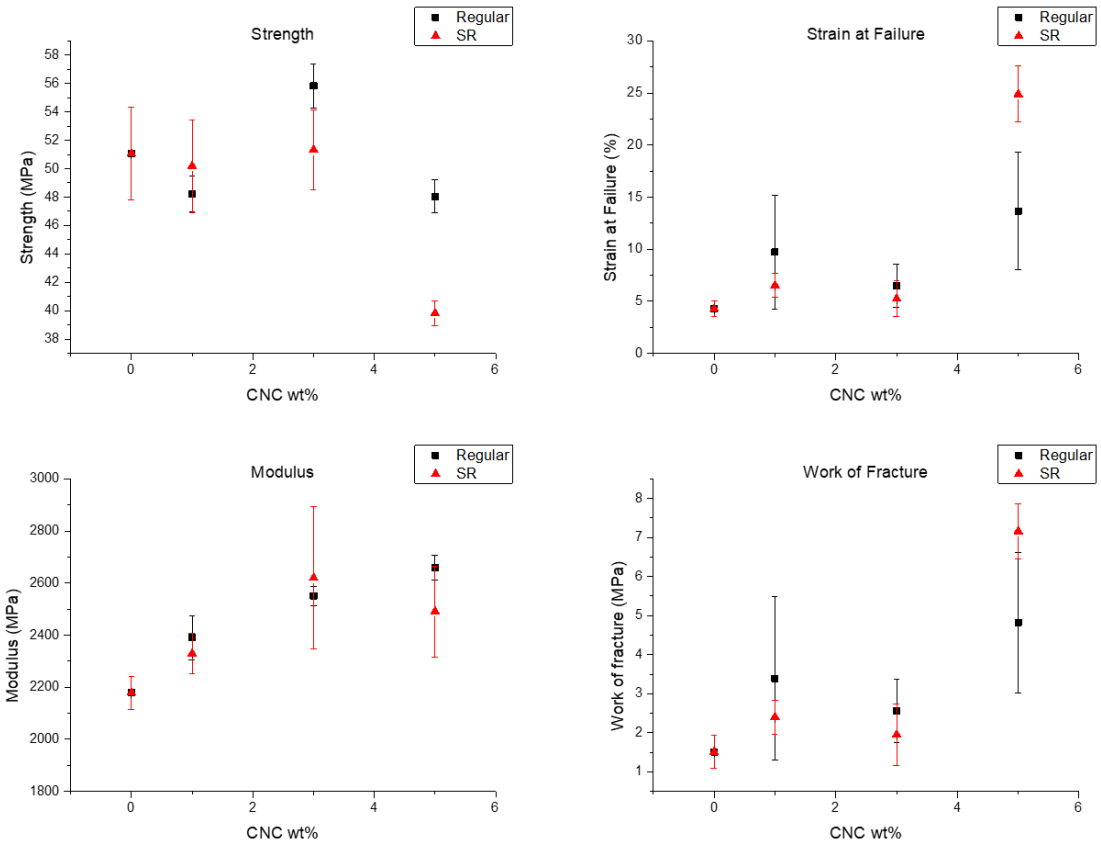

Figure 4.6 Mechanical properties of CNC/epoxy nanocomposite cured with D230

The thermomechanical properties of CNC/epoxy cured with D230 were evaluated using DMA. The results were illustrated in Figure 4.7 and Table 4.1. For both regular and solvent removal sample, glassy modulus and rubbery modulus were increased when more than 3 wt.% CNC was loaded. At low CNC content, a slight decrease in E' was found compared to neat epoxy as shown in Table 4.1. Storage modulus graph also shows that above T_g, the E' values in epoxy nanocomposites show evitable reinforced rubbery modulus at higher CNC loadings. This suggests that the strong interaction formed between epoxy and CNC through the hydrogen bonding network of the hydroxyls on the surface, that facilitate stress transfer. Thereby indicating constrained epoxy molecular motion when in contact with

CNC particles by shear between the interfaces. This observation was also analogs and in good agreement with other research studies [21-23].

Table 4.1 DMA data for CNC/Epoxy nanocomposite cured with D230

Sample	T_{g1}(°C)	T_{g2}(°C)	E′ at 35 °C (MPa)	E′ at 120°C (MPa)
Neat	N/A	98.8	2369±23	17.9±1.2
1CNC-R	71.8	98.3	1755±86	14.3±1.5
1CNC-SR	76	97.1	2041±125	14.2±3.6
3CNC-R	66.2	83.2	2343±38	16.9±2.2
3CNC-SR	73.4	92.4	2354±67	21.9±2.3
5CNC-R	62.1	79.4	2426±56	23.9±0.8
5CNC-SR	66.3	78.4	2494±88	26.9±1.2

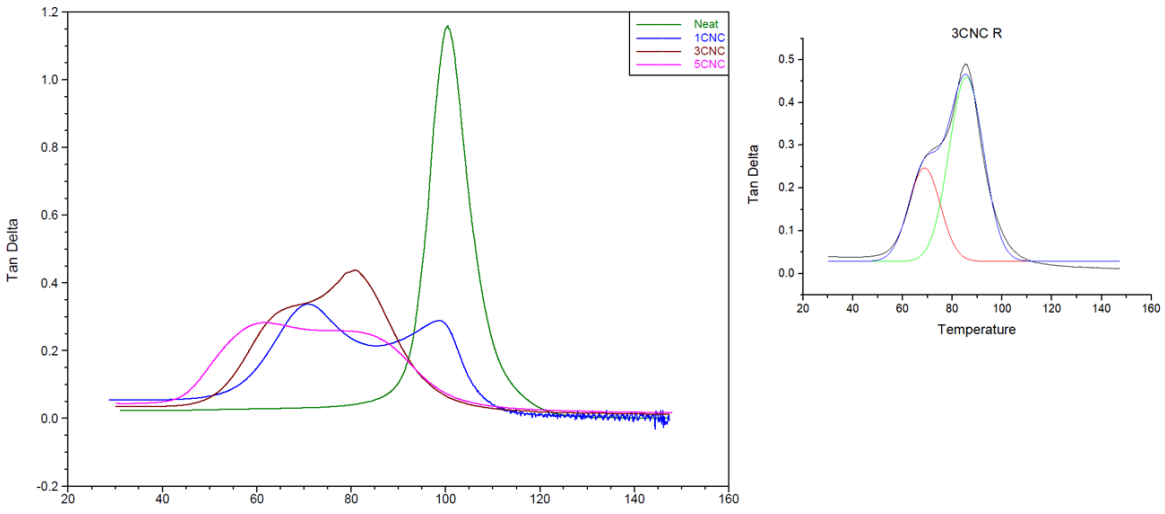

Figure 4.7 Left: values of the tan delta from DMA versus temperature for CNC/Epoxy nanocomposite (R) cured with D230 Right: a representative deconvoluted curve for 3CNC-R

Glass transition temperature (T_g) was calculated with the temperature at the peak of Tan δ curve, the results are summarized in Table 4.1, and some typical graphs of regular samples were shown in Figure 4.7. Neat epoxy has a singular sharp peak at 98.8 °C with peak height around 1.15, signifying a high degree of molecular mobility with narrow molecular weight distribution. All CNC filled epoxy nanocomposites showed two separate double peak and

the tan delta curves could be deconvoluted to two distinct curves as shown in Figure 4.7. Also, the height of the nanocomposite peaks was significantly lower than that of the neat epoxy, which could be related to the incorporation CNCs that could effectively dissipate the energy through the epoxy matrix and reduces the viscoelastic motions. We suggest that the reason for splits of Tg peaks was caused by the gradual change of crosslinking density across the thickness of the films. During the last curing treatment, samples were placed in a conventional oven and heated from 80 °C to 125 °C. The heat was coming from the bottom part of the oven and heat up the solvents near the bottom surfaces of the mold. The solvent would move up to the top surface and evaporate. This led to less trace of residual solvent left at the bottom side of the film and more entrapped solvent could be found near the sample/air surface. As we mentioned, a small trace of residual solvent would cause a significant influence in curing rate, resulting in different states of cure in the final product, in terms of crosslinking density. Thus, a densely crosslinked epoxy with higher M_w near the bottom of the film was formed and the T_{g2} of this part of the film match to the value of neat epoxy sample where no solvent was introduced. With an increase in solvent dosages, the solvent effect was more obvious, and a less crosslinked surface of the film with lower M_w cause results in a tremendous decrease in T_{g1} found in Table 4.1. One thing to notice was that the solvent removal step introduced had helped to alleviate the solvent effect for SR samples, and led to higher T_{g1} values for SR samples compared to the values of R samples.

4.3.3 Thermal Property of Nanocomposites

The values of T_g for composites made by the two processing methods were also determined using DSC measurements, and the DSC curves are shown below, and Table 2 summarized the Tg for all specimens. As expected, the DSC measurement also showed the similar trends of glass transition temperature as observed in DMA tests.

Table 4.2 Summary of T_g values from DSC measurements

Sample	T_g -Regular (°C)	T_g-SR (°C)
Neat	89.0±2.3	
1CNC	68.2±2.5	73.0±3.8
3CNC	60.8±2.2	60.9±3.6
5CNC	52.4±3.5	53.2±3.5

Unlike DMA which could disintegrate the two different viscous-elastic response of polymer chains with different degree of crosslinking or molecular weight. DSC only gave a generally heat response of the specimen preparation and the glass transition temperatures reported in the table are more likely to ascribe as bulk properties of each sample. Similar to data obtained by the DMA measurements, the T_g values decreased progressively with CNC contents. Also, the T_g values obtained from the samples produced by the solvent removal steps were generally higher than those prepared by regular methods.

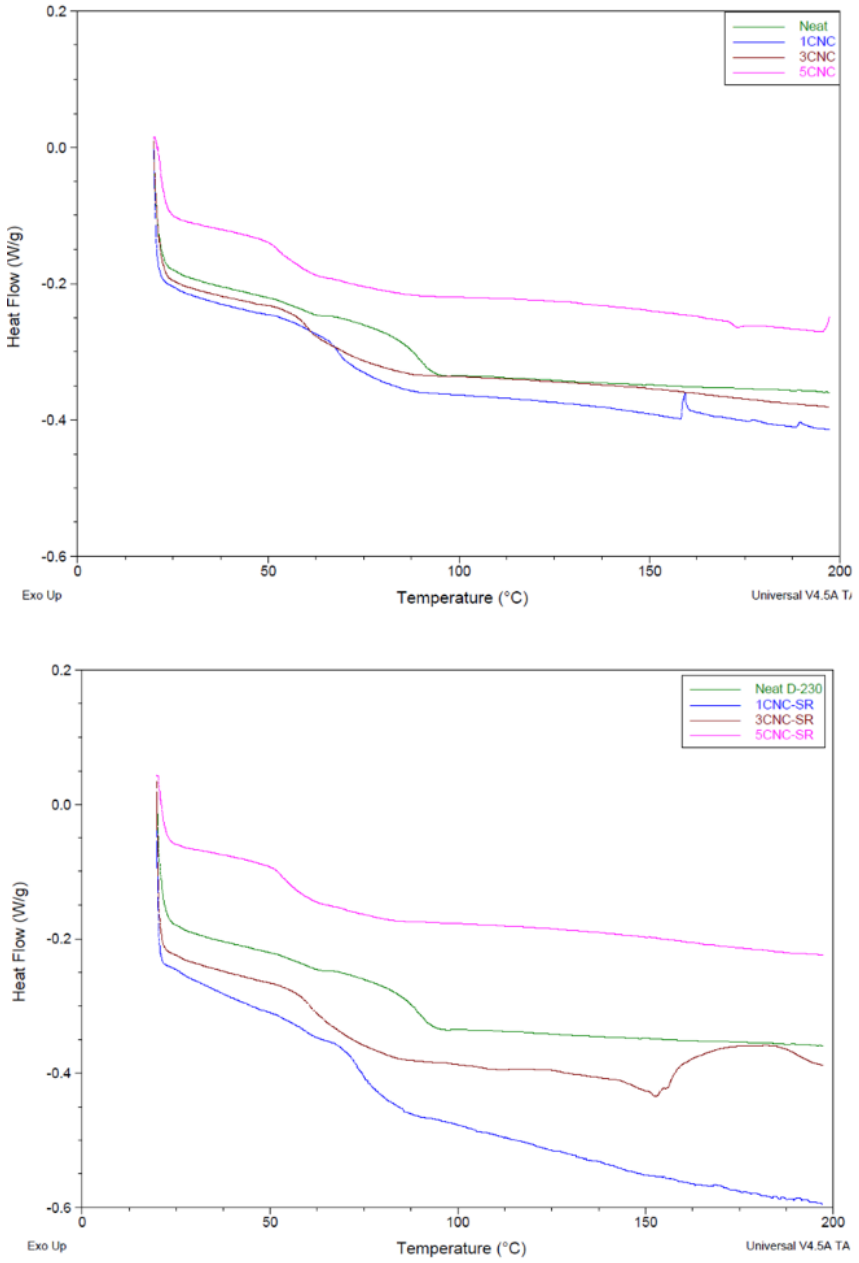

Figure 4.8 DSC curves for both Top: Regular and Bottom: solvent removal (SR) samples

Compare the DSC results for both epoxy composite samples made from D230 and ED600. Unlike the sample made with D230. There was no significant decrease in T_g values were for samples made with ED600, and some composite samples showed higher T_g than neat epoxy when using ED600 as a crosslinker. This reason behind this observation was the ED600 had a longer molecular backbone, thus the cured epoxy had a relatively low

crosslink density. The detrimental effect of residual solvent that plasticized the polymer was trivial, considering the epoxy already had a loose network. However, as the molecular weight of the amine crosslinker decreased, the epoxy cured with D230 showed a denser network, which the solvent left within the composite mixture could cause a severe plasticizing effect that lower the crosslink density and change the network structure.

Table 4.3 Water content, onset temperature, and temperature at maximum thermogravimetric decomposition peak for TGA data

Sample	Neat Epoxy	1CNC	5CNC	1CNC-SR	5CNC-SR	Neat CNC
Water content (%)	0.65±0.2	0.67±0.1	0.53±0.3	0.83±0.3	1.21±0.6	6.4+1.2
T_{onset} (°C)	357.0±4.6	356.2±3.8	350.9±0.4	352.3±2.3	350.0+1.2	235.0±3.0
T_{max} (°C)	373.4±2.3	378.7±4.2	379.4±0.8	375.1±6.2	378.8±3.5	244.1±3.2

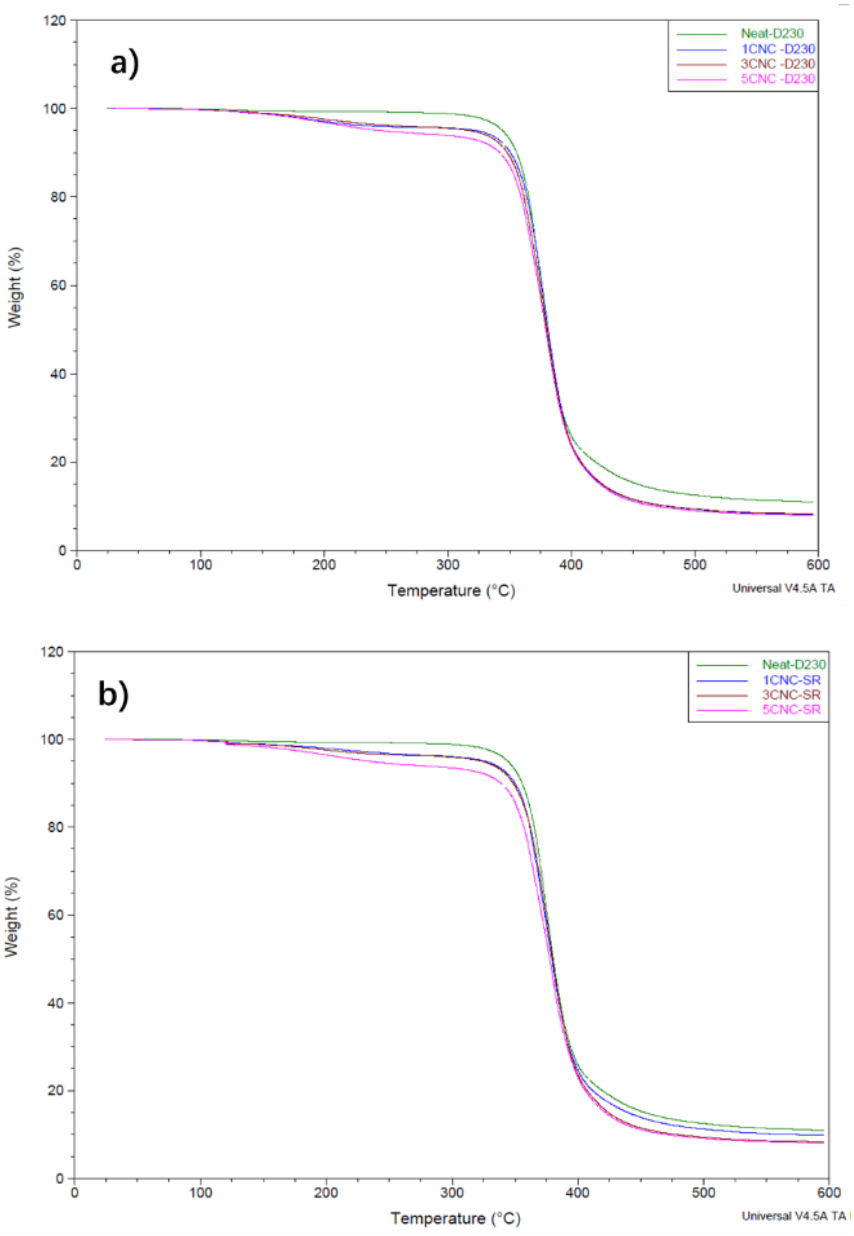

Figure 4.9 Thermogravimetric curves for a) regular and b) solvent removal (SR) composites films

Figure 4.9 shows the TGA data for neat epoxy and their composite prepared with two preparation protocols, including weight loss versus temperature. The water content, decomposition onset temperature (T_{onset}) and temperature at maximum weight loss (T_{max}) are summarized in Table 4.3. First, the water content of neat CNC was ten times higher

than that of neat epoxy. But there was no significant impact on water content on cured composite at all CNC loadings, indicates that CNCs did not bring extra water into the polymer matrix. This could be caused by physical blocking the hydrophilic sites on CNC surface by the densely packed epoxy matrix, or by the interaction between the epoxy moieties or backbones to the hydroxyl groups on the CNC surface. Second, the onset degradation temperature was reduced with increasing CNC concentration but showed no significant difference between regular and solvent removal methods. T_{onset} for composites were following the rule of mixtures model. The temperature at maximum weight loss increased with CNC content, but not significant.

From the curve, no significant decomposition profile was found for samples at 1 and 3 wt% CNC loading. However, at 5 wt.% CNC loading, the TGA curve shifted lower, that might indicate the significant structural change of the cured epoxy matrix at high solvent dosage. The low crosslink density of these samples made the polymer network more accessible to heat attack and degrade faster. One thing to notice was that all composite samples showed a lower char residue than that of the neat epoxy sample. This difference could be caused by the CNC fibers that were pyrolyzed at the last decomposition stage.

4.4 Conclusions

In this chapter, the compatibility of the CNC/epoxy system cured with PEA diamine crosslinker with different backbone structure was tested. From the last chapter, we showed the dropwise mixing protocols led to improved nanoparticle dispersion attributed from more intimate mixing between epoxy monomer and CNC/hardener mixture. No CNC aggregates were found from POM or SEM analysis with the cured composites sample, and

the mechanical performances were increased with up to 3wt.% CNC content, indicating good reinforcement of the polymer matrix. However, the plasticizing effect of residual solvent became prominent that significant changes to the cured composite structure at higher CNC loading. Higher flexibility and lower tensile strength, glass transition temperature/degradation temperature results found in composites with 5wt.% CNC loadings, which indicated the crosslink density of the epoxy matrices was decreased that compromised the properties of the composite. This means the solvent effect was more significant than the filler effect in this hardener system. Although the pre-solvent removal step could significantly reduce the amount of residual solvent in the composite mixture. Only moderate improvement in thermal performance was observed at the same CNC level. Overall, these two chapters highlighted the importance of understanding the compatibility of CNC with different polymer systems. Higher loadings of CNC solution could be incorporated into epoxy cured with a flexible and hydrophilic crosslinker such as ED 600, to improve its mechanical and even thermal properties the epoxy matrix properties. When switching to rigid and less hydrophilic systems, the detrimental effect of the solvent should be considered, and only low CNC loading should be incorporated into the polymer system.

Chapter 5. INFLUENCE OF HIGH LOADING OF CELLULOSE NANOCRYSTALS IN POLYVINYL ALCOHOL COMPOSITE FILMS

5.1 Introduction

In this Chapter, a more compatible PVA-CNC based nanocomposite was studied. High compatibility was due to the formation of hydrogen bonds between the hydrophilic surfaces on both CNC and PVA, and this led to the formation of a new biocompatible film. Water was used as the solvent for both PVA and CNC powders. Aqueous solution casting of CNC into PVA allows higher processability and easier drying, with advantages of reducing the costs and environmental concerns of using organic solvents. Thoroughly research the effect of various CNC loadings on the optical, thermal and mechanical properties of the nanocomposite films was studied.

By utilizing the current study to optimize the nanocomposite performance, further modifications on the PVA/CNC formulation could be tailor to different applications. The goal was to prepare CNC based composite films with promising potential to replace the petroleum-based counterpart with lower cost, and greener chemistry.

5.2 Experimental

5.2.1 Materials

Polyvinyl alcohol (M_w 89,000-98,000 and 99+% hydrolyzed) was purchased from Sigma Aldrich. Freeze dried CNC was purchased from the University of Maine, produced by the

U.S.D.A Forest Products Laboratory. The dimensions of these CNCs were determined to be 5-20 nm in diameter and 150-200 nm in length as provided by the supplier. Deionized (DI) water was used throughout the experimentation and was Millipore-processed (Darmstadt, Germany) with a resistivity of 18.2 MΩ-cm.

5.2.2 Preparation of PVA/CNC nanocomposite film

PVA powder (5g) was dissolved in DI water (100 mL) and stirred at 80 ºC for 6h. The PVA solution (5 wt.%) was allowed to cool to room temperature. Aqueous suspension of cellulose nanocrystals (3 wt.%) was prepared by dispersing 3g of freeze-dried CNC in 100 mL of DI water by continuous stirring at room temperature for 2h using a magnetic stirrer, followed by sonication in a bath sonicator (Crest CP500D, 120W, 42 kHz) for 24 h until a transparent suspension was achieved. Different proportion of CNC suspensions were added to the prepared PVA solution in order to produce composite with 3, 5, 10, 20, 30, 50, 70 wt.% cellulose nanocrystals; these samples were referred to as 3CNC, 5CNC, 10CNC, 20CNC, 30CNC, 50 CNC and 70 CNC, respectively. Stirring was continued for 2 h at room temperature. The final suspension was sonicated for 30 mins and degassed under vacuum to remove the air bubble. The solution was cast into a polystyrene petri dish and left to dry at room temperature for 48 h, followed by drying in an oven at 60 ºC for 24 h. Neat PVA and CNC films were also prepared using the same solution casting method and dried at same conditions. The resulting films were stored in a desiccator before further characterization to minimized moisture uptake.

5.2.3 Polarized light microscopy (POM)

The level of CNC dispersion in the PVA matrix was qualitatively analyzed using an Olympus BX51 microscope. Films were observed in the transition mode between two crossed polarizers with an objective of 5X magnification and at full extinction.

5.2.4 Scanning electrons microscopy (SEM)

To further characterize dispersion the fracture surface of the films after tensile testing were sputtered with gold and observed by scanning electron microscope (Phenom ProX Desktop SEM) at 10 kV.

5.2.5 Fourier-transform infrared spectroscopy (FTIR-ATR)

Nicolet iS50 FTIR (Thermo Scientific) equipped with Attenuated total reflection (ATR) mode was used to study the chemical structure of the composite membranes, as well as the interaction between the PVA and CNC. The spectra were collected in the range of 4000-600 cm^{-1} with a resolution of 1 cm^{-1} and a total of 32 scans.

5.2.6 Tensile Testing

The mechanical properties (tensile strength, modulus, and elongation at break) of nanocomposite membranes were determined using an Instron 5842 equipped with a 100 N load cell. Tensile specimens were prepared by die cutting the film into dog-bone samples following ASTM standard D638 Type V with the preset width and gauge length. The thickness of each specimen was measured with a digital micrometer in three different areas. At least five specimens of each composition were tested at room temperature. Samples with 20 and 30 wt.% CNC need to be rehydrated by wiping with a wet tissue paper before they

could be cut without cracking. Right after cutting, the dog-bone samples were placed on to a glass plate, covered with a microscope glass slide. Then placed in a drying oven at 60 ºC for 24 h. These samples were stored in a desiccator until testing. At higher CNC loading (i.e., 50 and 70 wt.% CNC), the samples were very brittle and broke easily during specimen preparation and attachment to the tensile testing machine. Therefore, tensile values for 50 and 70 CNC were not reliable and are not reported.

5.2.7 Dynamic mechanical analysis (DMA)

Dynamic mechanical analyzer DMA Q800 (TA Instruments) with air cooling system was used to investigate the dynamic properties of the nanocomposite membrane with varying CNC loading. Samples 3mm wide and 20 mm long were measured in tensile mode. The temperature range was 30 to 150 ºC at a heating rate of 3 ºC/min. Measurements were done at a constant frequency of 1Hz and strain amplitude of 0.05%.

5.2.8 Differential Scanning calorimetry (DSC)

Differential scanning calorimetry DSC Q200 (TA Instruments) was used to investigate the glass transition (T_g), melting (T_m) and cold crystallization (Tc) temperature of the specimens. 3-5 mg of samples were sealed in standard aluminum pans, and DSC tests were run under a nitrogen atmosphere. Samples were first heated from 30 to 250 ºC, then cooled back to 30 ºC, and finally heated to 250 ºC at 10 ºC/min under nitrogen atmosphere.

5.2.9 Thermogravimetric analysis (TGA)

Thermal stability and degradation behavior were investigated with thermogravimetric analysis (TGA) with TA Q50 (TA Instruments). Samples were tested under a flowing

nitrogen atmosphere with the sample size 5-7 mg and heated 10 ºC/min from room temperature to 600 ºC. The onset degradation temperature was determined with TA Universal Analysis software.

5.3 Results and discussions

5.3.1 Optical properties

As shown in Figure 5.1, the addition of up to 30 wt% CNC loading did not affect the optical transparency of the composite films, indicated good dispersion of CNC in the PVA matrix. This observation was due to similar refractive indices between the PVA (1.50) and nanocellulose (1.56) [125]. It was well known that PVA and CNC are highly compatible due to the strong interaction between the hydroxyl groups presented in both materials. Such hydrogen bonding interactions led to an abundant interconnected bond network. Thus well-dispersed CNC fillers in the PVA matrix could be achieved. The slightly opaque film shown in the composites with a higher concentration of cellulose nanocrystals (50 and 70 wt%) was due to macroscale aggregation of CNCs as suggested by Lee *et al*. [126].

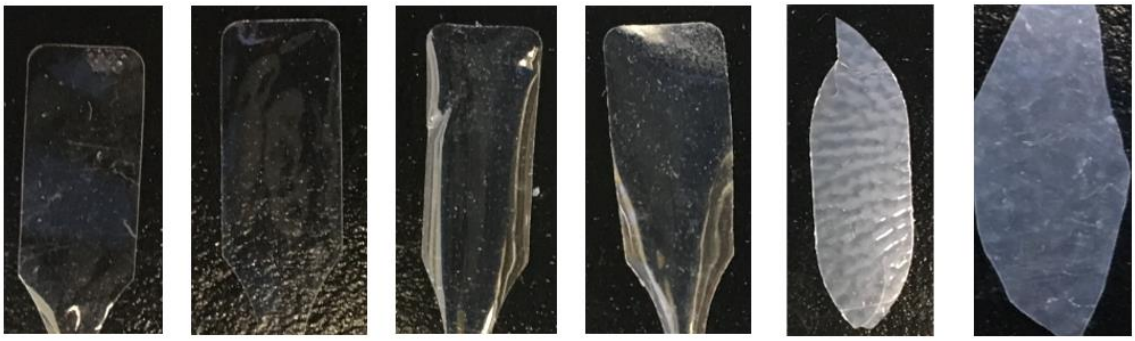

Figure 5.1 Photographic image of PVA/CNC films. From left to right: 0, 10, 20, 30, 50, 70 wt.% CNC.

To estimate the dispersion level of the CNC at the microscale, polarized optical microscopy images were collected and illustrated in Figure 5.2. A 530 nm red wave plate was used, giving an otherwise black image a magenta hue background, and birefringent domains due to agglomerated CNC have yellow-blue color. Even distribution of CNC in the PVA matrix

with no birefringence was observed for films with up to 20 wt.% CNC loading. At 30 wt.% CNC loading, an isolated birefringence region was found. The coloration of the 50 CNC and 70 CNC films were similar to that of neat CNC samples reported by Viet *et al*. [30]. They state the CNC films made by evaporation of water under ambient condition exhibit a delicate birefringent texture with a hazy appearance, which supports what we saw in Figure 5.1 and Figure 5.2. Viet showed that the sizes of birefringence would depend on the rate of formation of the films, as well as the processing history [30]. Therefore, the blue and yellow domains were mostly identical in 50 CNC and 70 CNC as they were prepared under the same conditions.

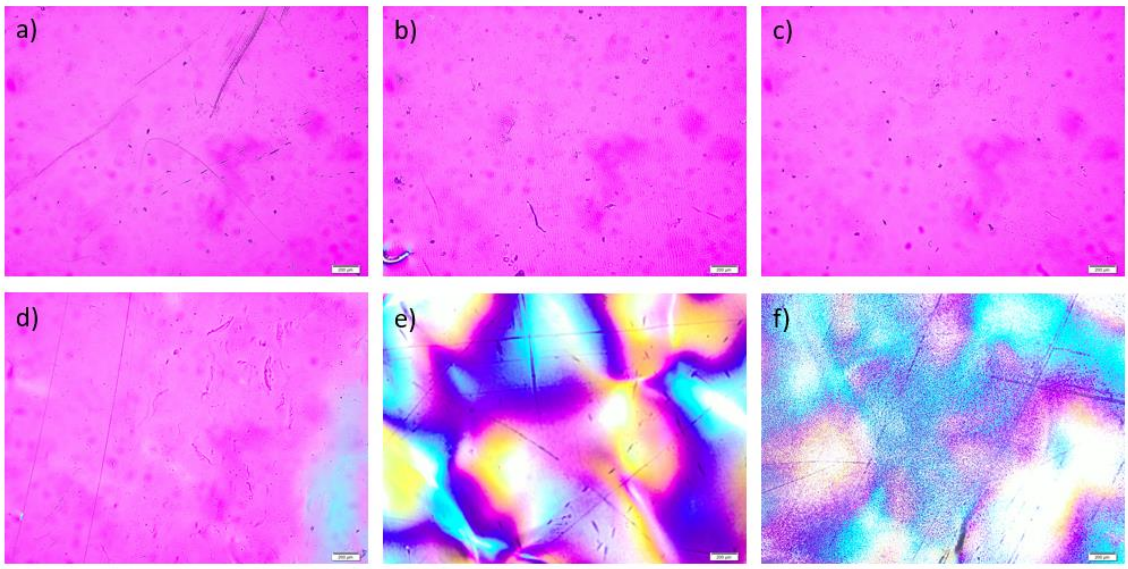

Figure 5.2 Polarized light microscope images of a) neat PVA, b) 10CNC, c) 20CNC, d) 30CNC, e) 50CNC and f) 70CNC films. Scale bar is 200 µm.

SEM micrographs could provide useful information about the distribution of cellulose nanocrystals in the polymer matrix. Low degree of micron-sized CNC agglomeration was found in the composite film with less than 30 wt.% CNC loading. In support of this, the

morphology of the fracture surface of PVA and PVA/CNC composites were presented in Figure 5.3. The neat PVA sample was significantly thinner in these images because of the large amount of plastic deformation during tensile testing, compared to the films loaded with CNC. It was shown that neat PVA film and composite with 10% CNC featured a homogeneous smooth surface which signals ductile failure. Most of the nanoparticles were embedded and dispersed uniformly in the fractured surface under 10 wt.% CNC in the PVA matrix as a stable continuous phase. However, the fracture surface became rougher at higher CNC loading, and many large granular particles were observed at the fractured surface, indicating possible aggregation occurred in the PVA matrix. Also, void space formed between CNC agglomerate which suggesting a negative effect on mechanical properties and was consistent with the results of the mechanical analysis in the following section.

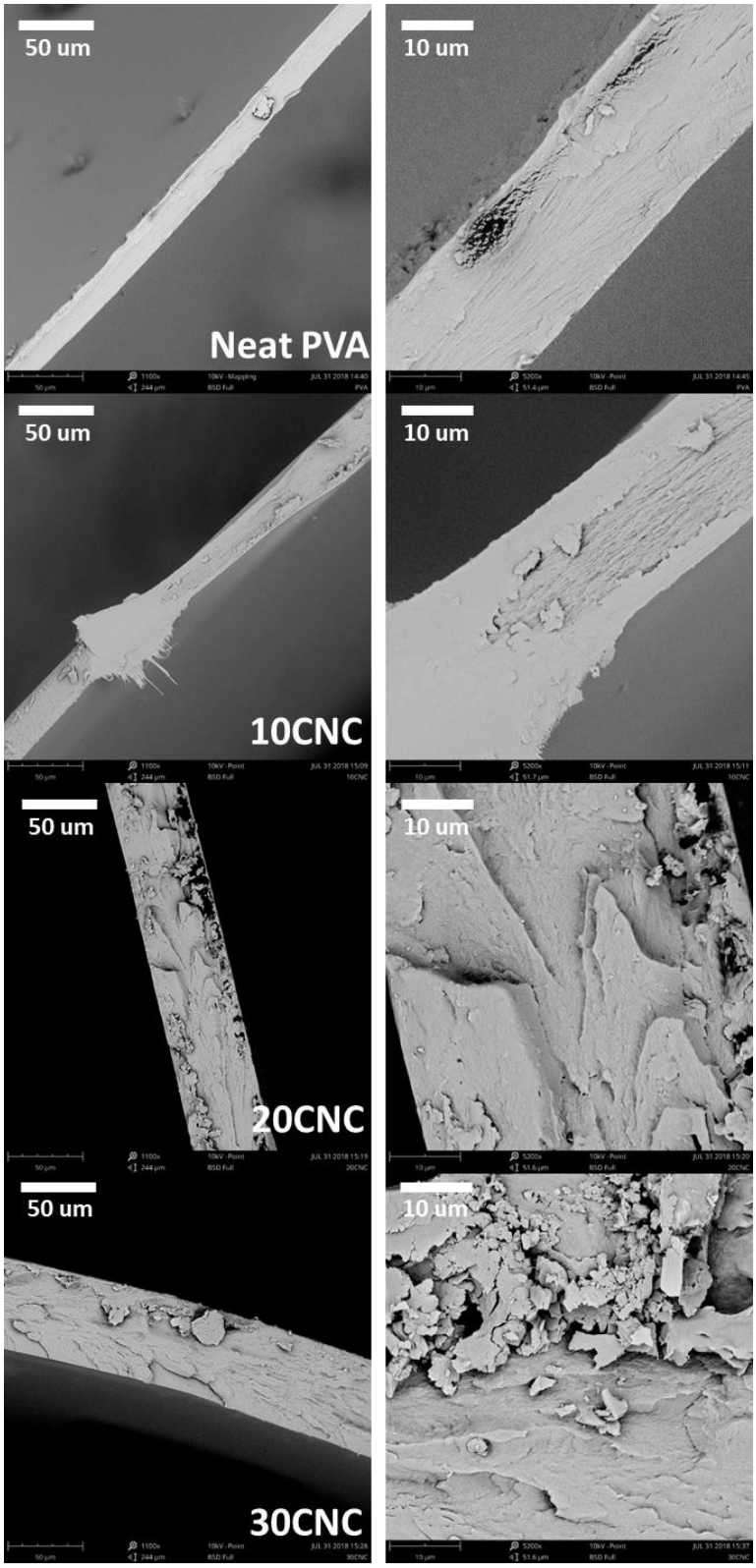

Figure 5.3 SEM images of cross-sections of PVA and PVA/CNC composites after tensile testing

5.3.2 Chemical analysis

The FTIR spectra of CNC/PVA nanocomposite films were depicted in Figure 5.4. A characteristic band of –OH group in PVA was observed around 3270 $cm^{-1,}$ and the peak shifted toward higher wavenumber upon the introduction of CNC. This band corresponds to the O-H vibration from the intramolecular, and intermolecular hydrogen bonding between the hydroxyl groups of PVA and CNC, which appears to indicate the good compatibility between these two polymers. C-H stretching vibration from alkyl groups was observed around 2939 cm^{-1} in neat PVA and its composites with CNC. An insignificant peak at 1706 cm^{-1} belongs to C=O stretching from the residual acetate groups in the PVA matrix. Peaks at 1417 cm^{-1} and 1327 cm^{-1} belongs to C-H bending vibration and were found in all spectra. The vibration peaks detected at 1142 cm^{-1} and 1086 cm^{-1} has been related to C-O stretching, and the intensity of these peaks decreased with the addition of cellulose nanocrystal, which supports the possible interaction between CNC and PVA [117]. The absorption band at 917 and 837 cm^{-1} of PVA was gradually reduced with increase CNC loading. This phenomenon was also found in previous literature and was attributed to possible PVA and CNC interaction [14, 117]. Two new bands were observed at 1065 cm^{-1} and 1028 cm^{-1} indicated the presence of ether bond and sulfonic acid groups respectively, by the introduction of CNC, and their intensities increased with increasing CNC loading. These were the characteristic bands by the contribution of C-O-C glycosidic bond in cellulose, and sulfate ester groups introduced with acid hydrolysis process.

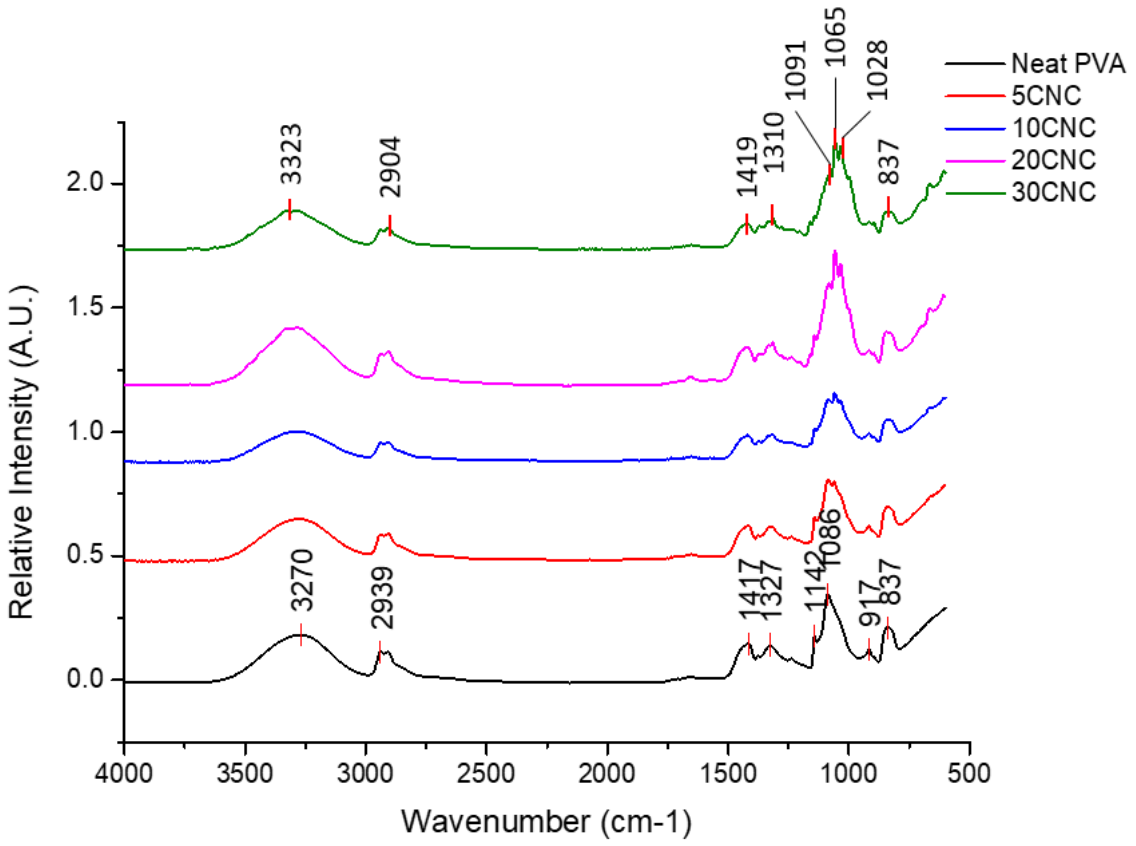

Figure 5.4 ATR-FTIR spectra of the neat PVA film and its composites.

5.3.3 Mechanical properties

Table 5.1 Mechanical properties of the neat PVA and nanocomposite films

Sample	**Neat PVA**	**5CNC**	**10CNC**	**20CNC**	**30CNC**
Tensile Strength (MPa)	77.3±7.7	113.5±5.0	127.3±3.1	103.1±19.0	68.1±24.6
Elastic Modulus (GPa)	4.4±0.2	6.4±0.4	6.8±0.7	6.4±0.6	5.7±0.7
Strain at break (%)	60.8±32.1	15.2±10.0	5.6±3.7	2.4±0.4	1.3±0.4
Glassy modulus (MPa)	4342±25	4450±12	5008±22	6293±65	7688±58
Rubbery Modulus (MPa)	87.2±12	267±8	338±21	747±39	1277±99

The tensile testing results for PVA and PVA/CNC films were given in Table 5.1 and Figure 5.5. All neat PVA specimens exhibit necking behavior confirmed it was a ductile polymer with high failure strain. After incorporation with CNC, the necking behavior start to weaken and completely diminished with 20 wt.% loading. In support for this, a trend of decreasing strain at the break with increase CNC loading was observed. For CNC reinforced specimens, the tensile strength and modulus were significantly increased up to 10 wt.% but decreased with further CNC loading. The tensile strength and modulus of neat PVA film were 77.3 MPa and 4.4 GPa, respectively. There was an approximately 65 % improvement in the tensile strength and 55% improvement in elastic modulus of the PVA nanocomposite film with the addition of CNC at 10 wt.% concentration. The enhancement in mechanical properties due to the addition of CNC might be a result of the inherent chain stiffness and rigidity in nanocellulose, which acts as a reinforcement phase and homogeneously distributed in the polymer system. The high compatibility between the fiber and matrix promotes interfacial interactions. The concentration of CNC used in this work was much higher than the percolation threshold mentioned in the literature (around 3 wt.%) [19, 23] . Thus the formation of a CNC percolation network in the PVA matrix results in an improvement in mechanical properties. Comparing 10 CNC to the 30 CNC films, the tensile strength and elastic modulus decreased to 68.1 MPa and 5.7 GPa respectively. A possible explanation of these difference was that change of specimen preparation method. 30 CNC samples must be wiped with DI water before they could be cut without cracking, where 10 CNC can be directly cut without hydration treatment. As both PVA and CNC are hydrophilic, the hydration treatment may affect the polymer structure, and the following hot-pressing procedure may introduce defects into the

composite film. Another explanation is due to the agglomeration tendency of the highly active CNC particles. CNC agglomeration was commonly found in composite systems with high CNC loading or in a polymer matrix that is not well compatible with CNC fiber and led to diminished mechanical properties [20, 23, 117]. Overall, hydration treatment could be the primary cause for mechanical depression, since 20 CNC films only showed small-scale CNC agglomerate from SEM micrographs.

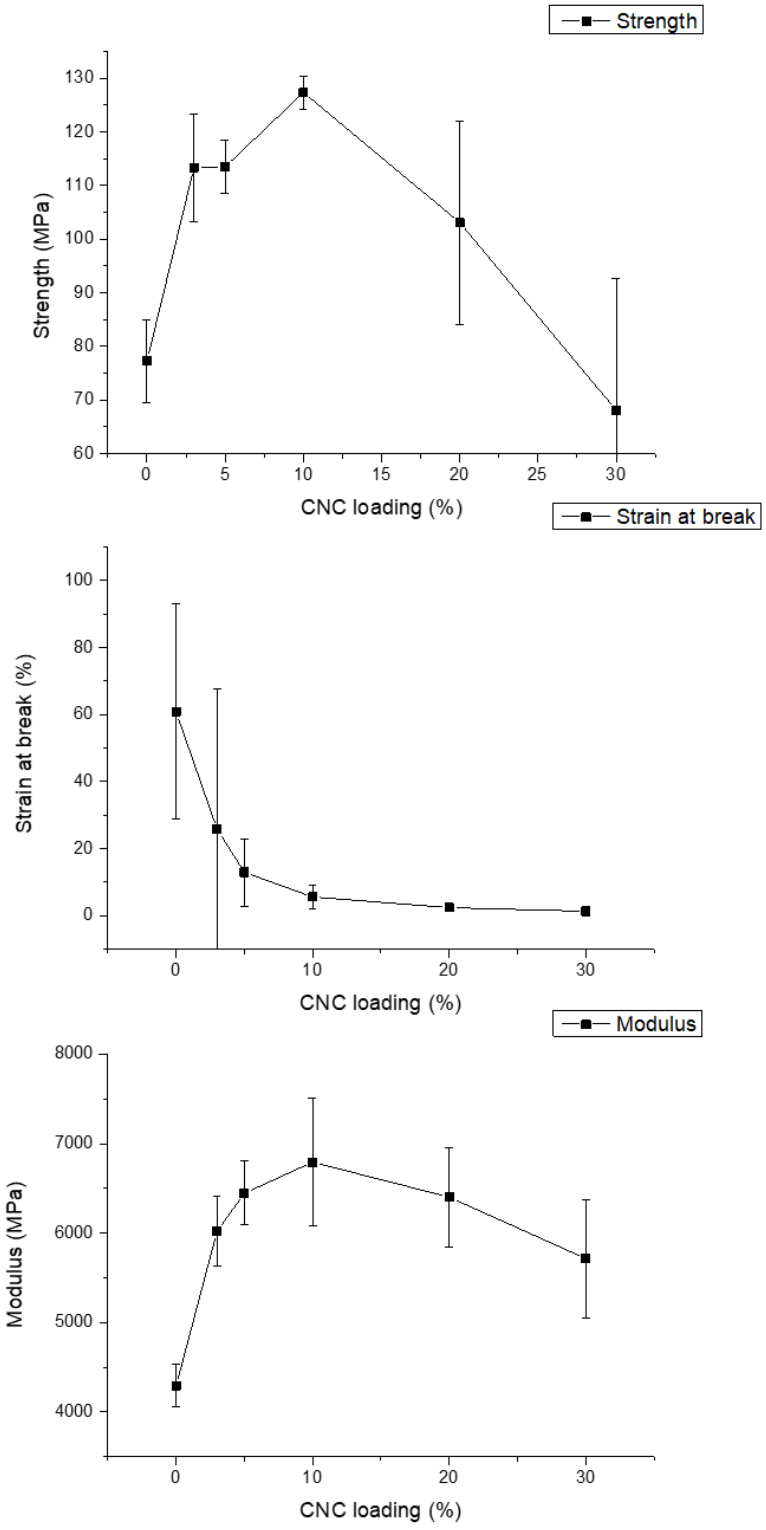

Figure 5.5 Effect of CNC content on the mechanical property of PVA-based nanocomposite films. Top-down: tensile strength, strain at break and tensile modulus

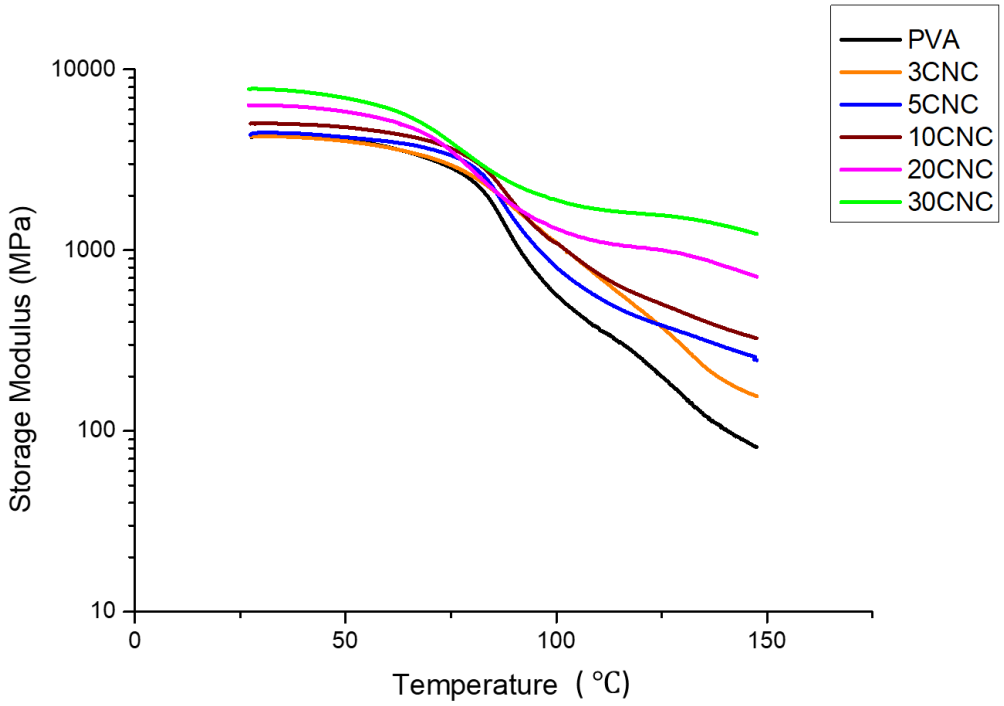

Figure 5.6 Dynamic mechanical analysis result of PVA and nanocomposite films

The DMA analysis of PVA and nanocomposite films was conducted to investigate their behavior in a range of temperature, and results were given in Table 5.1 and Figure 5.6. There was a systematic trend of increasing storage modulus with increasing CNC loading. This phenomenon highlights the reinforcing effect of CNCs in both the glassy and rubbery regions of the PVA matrix. As a point of reference, at low temperatures (35 ºC), the glassy storage modulus for PVA and composite with 10 and 30% nanofiber were 4342, 5008, and 7688 MPa, respectively. The differences in the storage modulus values were more noticeable above the glass transition temperature, in the rubbery region. It is found that the reduction in modulus with increasing temperature was less significant for films with increased CNC loading. At 130 ºC, the rubbery storage modulus of PVA, 10CNC, and 30CNC were 87.2, 338, and 1277 MPa, respectively. In other words, a 78% increased

glassy modulus versus a 15-time folds increase in rubbery modulus is found in the 30CNC sample, compared with neat PVA sample. This observation indicates that the filler and polymer interaction and CNC percolation network within the films improved the thermo-mechanical properties. The CNC percolation network in the composite bears a significant amount of load via stress transfer through hydrogen bonds, especially at a higher temperature in the rubbery regions.

5.3.4 Thermal properties

TGA and DTG were undertaken to investigate the thermal performance of PVA-based nanocomposite films with various CNC loading as reinforcement and were shown in Figure 5.8 and Table 5.2. The nanocomposites had better thermal stability (e.g. higher onset temperature or char content) depending on the CNC loading compared to both neat PVA and CNC film in nitrogen. The results were supervising because incorporation of cellulosic reinforcement is usually known to reduce the thermal stability of thermoplastic matrices[16, 44]. This unusual behavior of CNC-polymer composites having greater thermal stability than neat polymer and the neat CNC has been reported before, particularly when using PVA as the matrix [12, 14, 79].

Table 5.2 Summary of onset temperature of PVA/CNC films with different CNC loading

Sample	PVA	3CNC	5CNC	10CNC	20CNC	30CNC	CNC
T_{onset} (°C)	247±12	248±8	254±16	263±9	316±24	233±32	232±17

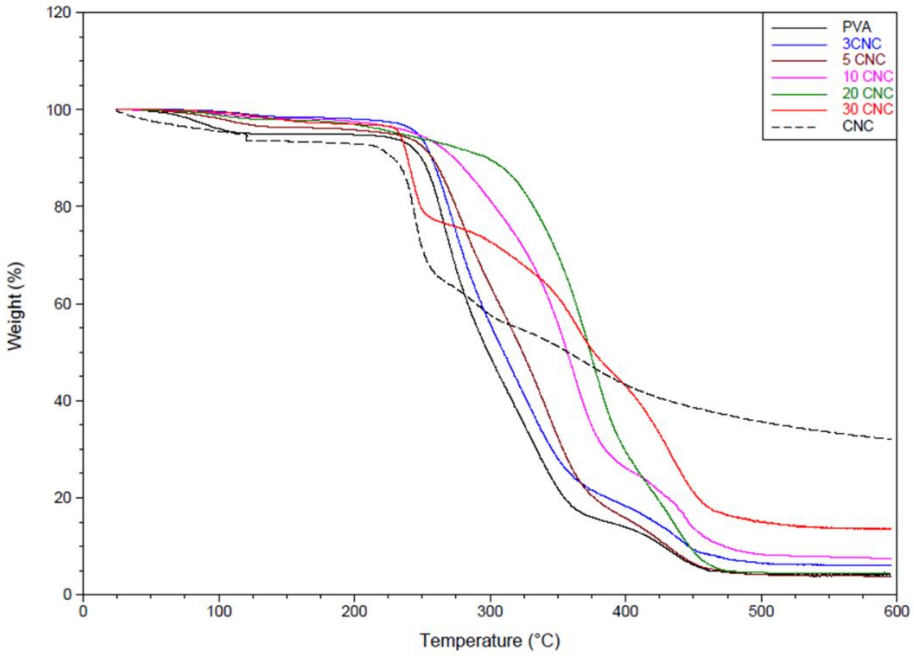

Figure 5.7 TGA curves for PVA and its composites with different CNC loading. Thermogram of pure CNC is used as a reference

It was shown in Table 5.2 that the inclusion of cellulose nanocrystals resulted in an improvement in initial degradation temperature of nanocomposite with up to 20 wt.% CNC loading. This improvement is possibly due to the formation of hydrogen bonds between the polymer and incorporated nanofiller and restriction of the mobility of polymer chains caused by the homogeneous distribution of CNC in the matrix. For instance, T_{onset} for PVA was 247 ºC while it increased to 263 ºC for nanocomposite with 10% CNC loading. The 20CNC sample showed the highest T_{onset} of 316 ºC, which is a 28% increase compared to the neat polymer.

The TGA and DTG curves for PVA and PVA/CNC composites revealed three weight loss regions. The initial weight loss about 40-120 ºC was due to evaporation of the absorbed moisture on the surface of the samples. The weight loss in this temperature range was much lower for all nanocomposite films compared to the pure polymer and neat CNC. This could

be attributed to a more compact structure of the composite with lower free volume to retain water, or the hydrogen bonding network could hold the water molecules more efficiently that requiring a higher temperature to remove the tightly bounded water from the sample surface. For PVA sample, the next two stages of weight loss were due to thermal degradation of PVA, occurred in the range of 230-380 ºC and 400-500 ºC, which may be contributed to the structural degradation of PVA and decomposition of carbonaceous materials, respectively. For neat CNC sample, the pyrolysis also occurred in two separate stages, i.e., between 200 to 320 ºC and 300 to 500 ºC. Dehydration of the cellulose chain started first at a lower temperature, catalyzed by acidic sulfate groups present on the CNCs prepared by acid hydrolysis[23, 127]. Afterward, the second phase occurred at a higher temperature with a broad peak in the DTG curve corresponding to the decomposition of the unsulfated crystal interiors, that slowly degraded and formed char product.

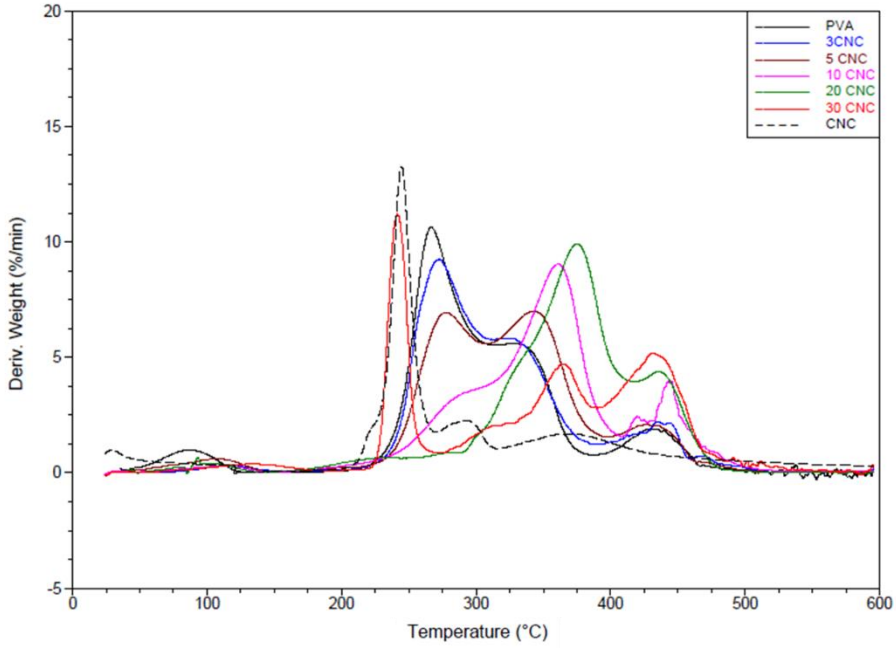

Figure 5.8 DTG curves for PVA and its composites with different CNC loading. Thermogram of pure CNC is used as a reference

Incorporation of CNCs into PVA matrix remarkably changed the thermal stability. The deformation temperature of CNC reinforced PVA films provided a shift of TGA curves. As the nanocellulose loading increased, the thermal stability of the composite films increased. This thermal stability improvement peaked at 20 wt.% CNC loading, but suddenly dismissed at higher loading. Compared to the distinguished thermal decomposition peaks of PVA and CNC represented in Figure 5.8, the bimodal shape of the DTG curves with two different peak values for PVA/CNC composite confirmed the synchronized decomposition behavior of both PVA and CNC. The major weight loss of CNC occurred between 200 to 260 ºC disappeared, indicating a good interaction between the surface functional groups of CNC and the macromolecular chains of PVA via noncovalent interaction. Also, it was quite apparent from the DTG thermogram that the incorporation of CNC slows down the structural degradation of the composite film in the range of 220 to 400 ºC. Therefore, shifting the major weight loss to the last stage of thermal degradation. The presence of residual sulfate groups may also catalyze the cleavage of the PVA backbone might be another explanation. It is noteworthy that the composite film with 30 wt.% CNC loading has the initial degradation peak coincide with neat CNC curve. This result suggested that a micro-sized agglomerate might be formed, and it decomposed without interacting with the polymer matrix.

The glass transitions, crystallization and melting behavior of PVA/CNC films were studied using differential scanning calorimetry (DSC), and the obtained curves and thermal transition values are presented in Figure 5.9 and Table 5.3. In all cases, the studies were undertaken by a heating-cooling-heating cycle. The moisture and thermal history of the composite films can be eliminated during the first heating cycle.

Table 5.3 Effect of CNC loading on melting temperature (T_m), crystallization temperature (T_c), glass transition temperature (T_g) and degree of crystallinity(X_c) of composite films

Sample	T_m (°C)	T_c (°C)	T_g (°C)	Δh_c(J/g)	X_c(%)
PVA	226.5	200.0	75.9	49.2	35.5
3CNC	225.1	205.6	75.9	41.9	30.2
5CNC	223.7	204.1	79.2	37.4	27.0
10CNC	223.8	201.7	79.9	29.7	21.4
20CNC	222.4	193.7	82.7	28	20.2
30CNC	221.8	N/A	76.2	N/A	N/A

The melting temperature of PVA in the PVA/CNC films was not largely affectedly by the addition of CNC. The DSC thermogram displayed a significant melting endotherm at around 225 ºC, whereas the endotherm was broadening and shifted to lower temperature with the addition of CNC. The sharp endotherm peak is assigned to the melting of the crystalline portion of PVA. Therefore, this depression in melting temperature could be ascribing to change of the crystallization of PVA with CNC. On further investigation of the cooling cycle. It showed that PVA sample has a sharp exothermic crystallization peak at 200 ºC, while the crystallization peak of its nanocomposite containing 3 wt.% of CNC was weaker and shifted to 205.6 ºC. Subsequently, the T_c of nanocomposites with higher CNC loading has decreased and extinguished at 30 wt.% CNC content. These results likely indicated that the structure of the CNCs limited the crystallization of PVA. The homogeneous phase nucleation dominates the formation of crystals which appears to be uniform in size and shape during cooling in the PVA film. Arup et al. reported that the

CNC fillers could act as a crystallization nucleation points for polymer [117]. Incorporation of CNC provided more nucleation sites with the large surface area that leads to heterogeneous phase nucleation which forms a large number of small crystallites varying in size [14]. The degree of crystallinity for all samples was presented in Table 5.3, and its values decreased upon addition of CNCS. Therefore, the low crystalline form of PVA/CNC composites show a weaker melting transition and spread over a broader range of temperature compared to neat PVA.

It should be noted that the glass transition temperature showed the same trend as the onset degradation temperature from TGA analysis. Firstly, T_g increased with the addition of CNC from the 75.9 ºC for the neat PVA to 82.7 C for the 20CNC nanocomposite film, then suddenly dropped to 76.2 ºC for 30 CNC sample. The first increase in T_g with the addition of up to 20 wt.% CNC loading is ascribed to the limitation of the matrix mobility by the interfacial force acted between PVA and CNC surface, and this effect was magnified at higher CNC loading. However, the large aggregates of CNC formed in 30 CNC sample may cause the depression of T_g. In this work, a neat CNC sample did not show any significant glass transition in the temperature range of the DSC scans.

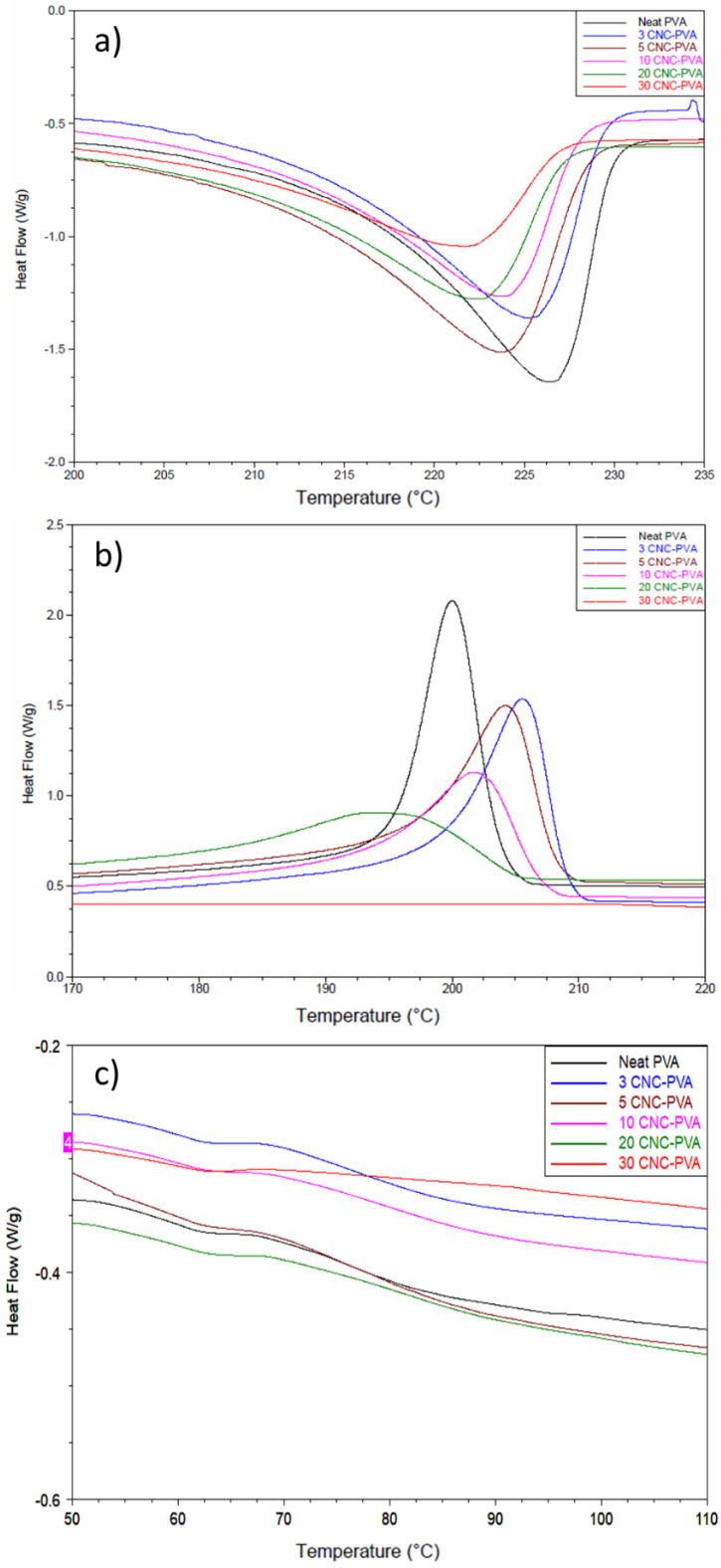

Figure 5.9 DSC results of films at a) melt transition, b) crystallization transition and c) glass transition

5.4 Conclusions

Renewable and bio-based nanocomposite films with robust thermo-mechanical properties were prepared via the solution casting of polyvinyl alcohol (PVA) and cellulose nanocrystal (CNC). PVA/CNC films with up to 30 wt.% CNC loading were optically transparent. SEM micrographs showed homogeneous distributions of CNCs within PVA matrix at lower CNC concentration. However, at higher CNC proportion (20 and 30 wt.%), small granular particles were observed at the fractured surface, indicating possible aggregation occurred in the PVA matrix. These observations are consistent with mechanical testing results. Comparing the neat PVA to the 10 wt.% CNC loaded film, the elastic modulus increased from 4.3 to 6.8 GPa, the tensile strength increased from 77 to 127 MPa, respectively, while the mechanical properties decreased at higher CNC loading. The glassy storage modulus of PVA increased from 4.3 to 7.7 GPa at 30 wt.% CNC loading. The addition of CNC significantly changed the thermal performance of PVA. Thermal stability of the composite films with up to 20 wt.% CNC content was greater than both neat PVA and neat CNC. Composite films showed higher onset degradation temperature with a delayed structural degradation in the range of 220 to 400 ºC. The T_g values also showed a similar trend, increased from 76 ºC for the neat polymer to 83 ºC at 20 wt.% CNC loading. These mechanical and thermal results indicated good compatibility of PVA and CNC via hydrogen bonding network between hydroxyl groups of CNC and polymer matrix and evidenced well-dispersed nanofillers within the PVA. The matrix structure of the PVA was strongly affected by the addition of CNC. The degree of crystallinity was decreased with increasing CNC loading, which also caused depression in melting temperature.

Chapter 6. PREPARATION AND CHARACTERIZATION OF POLYVINYL ALCOHOL/CELLULOSE NANOCRYSTAL-BASED NANOCOMPOSITE FOR FUEL CELLS APPLICATIONS

6.1 Introduction

Commercially available proton conducting membranes such as Nafion® are petroleum-based polymers that are expensive and difficult to recycle. High methanol crossover and low conductivity performance at elevated temperature are the two main drawbacks of Nafion® film. Therefore, there is a persistence need for developing alternative polymeric electrolytes for the DMFCs that are cheaper and more biofriendly compare to perfluoro sulfonate polymers.

In the current research, cellulose nanocrystal was blended with polyvinyl alcohol (PVA) to make a free-standing and flexible film. PVA is a low-cost polymer with good film-forming capability with superior chemical, mechanical and thermal stability. Its high selectivity of water over methanol or alcohols can function as an excellent methanol barrier and PVA is intrinsically compatible with CNC phases due to the formation of hydrogen bonds between the hydrophilic surfaces. From the last chapter, the PVA with 10 wt.% CNC loading showed the best mechanical performance with good handleability. Therefore, this composite composition was selected for the current study. Since both PVA and CNC are soluble in water and have a high degree of swelling, the hydrophilicity of the composite film was controlled by covalent crosslinking using various compositions of sulfosuccinic acid (SSA). The sulfonic acid groups attached to sidechain of SSA could also serve as sites

for proton transfer, which could raise the proton conductivity to the PVA/CNC membrane. The fabricated membranes were characterized by using Fourier transfer infrared spectroscopy (FTIR), differential scanning calorimetry (DSC) and thermogravimetry analysis (TGA). Proton conductivity and methanol permeability were also measured. Eventually, the object of this study is to provide the insight of to prepare a bio-based crosslinked polymeric electrolyte membrane with a simple method of functionalization and to evaluate its potential for application in direct methanol fuel cells.

6.2 Experimental

6.2.1 Materials

Polyvinyl alcohol (PVA, M_w 89,000-98,000 and 99+% hydrolyzed) and sulfosuccinic acid (SSA, 70 wt% in water) were purchased from Sigma Aldrich and used as received without further purification. Freeze dried CNC was purchased from the University of Maine, produced by the U.S.D.A Forest Products Laboratory. The dimensions of these CNCs were determined to be 5-20 nm in diameter and 150-200 nm in length as provided by the supplier. Deionized (DI) water was used throughout the experimentation and was Millipore-processed (Darmstadt, Germany) with a resistivity of 18.2 MΩ-cm.

6.2.2 Preparation of crosslinked PVA/CNC nanocomposite film

PVA powder (5g) was dissolved in DI water (100 mL) and stirred at 80 ºC for 6h. The PVA solution (5 wt%) was allowed to cool to room temperature. Aqueous suspension of cellulose nanocrystals (3 wt%) was prepared by dispersing 3g of freeze-dried CNC in 100 mL of DI water by continuous stirring at room temperature for 2h using a magnetic stirrer,

followed by sonication in a bath sonicator (Crest CP500D, 120W, 42 kHz) for 24 h until a transparent suspension was achieved. Aqueous CNC was added to PVA solution to obtain a final CNC content of 10 wt% and stirred for 2 h at room temperature. Different amounts of SSA were added into the PVA/CNC mixture and stirred overnight at room temperature. The concentration of SSA was changed from 3.5 to 20 wt% relative to the total amount of PVA and CNC in solution. The polymer solution was cast into a polystyrene petri dish and left to dry at room temperature for 48 h, followed by drying in an oven at 60 ºC for 24 h. The obtained membranes were peeled off from the dishes and then annealed for 2h in a thermoset oven at desired temperature 100 and 120 ºC, respectively to induce crosslinking reaction. Freestanding and flat membranes were obtained with a thickness of 60-100 µm. The pristine recast Nafion® membrane was also prepared and treated in a similar manner which was dried at 60 ºC for 24 h and then annealed at 120ºC for 12 h.

6.2.3 Fourier-transform infrared spectroscopy (FTIR-ATR)

Nicolet iS50 FTIR (Thermo Scientific) equipped with Attenuated total reflection (ATR) mode was used to record the spectra of the SSA crosslinked PVA/CNC film. The spectra were collected in the range of 4000-600 cm^{-1} with a resolution of 1 cm^{-1} and a total of 32 scans.

6.2.4 Water uptake and swelling in thickness

Water uptake (WU) was determined the mass change before and after the complete hydration of the membrane with water. A dry membrane was swelled in DI water for 24 h then the surface of the membrane was quickly wiped with a filter paper to remove the excess surface water and was weighed (W_{wet}). Then samples were dried in an oven at 60

ºC for 24 h and then weighed again (W_{dry}). Three independent tests were conducted on each SSA composition. The WU was calculated using the expression:

$$WU = \frac{(W_{wet} - W_{dry})}{W_{dry}} \times 100\% \quad (1)$$

Swelling behavior in the thickness direction was calculated by the same experiment using the following equation:

$$Swelling\ ratio\ (\%) = \frac{T_{wet} - T_{dry}}{T_{dry}} \times 100\% \quad (2)$$

Where T_{dry} is the thickness of the film in dried state and T_{wet} is the thickness of the sample at the same position in the swelled state.

6.2.5 Ion exchange capacity (IEC) and hydration number (λ)

The ion exchange capacity was measured by a titration method. The pre-weighed membrane was immersed in 1M NaCl solution for 24 h, where the H^+ exchanged with Na^+ ions were titrated against 0.01M NaOH solution with a pH meter (PHH-63 Omega). The IEC values were calculated from the following expression:

$$\text{IEC (mmol/g)} = \frac{V_{NaOH} \times M_{NaOH}}{\text{Weight (polymer)}} \quad (3)$$

Where V_{NaOH} and M_{NaOH} are the volume and normality of the NaOH solution, respectively. The ratio of water molecules to the ion exchange sites, denoted as hydration number *λ,* was calculated by eqn (4).

$$\lambda = \frac{WU}{IEC \times 18} \quad (4)$$

6.2.6 Differential scanning calorimetry

The amount of free water and bound water in the membranes were determined by melting transition in differential scanning calorimetry (DSC, Q200 TA Instruments). The membrane samples were fully hydrated in deionized water for 24 h. The surface water on the membrane surface was wiped off, and around 5 mg samples were weighed and enclosed in an aluminum pan. Each sample was cooled from 25°C to -50°C and then heated to 25°C at a heating rate of 5°C/min. The weight fraction of free water (ω_f) was calculated by eqn (5).

$$\omega_f = \frac{\Delta H_m}{Q_{melting}} = \frac{\int \Delta C_p dT}{Q_{melting}} \quad (5)$$

Where ΔH_m is the total melting enthalpy obtained by integration of the freezing peak over the broad melting transition and $Q_{melting}$ is the enthalpy of fusion of bulk ice (334 J/g). The weight fraction of bound water (ω_b) is calculated by subtracting the amount of freezing water (ω_f) from the total water uptake (WU).

6.2.7 Proton conductivity

Proton conductivity measurement of hydrated membranes was carried out using a four-probe, in-plane electrochemical impedance spectrometer (Parstat 2273). The membranes of 1cm x 4cm size were soaked in water for 24 h and fitted in between Pt electrodes of the test cell. AC impedance measurement for resistance evaluation was performed over the frequency range of 1-10^6 Hz. Temperature dependence of proton conduction was also analyzed in the range of 20 to 80 °C. The in-plane proton conductivity was calculated from the equ (6).

$$\sigma = \frac{L}{RA} \quad (6)$$

Where σ is the proton conductivity in S cm^{-1}, L is the distance between the reference electrodes, A is the cross-sectional area of the membrane sample, and R is the resistance.

6.2.8 Methanol permeability and selectivity

Methanol permeability was measured at room temperature in a simple glass vial set-up reported by several authors[128-130]. 4 mL glass vials were filled with 2 mL pure methanol. The membranes were clamped between the mouth of the glass and the cap. The cap had an 8.5 mm diameter hole so that the methanol vapor could escape only through the hole. The weight loss was recorded as a function of time. The methanol permeability (P) was calculated by applying equ (8) derived form of Fick's first law (7):

$$J\left(\frac{N}{A \times t}\right) = -D\frac{dC_m}{dx} = -DK\frac{\Delta C_g}{l} = -P\frac{\Delta P}{l} \quad (7)$$

Where J is the molar flux of methanol, D is the methanol diffusivity, K is the partition coefficient of methanol in the membrane, C_m is the methanol concentration in the membrane and ΔC_g is the methanol concentration in the gas phase, which could be approximated using the vapor pressure of methanol.

$$P = \frac{N \times l}{\Delta P \times A \times t} \quad (8)$$

N is the number of moles of methanol lost (moles), l is the thickness of the membrane (cm), ΔP is the saturated vapor pressure of methanol (16,077 Pa), A is the area of the small hole on the cap (cm^2), and t is the time (days). The relative permeability of the Nafion® sample to the composite membrane (P/ P_{Nafion}) was also reported as a parallel comparison.

6.2.9 Thermal and hydrolytic Stability

Thermal stability of the membranes was analyzed by thermogravimetric analysis (TGA, Q50 TA Instrument). TGA measurements were performed under a nitrogen atmosphere from 40 to 600 ºC at a heating rate of 10 ºC /min.

The hydrolytic stability of the membranes was evaluated by soaking the membranes in 60 ºC water for up to 2 weeks while monitoring the change in proton conductivity values. The proton conductivity was determined in HPLC-grade water at room temperature.

6.3 Results and discussions

6.3.1 Chemical Analysis

Figure 6.1 showed the crosslinking mechanism for the CNC/PVA with SSA. Both CNC and PVA could be thermally crosslinked with SSA via the esterification between –OH of Cellulose and PVA and –COOH of SSA. The degree of crosslinking was controlled by varying the SSA composition, as well as the crosslinking environment (temperature and time). The resultant crosslinked membrane was designated 10CXS-Y, where X denotes the weight percentage of SSA based on the weight of PVA and CNC in the film, and Y denotes the temperature for crosslinking. Because SSA contains sulfonic acid group, thus it acted as both crosslinking agent and proton conductor.

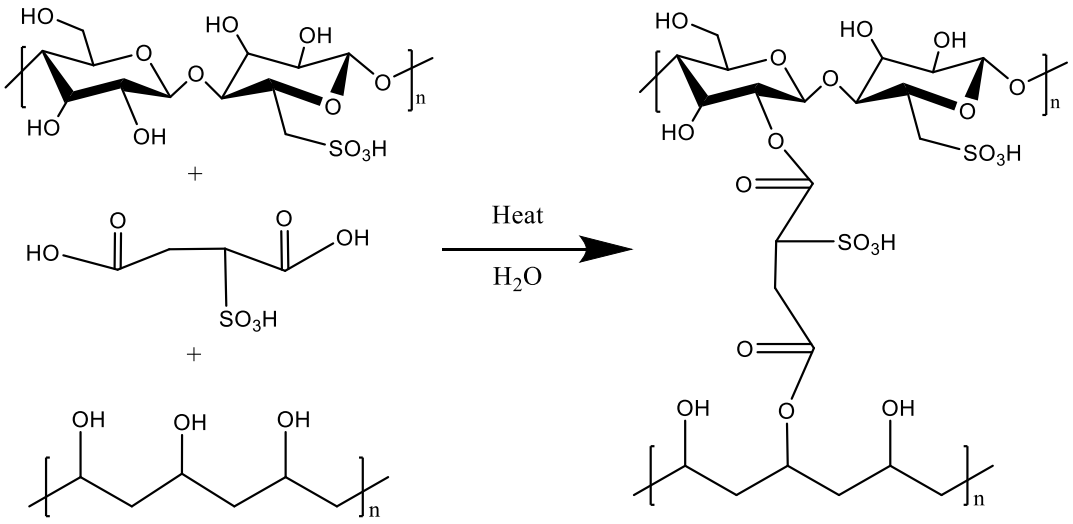

Figure 6.1 The presumptive crosslinking mechanism and structure of crosslinked PVA/CNC membrane with SSA

The chemical structure of PVA/CNC membranes comprising SSA as a crosslinking agent was investigated by ATR-FTIR spectra as shown in Figure 6.2. Two characteristic bands of –OH group and C-H stretching vibration from alkyl group was observed around 3270 cm^{-1} and 2939 cm^{-1}, respectively, in pristine PVA/CNC film. The band at 1730 cm^{-1} represented the ester group formed during crosslinking, and its intensity increased with the amount of the SSA, as well as increasing crosslinking temperature. Two significant bands at 1236 and 1030 cm^{-1} were related to the sulfonic acid group that could be presented in acid-hydrolyzed CNC and by the introduction of SSA. The increase in these two bands was also observed with increasing SSA loading and crosslinking temperature. The results indicate that the sulfonic acid groups were incorporated and the crosslinking reaction depending on the amount of SSA, and temperature.

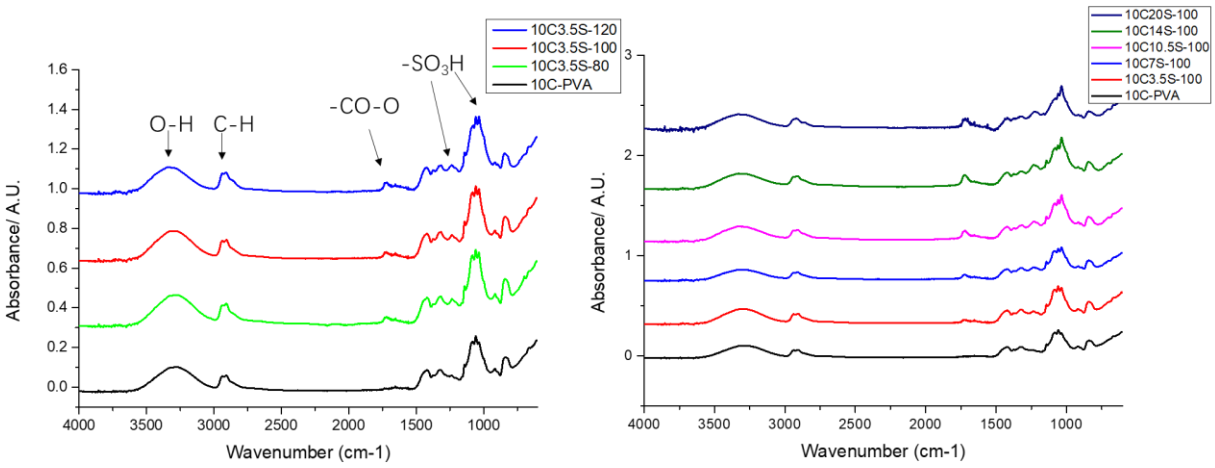

Figure 6.2 ATR-FTIR spectra of the crosslinked PVA/CNC membrane for 2h. Left: crosslinked at different temperature with 3.5 wt.% SSA. Right: crosslinked at 100 ºC with different SSA composition

It was well known that water resides in the hydrophilic region of the ionomers, facilitate proton transportation. However, both PVA and CNC were soluble in hot water, result in the loss of structural stability and cause the leakage of the composite membrane. In this regard, after the crosslinking treatment, the hydrophobicity of the CNC/PVA membrane could be controlled, which led to higher dimensional stability in water. Meanwhile, the presence of sulfonate groups could open-up the PVA/CNC interfaces, results in more space to accommodate water molecules.

6.3.2 Water uptake, IEC and thermal analysis

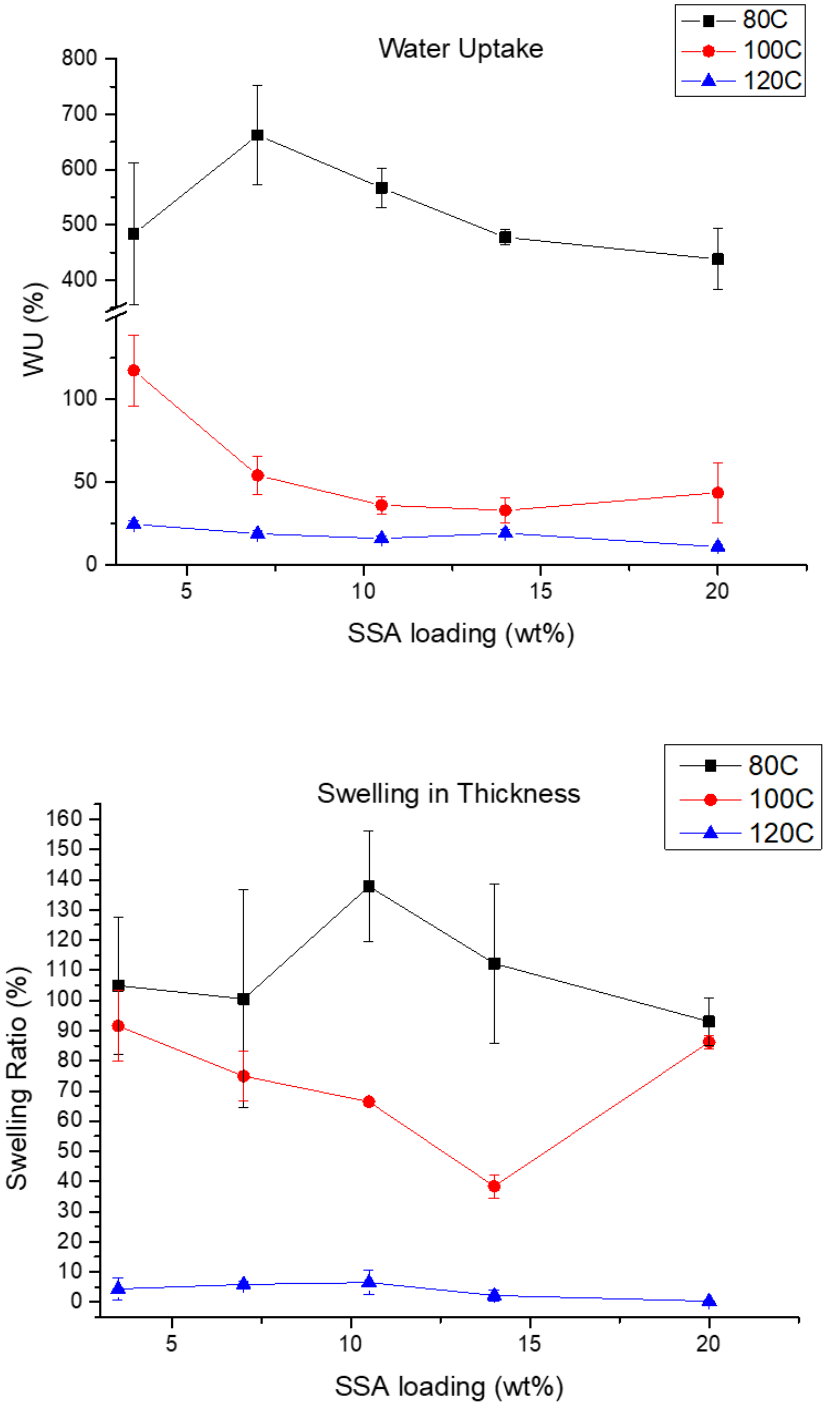

Figure 6.3 Top: Water uptake and Bottom: Swelling behavior of PVA/CNC/SSA membranes as a function of SSA concentration

Water uptake and swelling in the thickness direction of crosslinked PVA/CNC/SSA membrane with different amount of SSA and crosslinking condition were shown in Figure 6.3. It was shown that high water uptake was found in all membrane prepared at 80 ºC, although the water content decreased with increasing crosslinking time. This indicates that the membranes were only partially crosslinked, which consequently led to excessive swelling and dissolution. Change of temperature to 100 ºC would significantly improve the crosslink density through the esterification. The membranes crosslinked at 120 ºC showed minimal water uptake, which is similar to the WU found in hydrophobic Nafion® membrane (20-30%).

On the other hand, the WU of the membranes crosslinked at 100, and 120 ºC decreased with the SSA concentrations up to 14 wt.%, indicating that more rigid and compact polymer structure was formed by increasing the degree of crosslinking. Above this concentration, the WU and % swelling in the membrane crosslinked at 100 ºC increased slightly again and the membranes crosslinked at 80 and 120 ºC decreased continuously. The abrupt change in water uptake when high SSA concentration introduced was reported before [106, 109, 131]. The increase in hydrophilicity in 10C20S-100 membrane was presumably due to the fact the increase of sulfonic acid group suppresses the effect of crosslinking at this condition.

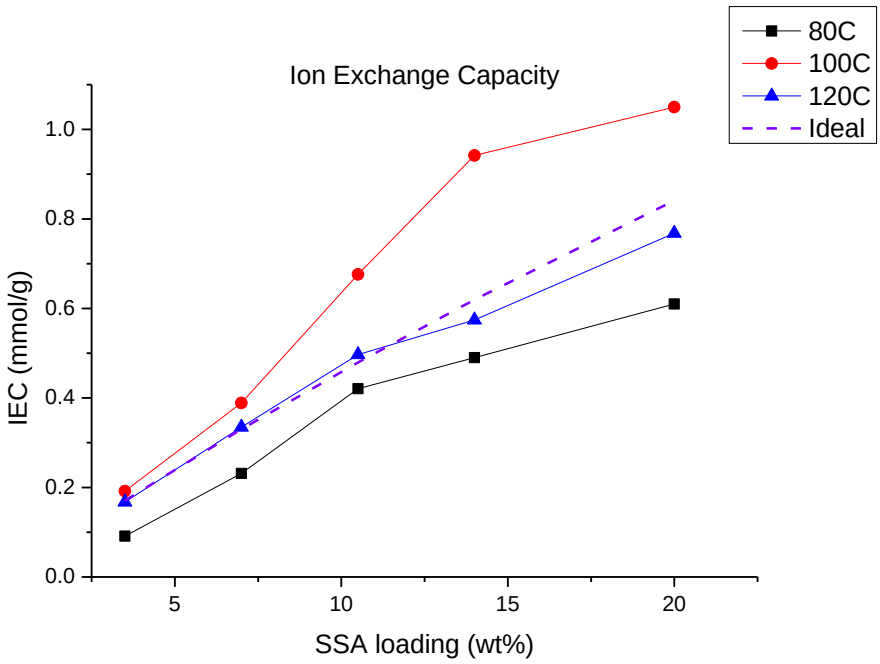

Figure 6.4 IEC values in the PVA/CNC/SSA membranes as a function of SSA concentration and the crosslinking temperature

Figure 6.4 shows that Ion exchange capacity in the PVA/CNC/SSA membranes depends upon the SSA content. The IEC values represent the molar content of the ion exchange site to membrane weight. The IEC values of the membranes crosslinked at 80, 100 and 120 ºC increased with the amount SSA, mostly due to the increased content of sulfonic group incorporated into the polymer. The IEC of membranes treated at 120 ºC almost coincide with the theoretical values, indicating a fully crosslinked network. Membranes treated at relatively low temperature are not fully crosslinked. Membranes crosslinked at 100 ºC would have unreacted carboxylic acid groups in the SSA, which can also act as ion-exchangeable sites and thus had higher IEC values than theoretical prediction. Membranes crosslinked at 80 ºC, however, had more unreacted SSA that were likely to be washed off during sample preparation, which led to lower IEC values. Also, the membranes crosslinked at 80 ºC were re-dissolve in hot water during conductivity measurement, thus

were not analyzed for the rest of the tests. Therefore, it might be important to precisely control the crosslinking conditions regarding SSA concentration and thermal treatment condition. It was worth to note that the IEC value of 10C20S-100 is close to the IEC value of commercial Nafion® Membrane which is around 1 mmol/g. According to the water uptake and IEC results, the water molecules per ionic exchange group (λ) were summarized in Table 6.1. Similar to water uptake, membranes treated at lower temperature had larger hydration number than the ones treated at a higher temperature, which may indicate higher water utilization in the membranes crosslinked at 100 ºC.

Table 6.1 Water uptake, IEC, hydration number, free water and ionic conductivity of CNC/PVA/SSA membranes

Sample	Water Uptake （%）	IEC (mmol/g)	Hydration Number (λ)	Enthalpy of freeze peak (J/g)	W_f (%)	W_b (%)
10C3.5S-100	117.3	0.19	33.98	69.54	20.8	96.5
10C7S-100	54	0.39	7.71	34.41	10.3	43.7
10C10.5S-100	36	0.68	2.96	7.84	2.3	33.7
10C14S-100	32.8	0.94	1.93	14.54	4.4	28.4
10C20S-100	43.5	1.05	2.54	23.57	7.1	36.4
10C3.5S-120	24.5	0.17	8.13	0.00	0	24.5
10C7S-120	18.7	0.33	3.10	0.00	0	18.7
10C10.5S-120	15.9	0.50	1.78	0.00	0	15.9
10C14S-120	19.1	0.57	1.85	0.00	0	19.1
10C20S-120	10.9	0.78	0.78	0.00	0	10.9

Water is a crucial molecule for ionomeric membranes. The water molecules reside in the polyelectrolyte membrane facilitate proton transportation via the Grotthuss mechanism. Thus, the higher water content in the film could contribute to greater proton conductivity. There are two types of water occurs in the membrane, free and bound (freezable and non-freezable) water. With increasing temperature, free water is removed first, which leads to an increase in electrolyte ohmic resistance. Also, too much free water could result in flooding of the ionomeric channels and reduce the efficiency of proton transport or loss of mechanical stability. Meanwhile, non-freezable water is bound to an ion or polar polymer surface and remain in the membrane to assist proton transportation at elevated temperature. The state of water in the crosslinked membranes was investigated by DSC. The melting peaks of free water in the DSC thermograms were shown in Figure 6.5. The weight percentage of free water and bound water were summarized in Table 6.1. There were no melting peaks observed for membranes crosslinked at 120 ºC, indicates the all the water being absorbed are bound water. In the case of membranes crosslinked at 100 ºC, the amount of free water decreased abruptly at the SSA content of 10.5 wt.% and then increased with more addition of the SSA. The fraction of bound water for membranes crosslinked at 100 ºC is 2-4 times higher than membrane crosslinked at 120ºC with the same SSA content. Thes results indicated the crosslinking condition could be optimized to achieve a high fraction of water molecules in the bounded state with little free water.

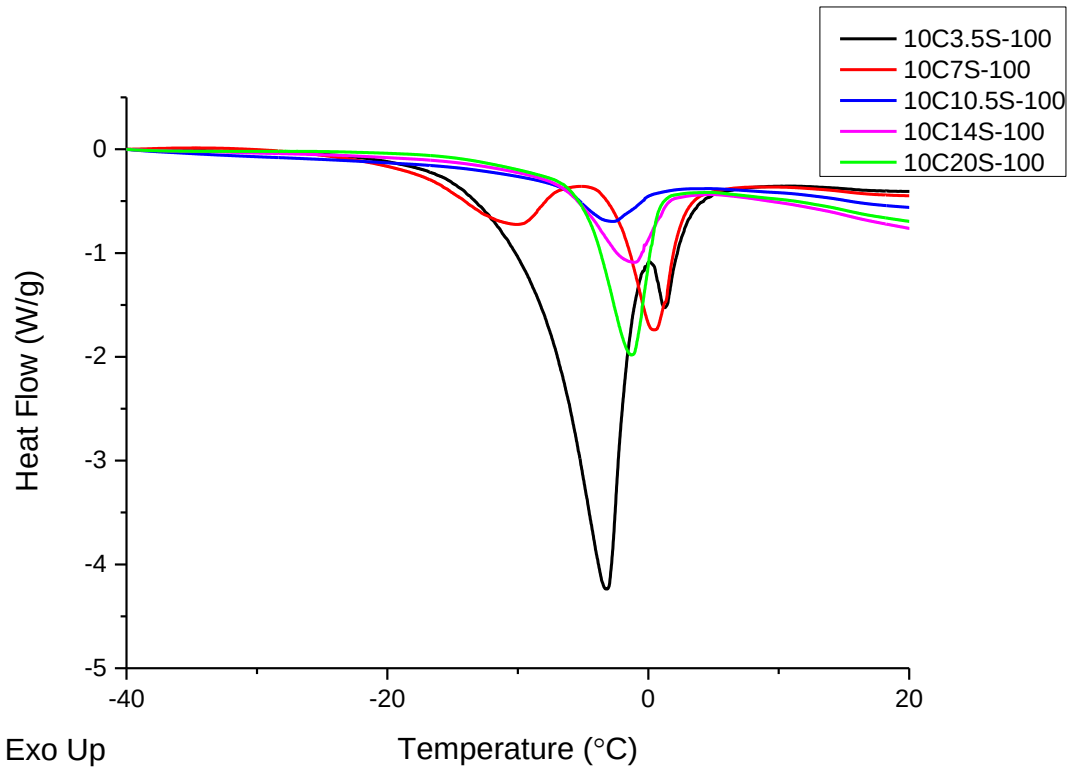

Figure 6.5 Melting curves of PVA/CNC/SSA film with different SSA content at the vicinity of 0 ºC

6.3.3 Proton conductivity measurement

Proton conductivity in polymeric systems is a critical issue in the development of new PEM. An Ideal PEM should allow fast proton transportation that matches up to the performance of well-established proton conductor such as Nafion®. Most of the alternative membrane showed the conductivity in the range of 10^{-5} to 10^{-2} S/cm. Figure 6.6 and Figure 6.7 showed the variation of proton conductivity with temperature for both recast Nafion® and PVA/CNC based membranes crosslinked at different temperatures. The conductivity of the composite membrane seems to be dependent upon the SSA loading and the crosslinking temperature. Since sulfonic acid groups present in SSA could provide an accessible pathway for proton migration, the value of conductivity was improved by increasing the

SSA content. Membranes crosslinked at 100ºC showed higher conductivity values as compared with the membranes crosslinked at 120ºC. As mentioned, the degree of crosslinking will be significantly changed by varying the crosslinking temperature. Membrane crosslinked at a higher temperature will have a more compact structure with narrower or dead-end conduction nano-channel causing the counter effect. For the membranes crosslinked at a lower temperature, the unreacted carboxylic acid groups present in the ionomers could also act as proton conductors. Also, more hydrophilic ionic channels formed by the arrangement of the hydrophilic polymeric group through hydrogen bonds between the hydroxyl group of PVA or CNC, and the sulfonic and carboxylic acid group of SSA. In accordance with DSC results, it was suggested that a critical hydrophilic domain in a polymer matrix should be considered to provide free volume for the bound water, which helped proton transport in those regions. However, the proton conductivity of the best-performed membrane 10C20S-100 was still about three times lower than the recast Nafion® membrane over the whole temperature range of investigation (20-80ºC). Further optimization of the composite membrane, aiming in particular for the increase in proton conductivity was not been considered in this work.

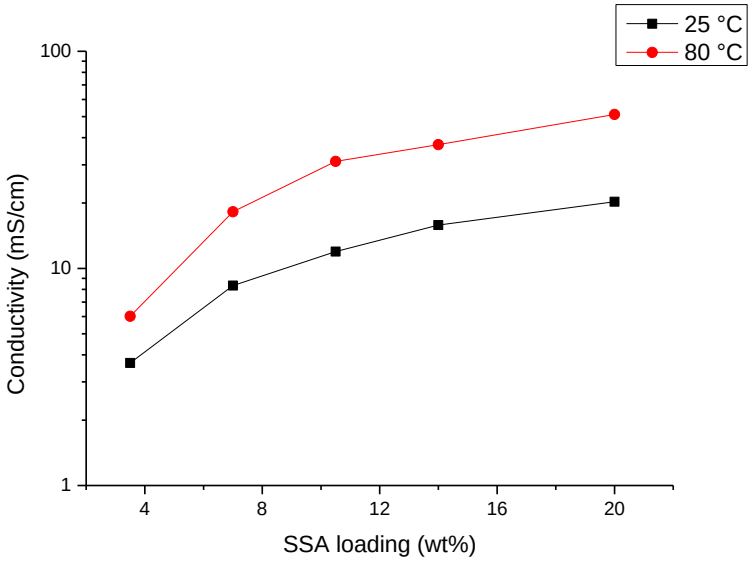

Figure 6.6 Effect of SSA loading on the proton conductivity of PVA/CNC membrane crosslinked at 100 ºC

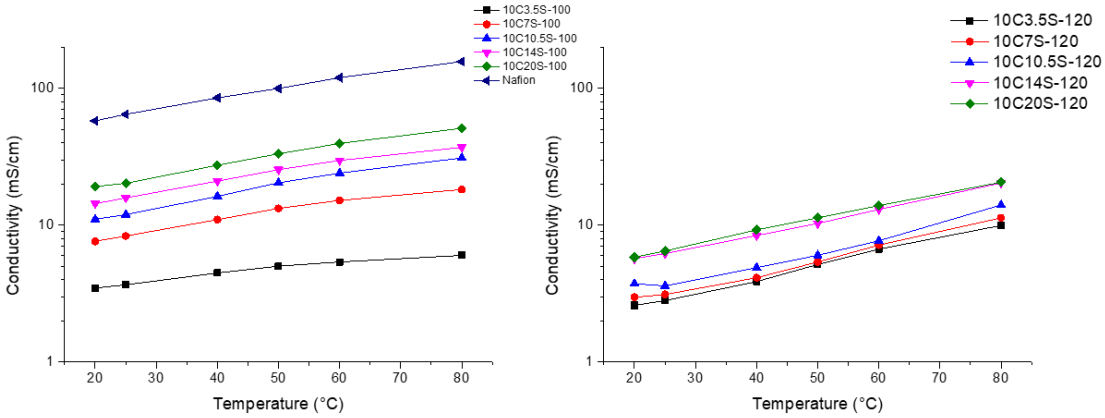

Figure 6.7 Proton conductivity as a function of the temperature of PVA/CNC membrane crosslinked at Left: 100 ºC Right： 120 ºC

Generally, the proton conductivity increases with temperature and follows the Arrhenius relationship with the equation:

$$\sigma = \sigma_0 \exp(-\frac{E_a}{RT}) \qquad (9)$$

where σ is the proton conductivity, σ_0 is a fitting parameter, E_a is the activation energy of proton transport, R is the universal gas constant (8.314472 $Jmol^{-1}K^{-1}$), and T is the absolute temperature in K. Table 6.2 summarized the activation energy fitted from the Arrhenius equation. The membrane crosslinked at 100 ºC showed a similar activation value, about 13 to 15 kJ mol^{-1}, to the value of Nafion® except for 10C3.5S-100 (E_a= 8.15 kJ mol^{-1}). This indicated that the same proton conduction mechanism in both types of samples. The activation energy for the membranes crosslinked at 120 ºC was slightly higher with the value in a range of 18 to 22 kJ mol^{-1}.

Table 6.2 Obtained parameters from Equation 9

Sample	**Fit Equation**	**R^2**	**σ_0 (mS cm^{-1})**	**E_a (kJ mol^{-1})**
10C3.5S-100	lnσ=-0.987T^-1-2.278	0.981	0.10	8.15
10C7S-100	lnσ=-1.558T^-1+0.457	0.990	1.58	12.95
10C10.5S-100	lnσ=-1.845T^-1+1.785	0.996	5.96	15.34
10C14S-100	lnσ=-1.679T^-1+1.496	0.995	4.46	13.96
10C20S-100	lnσ=-1.755T^-1+2.014	0.997	7.49	14.59
10C3.5S-120	lnσ=-2.373T^-1+2.089	0.994	8.08	19.73
10C7S-120	lnσ=-2.593T^-1+2.756	0.986	15.70	21.56
10C10.5S-120	lnσ=-2.290T^-1+2.078	0.951	7.99	19.04
10C14S-120	lnσ=-2.181T^-1+2.225	0.991	9.25	18.13
10C20S-120	lnσ=-2.180T^-1+2.278	0.999	9.76	18.13
Nafion®	lnσ=-1.709T^-1+2.999	0.999	20.07	14.21

Generally, there are three proton migration mechanisms take place in electrolyte membranes. The dominant one is the Grotthuss mechanism, where a proton is passed through a chain of water molecules via formation and cleavage of hydrogen bonds. The second transport mechanism is the vehicle mechanism. In this case, proton combines with water molecules and diffuses as hydronium ions. The last mechanism is associated with proton hopping along with the sulfonic and carboxylic acid groups along the nanochannel surface. Together with DSC and water uptake result, the dominant proton transport in the composite membranes should occur close to the ion exchange sites, with the assistant of bound water to perform the Grotthuss-like mechanism. Additionally, free water in the membranes assist vehicle mechanism and the presence of acid groups provide the formation of more reachable places for protons to hop. From these results, lack of free and bound water molecules in composite membranes crosslinked at 120 ºC due to the over-crosslinked structure led to high activation energy and restrict the proton conduction.

6.3.4 Methanol permeability and selectivity measurement

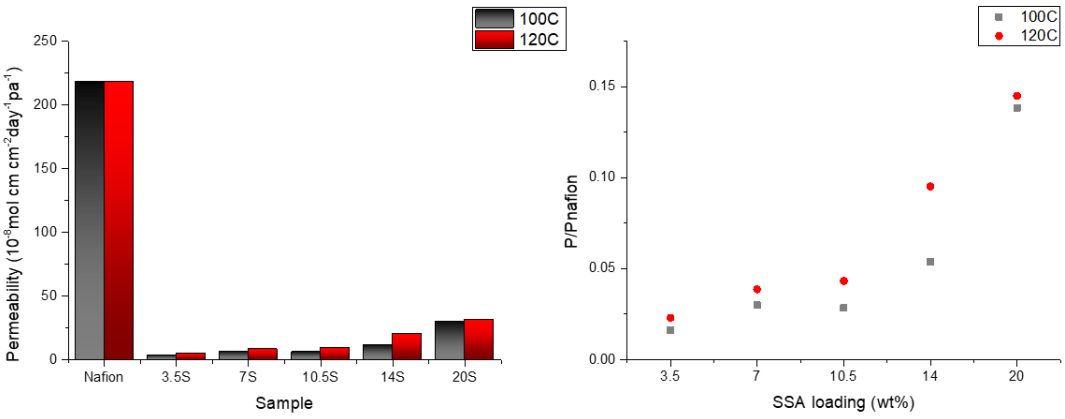

Figure 6.8 Methanol permeabilities of the PVA/CNC/SSA membranes in comparison to Nafion® at Room Temperature

One of the essential criteria for PEM used in a fuel cell is to have an effective barrier for fuel crossover. Methanol permeation across the electrolyte membranes in DMFCs causes chemical oxidation of methanol at the cathode with the help of the catalyst. Thus, diminishes fuel cell efficiency and performance[89]. Methanol permeability measurements were shown in Figure 6.8. The notable feature in the left figure was that the PVA/CNC based membranes show significant improvement in the methanol barrier property compared to Nafion®. The methanol permeability of the PVA/CNC/SSA membranes were only about 2-14 % of that of Nafion®. Such favorable property is the result of the crosslinking structure and good filler-matrix interaction, which creates a tortuous path for methanol penetrants as well as reduced membrane's void due to strong H-bonding. The enormous hydroxyl groups presented on the PVA surface gave rise to the high polarity and thus made PVA more accessible with high polar molecules like water and was very resistance to hydrocarbons. This made crystalline PVA an effectivity barrier for alcohol compounds. Increased degree of crosslinking by introducing more acid and higher temperature treatment would significantly consume the hydroxyl groups presented on both PVA and CNC surface, thus led to this decrease in its barrier properties. It also could be seen that the methanol transport behavior was consistent with the IEC behavior of the membranes, with increasing SSA loading, the methanol permeation rate increases, which is associated with the hydrophilic nature of the sulfonic acid groups. It was also interesting that the methanol permeability of the PVA/CNC/SSA depends on the crosslinking temperature. Membranes crosslinked at higher temperature have more rigid structures that should reduce the methanol transport path. However, the crosslink reaction could also prohibit the formation of the crystalline structure of PVA. The decrease in the crystallinity

could make it easy for methanol to be transported through the polymer membrane. Meanwhile, the membranes treated at 120 ºC became brittle and could form micro defects during specimen fabrication and sample attachment, influencing the test results.

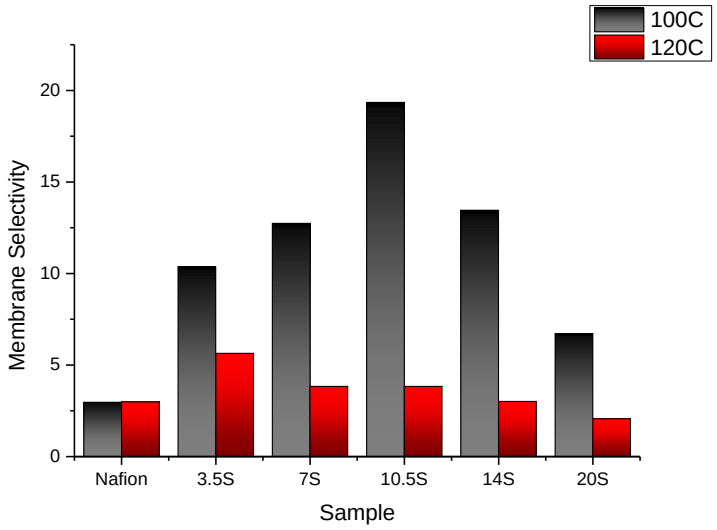

Figure 6.9 Membrane selectivity of crosslinked PVA/CNC membranes compared to Nafion®

An electrolyte with high proton conductivity and low methanol crossover is the crucial elements of direct methanol fuel cells. Selectivity, which is the ratio of the ionic conductivity to the methanol permeability is usually calculated to evaluate the performance of a membrane in DMFC applications. As shown in Figure 6.9, the 10C10.5S-100 sample had the highest selectivity value, which was about six times higher than that of Nafion®. The experiment result showed that at lower SSA concentrations (below 10.5wt%), the restriction to methanol diffusion overplays the promotion of proton transport by the incorporation of sulfonic acid groups. At higher SSA loading, the increase of sulfonic

groups exacerbates the methanol diffusion problem and results in a decreased membrane selectivity.

6.3.5 Hydrothermal stability

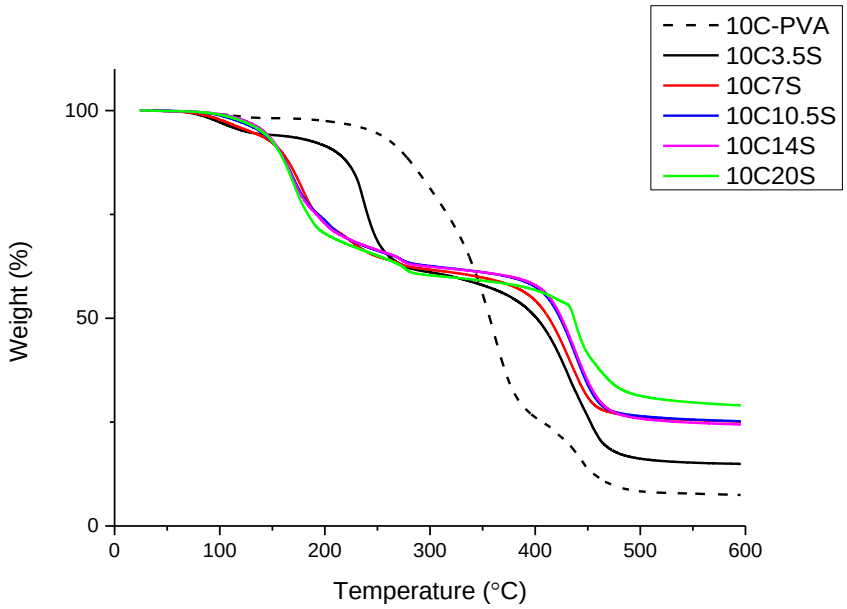

Figure 6.10 TGA thermograms of unmodified and crosslinked PVA/CNC based membranes (100 ºC)

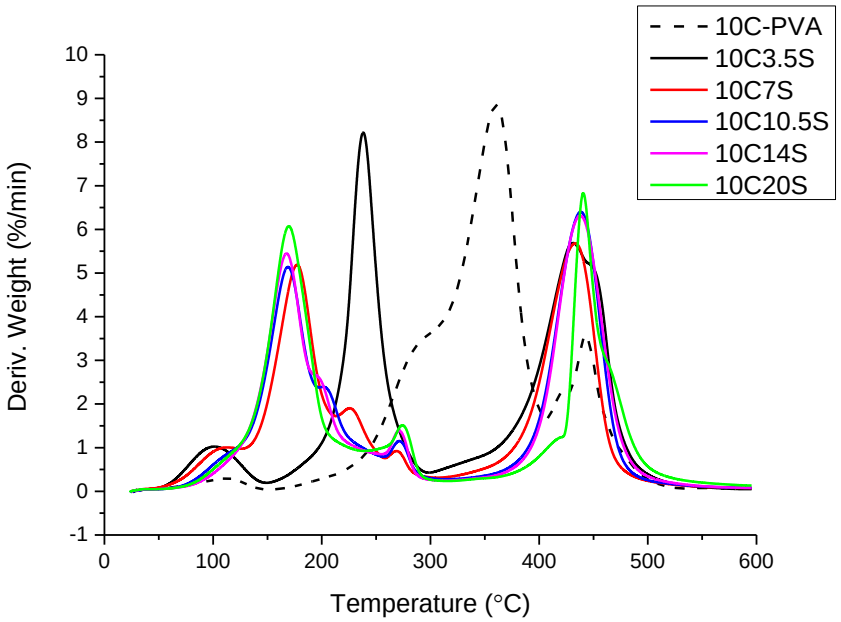

Figure 6.11 Derivative TGA curves of the unmodified and crosslinked PVA/CNC based membranes (100 ºC)

The thermal stability of the unmodified and crosslinked PVA/CNC membranes was evaluated through the TGA experiments. It was found that the CNC reinforced PVA nanocomposite showed three major weight loss regions. As seen from

Figure 6.10, the initial weight loss of 30-140 ºC was attributed to the evaporation of the water of the composite films. The second stage of thermal degradation occurred at around 220 -380 ºC and with the total weight loss around 70%. This loss is mainly due to the structural degradation of the PVA and CNC and involves the elimination of side groups such as sulfonic acid groups. The last degradation process started above 400 ºC, dominated by cleavage of the long PVA chains and the decomposition of the carbonaceous materials. Incorporation of SSA in the PVA/CNC matrix clearly affects the thermal stability. The initial weight loss became much more significant with the presence of SSA as a consequence of water formed as a by-product of further esterification. The increasing of the sulfonic acid group shifted the second degradation stage to lower temperature as seen in Figure 6.11. It was seen that the weight loss over the second degradation stage was decreased by increasing the SSA content of the membranes. This result implied higher thermal stability was achieved by crosslinking the membrane. About 30% weight loss during this stage could be attributed to the loss of sulfosuccinic acid and breakage of the ester bonds. Meanwhile, the structural degradation of PVA and CNC may be accelerated by the acid environment of the sulfonic acid groups added by SSA [77, 110]. The remaining char content of membranes upon reaching 600 ºC was also increased with the increase of SSA concentration. It was noteworthy that all crosslinked membranes were thermally stable at the desired operating temperature range for DMFC applications.

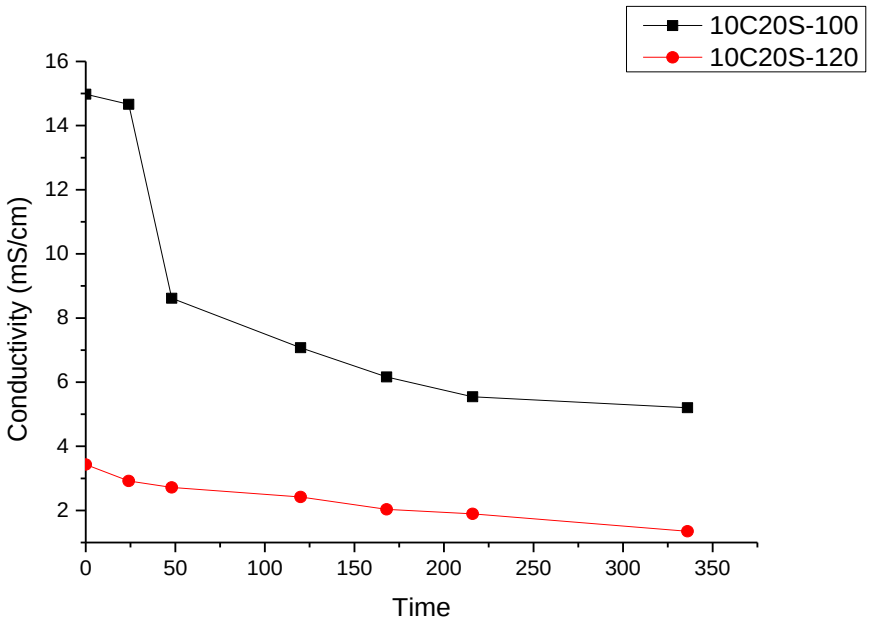

Figure 6.12 Hydrolytic stability of the PVA/CNC/SSA membranes at 60 ºC

Long-term hydrolytic stability of PEMs is of great importance for DMFC applications. The hydrolytic stability was evaluated by monitoring the proton conductivity of the membranes soaked in 60 ºC water over 2 weeks. As shown in Figure 6.12, the percent of conductivity reduction was found to be 65% and 61% for 10C20S-100 and 10C20S-120 after 2 weeks, respectively. Although near no change in proton conductivity was observed in 10C20S-100 sample after 24 h, indicating the crosslinked structure was stable for that short period. This result confirmed the unstable covalently cross-linked structure, mainly due to the hydrolysis of the ester linkage, especially with the sulfonic acid groups act as an acid catalyst. An alternative approach to increase membrane stability should be considered before starting the single cell performance tests with the membrane electrode assembly (MEA). By using different types of crosslinker or binary crosslinking agents, such as the switch from aliphatic to aromatic dicarboxylic acids or use dialdehyde and diisocyanate

crosslinker [111, 132]. A membrane with better thermal and hydrolytic stability, as well as increased proton conductivity may be fabricated.

6.4 Conclusion

A series of crosslinked PVA/CNC membranes, comprising different amounts of sulfosuccinic acid were prepared and evaluated as a potential polymer electrolyte membrane for direct methanol fuel cell applications. FTIR spectroscopy showed the successful incorporation of SSA into the PVA/CNC matrix via esterification reactions. IEC value and proton conductivity of the composite membranes were increased with SSA loading. Both SSA content and crosslinking temperature controlled the degree of crosslinking. It was found that the crosslinking level should be controlled to obtain a critical room to retain bond water, which played the dominant role in the proton transport within the membranes. The composite membranes had the proton conductivity in the range of 10^{-3} to 10^{-2} S/cm, which matched with Nafion® membrane. The membrane crosslinked at 100 ºC showed similar activation energy to the value of Nafion®, indicated that the same proton conduction mechanism. The methanol permeability of the PVA/CNC/SSA membranes were about 2-14 % of that of Nafion®, which means the methanol crossover problem was significantly alleviated. Together, the optimum sample 10C10.5S-100, provided membrane selectivity that was six times higher than the value of Nafion®. Considering these advantages of the synthesized membrane, including low cost, convenient preparation method, and high selectivity, such bio-based nanocomposite PEMs could be a good candidate for DMFC applications.

Chapter 7. CONCLUSIONS AND FUTURE DIRECTIONS

This work provides a basis for designing CNC based composites with different polymer systems, processing methods, and for targeting different end applications to help to identify CNC's value in the market. In this chapter, a summary of the major findings of the CNC based polymer nanocomposites systems was presented. Based on the results and experimental observations, potential future works will be outlined.

7.1 Concluding Remarks

The project mainly used the solution casting process and impregnation technique for sample preparations. In Chapter 3 and 4, the role of residual solvent and the compatibility between different epoxy matrix and CNC was analyzed. We found the optimized dispersion methods and processing strategies for cellulose nanocrystal in epoxy resins with improved nanofiller distribution. Through this research, an increased understanding of the processing-structure-property relationships of CNC/polymer nanocomposite is obtained and provide useful insight for designing the CNC/epoxy formulations.

In Chapter 3, two processing strategies to prepare CNC/epoxy composites were studied, with bulk or dropwise mixing. For both cases, CNC solution would first combine with hardeners to make a homogeneous, well-dispersed CNC/hardener mixture before mixing with the epoxy monomer. There was a trend of increase tensile strength and elastic modulus with increase CNC loading. Higher tensile properties of the composites were found by dropwise mixing than that of the composites prepared by bulk mixing. The considerable difference observed in composite samples could be mainly resulted from an improved level

of CNC dispersion and CNC/hardener distribution in the epoxy matrix when adding both solutions dropwisely. The effect of solvent was also studied. Dispersing freeze-dried CNCs into the hardener without the aid of the solvent led to the aggregation of CNCs at microscale which could be observed from the microscopic analysis. No significant difference in tensile performances was found when preparing nanocomposite at full or partial solvent residues prior to curing using bulk dispersion strategy. However, higher tensile strength, modulus, and work of fracture of the nanocomposite were observed for regular sample compared to solvent removal samples when using dropwise mixing method. This indicates a certain level of solvent should be retained in the composite solution, to lower its viscosity and thus allow better mixing. No significant change was found in thermal properties with respect to different residual solvent dosages or mixing protocols. This study highlights the effect of processing methods and the use of a proper solvent to disperse CNC into a polymer system with low compatibility.

In Chapter 4, a different crosslinking agent was selected to test the compatibility of CNC with this new system by evaluating the composite performance. Unlike the results found in the last chapter, whereas the filler effect was more significant than the solvent effect in previous crosslinker system. In this study, nanocomposite cured with PEA diamine crosslinker with a more hydrophobic backbone structure showed an optimum tensile performance with 3 wt.% CNC loading. The plasticizing effect of residual solvent became prominent that significantly changes the cured composite structure at higher CNC loading or higher solvent dosage. A clear brittle to ductile transition was found at 5 wt.% CNC loading, with a sudden drop in tensile strength and five times increases in the strain at failure compare to sample prepared at 3 wt.% CNC loading. The split of T_g peaks found

from DMA measurement suggests that the gradual change of crosslinking density across the thickness of the films. The pre-solvent removal step could moderately improve thermal performance compared to regular samples. For solution cast CNC/Epoxy systems, more effective reinforcement of CNCs was attained when using higher hydrophilic hardener. When switching to rigid and less hydrophilic systems, the detrimental effect of the solvent should be considered, and only low CNC loading should be incorporated into the polymer system.

From our second design, a more compatible PVA-CNC based nanocomposite was studied. Aqueous solution casting of CNC into PVA allows larger solution processing and easier drying, with advantages of reducing the costs and environmental concerns of using organic solvents. No macroscopic scales of CNC agglomerations were found in the composites film up to 30 wt.% CNC loading. Effect mechanical reinforcement of CNC was achieved for low CNC loadings (10 wt.%), however, at high CNC loading of 20 and 30 wt.%, the films were brittle in nature and change of specimen preparation method for these samples may affect the polymer structure and introduce defect into the films. From the thermal analysis, percent crystallinity decreased with increasing CNC content due to the micro-crystallization of PVA near CNCs. Thermal stability of the composite films with up to 20 wt.% CNC content was greater than both neat PVA and neat CNC. Increased T_g was also observed up to 20 wt.% CNC loading due to the restriction of the CNCs on the polymer chains and near-surface micro-crystallization. This study illustrated good compatibility of PVA and CNC, and the processing-structure-property relationship of CNC/PVA nanocomposite systems was assessed. This robust, renewable and biodegradable films can be formulated for different applications. Considering the handleability and possible post-

chemical treatment of the film, a composite film at 10 wt.% CNC loading was recommended.

Finally, the use of PVA/CNC based membrane for direct methanol fuel cell application was evaluated. Sulfosuccinic acid (SSA) was used as both crosslinking agent and proton conductor to synthesis the ionomers with a series of crosslinking conditions. The composite films prepared had a proton conductivity in the same magnitude with much lower methanol permeability compared to a commercial perfluorinated membrane (Nafion®). The optimum composition of the composite membrane was six times higher in selectivity than the corresponding value for Nafion®. The convenient preparation method, low cost, thermal stability, and recycling potential demonstrated such bio-based nanocomposite PEMs could be a good candidate for DMFC applications.

7.2 Suggested Future Works

As discussed in Chapter 2.2.1, there are two possible organic solvents that can be used to dissolve/disperse both CNC and epoxy, dimethylformamide (DMF) and dimethyl sulfoxide (DMSO). Our current work focusing on using DMF due to the limitation of the processability in the lab. A recent study indicates that DMSO/H_2O co-solvent can help to individualize the CNC nanofibers in the system better than DMF/H_2O co-solvent. Also, DMSO is another solvent widely used in the industry as it does not cause reproductive problems. Therefore, further study of the reformulation is required to validate the use of DMSO over DMF. If the sample does not perform optimally, we can screen DMF/DMSO/H_2O solvent mixtures.

Another future study for the CNC/epoxy composite could be directed by blending of ED 600 with other diamine crosslinkers. ED 600 can act as both epoxy crosslinker and non-ionic surfactant for CNC, and to tailor the compatibility of hygroscopic properties between CNC and epoxy system. To better stabilize the emulsion of the composite mixture, CNC solution should always mix with ED 600, prior to adding any other epoxy components into the solution.

Further research on scalable processing of aqueous CNC/PVA system is needed, particularly focusing on speed up the drying process to match the productivity in film industries and studies the effect of different speed drying methods and understand the process-structure-property relationship. Different end-applications such as membrane, packaging, paper or filter of PVA/CNC based film should be reviewed and a twist of the polymer formulation accordingly if required.

Future research on further developing bio-based electrolyte membrane in DMFC application is required. Our current CNC/PVA/SSA systems showed limited hydro-thermal stability that hindered the next step fuel cell design, which required to integrate the proton-exchange membrane into a membrane electrode assemblies (MEAs) and test it under DMFC operation condition. As mentioned in Chapter 2.3, chemical crosslinking of the polymer/CNC network is an effective method to improve thermo-mechanical performance and dimensional stability of the proton-exchange membrane. Currently, esterification between the hydroxyl groups on CNC or PVA with the carboxyl group on SSA is not stable enough in hot aqueous condition. The future design should focus on using more thermally stable crosslinkers that contain proton conductive sites, such as poly (styrene sulfonic acid-co-maleic acid) (PSSA-MA). Another approach is to utilize aldehyde based crosslinker to

chemically react with the hydroxyl groups to form hemiacetal or acetal compound with the aid of acid catalyst if it is required. A mix of different crosslinker/conductor or dual-crosslinker to achieve a better combination of electrochemical and thermo-mechanical performance is also recommended.

REFERENCES

1. Abraham, E., et al., *Highly Modified Cellulose Nanocrystals and Formation of Epoxy-CNC Nanocomposites.* ACS Appl Mater Interfaces, 2016.

2. Kwong Siong Kiew, S.H., Md Rezaur Rahman, *Comparative Study of Dielectric Properties of Chicken Feather/Kenaf Fiber Reinforced Unsaturated Polyester Composites.* BioResources, 2013. **8**(2).

3. Moon, R.J., et al., *Cellulose nanomaterials review: structure, properties and nanocomposites.* Chem Soc Rev, 2011. **40**(7): p. 3941-94.

4. Ng, H.-M., et al., *Review of Nanocellulose Polymer Composite Characteristics and Challenges.* Polymer-Plastics Technology and Engineering, 2016. **56**(7): p. 687-731.

5. Salas, C., et al., *Nanocellulose properties and applications in colloids and interfaces.* Current Opinion in Colloid & Interface Science, 2014. **19**(5): p. 383-396.

6. Junior de Menezes, A., et al., *Extrusion and characterization of functionalized cellulose whiskers reinforced polyethylene nanocomposites.* Polymer, 2009. **50**(19): p. 4552-4563.

7. Sapkota, J., et al., *Fabrication and Properties of Polyethylene/Cellulose Nanocrystal Composites.* Macromolecular Materials and Engineering, 2017. **302**(1): p. 1600300.

8. Jiang, H. and D.P. Kamdem, *Development of poly(vinyl chloride)/wood composites. A literature review.* Journal of Vinyl and Additive Technology, 2004. **10**(2): p. 59-69.

9. L. CHAZEAU, M.P., J. Y. CAVAILLE, *Plasticized PVC Reinforced with Cellulose Whiskers. I. Linear Viscoelastic Behavior Analyzed through the Quasi-Point Defect Theory.* J Polym Sci B: Polym Phys, 1999. **37**: p. 2151-2164.

10. Bondeson, D. and K. Oksman, *Polylactic acid/cellulose whisker nanocomposites modified by polyvinyl alcohol.* Composites Part A: Applied Science and Manufacturing, 2007. **38**(12): p. 2486-2492.

11. Lin, N., et al., *Surface acetylation of cellulose nanocrystal and its reinforcing function in poly(lactic acid).* Carbohydrate Polymers, 2011. **83**(4): p. 1834-1842.

12. El Miri, N., et al., *Bio-nanocomposite films based on cellulose nanocrystals filled polyvinyl alcohol/chitosan polymer blend.* Journal of Applied Polymer Science, 2015. **132**(22): p. 42004-.

13. Gaur, S.S., et al., *Thermo-mechanically stable sustainable polymer based solid electrolyte membranes for direct methanol fuel cell applications.* Journal of Membrane Science, 2017. **526**: p. 348-354.

14. Jahan, Z., M.B.K. Niazi, and Ø.W. Gregersen, *Mechanical, thermal and swelling properties of cellulose nanocrystals/PVA nanocomposites membranes.* Journal of Industrial and Engineering Chemistry, 2018. **57**: p. 113-124.

15. Peresin, M.S., et al., *Crosslinked PVA nanofibers reinforced with cellulose nanocrystals: Water interactions and thermomechanical properties.* Journal of Applied Polymer Science, 2014. **131**(11):

16. Ramezani Kakroodi, A., et al., *Mechanical, Thermal, and Morphological Properties of Nanocomposites Based on Polyvinyl Alcohol and Cellulose Nanofiber fromAloe veraRind.* Journal of Nanomaterials, 2014. **2014**: p. 1-7.

17. Cao, X., Y. Habibi, and L.A. Lucia, *One-pot polymerization, surface grafting, and processing of waterborne polyurethane-cellulose nanocrystal nanocomposites.* Journal of Materials Chemistry, 2009. **19**(38): p. 7137.

18. Xiaodong Cao, H.D., and Chang Ming Li, *New Nanocomposite Materials Reinforced with Flax Cellulose Nanocrystals in Waterborne Polyurethane.* Biomacromolecules, 2007. **8**: p. 899-904.

19. Luo, J., et al., *Influence of high loading of cellulose nanocrystals in polyacrylonitrile composite films.* Cellulose, 2017. **24**(4): p. 1745-1758.

20. Peng, S.X., R.J. Moon, and J.P. Youngblood, *Design and characterization of cellulose nanocrystal-enhanced epoxy hardeners.* Green Materials, 2014. **2**(4): p. 193-205.

21. Peng, S.X., et al., *Enhanced dispersion and properties of a two-component epoxy nanocomposite using surface modified cellulose nanocrystals.* Polymer, 2017. **112**: p. 359-368.

22. Tang, L. and C. Weder, *Cellulose whisker/epoxy resin nanocomposites.* ACS Appl Mater Interfaces, 2010. **2**(4): p. 1073-80.

23. Xu, S., et al., *Mechanical and thermal properties of waterborne epoxy composites containing cellulose nanocrystals.* Polymer, 2013. **54**(24): p. 6589-6598.

24. Ansari, F., et al., *Cellulose nanofiber network for moisture stable, strong and ductile biocomposites and increased epoxy curing rate.* Composites Part A: Applied Science and Manufacturing, 2014. **63**: p. 35-44.

25. Ansari, F., M. Skrifvars, and L. Berglund, *Nanostructured biocomposites based on unsaturated polyester resin and a cellulose nanofiber network.* Composites Science and Technology, 2015. **117**: p. 298-306.

26. Yuzuru Shimazaki, Y.M., Yoshitaka Takezawa, Masaya Nogi, Kentaro Abe, Shinsuke Ifuku, and Hiroyuki Yano, *Excellent Thermal Conductivity of Transparent Cellulose Nanofiber/Epoxy Resin Nanocomposites.* Biomacromolecules, 2007. **8**: p. 2976-2978.

27. Ghaderi, M., et al., *All-cellulose nanocomposite film made from bagasse cellulose nanofibers for food packaging application.* Carbohydr Polym, 2014. **104**: p. 59-65.

28. Ma, H., et al., *Green composite films composed of nanocrystalline cellulose and a cellulose matrix regenerated from functionalized ionic liquid solution.* Carbohydrate Polymers, 2011. **84**(1): p. 383-389.

29. Zhang, J., et al., *All-Cellulose Nanocomposites Reinforced with in Situ Retained Cellulose Nanocrystals during Selective Dissolution of Cellulose in an Ionic Liquid.* ACS Sustainable Chemistry & Engineering, 2016. **4**(8): p. 4417-4423.

30. Viet, D., S. Beck-Candanedo, and D.G. Gray, *Dispersion of cellulose nanocrystals in polar organic solvents.* Cellulose, 2006. **14**(2): p. 109-113.

31. Okura, H., M. Wada, and T. Serizawa, *Dispersibility of HCl-treated Cellulose Nanocrystals with Water-dispersible Properties in Organic Solvents.* Chemistry Letters, 2014. **43**(5): p. 601-603.

32. Huber, T., et al., *A critical review of all-cellulose composites.* Journal of Materials Science, 2011. **47**(3): p. 1171-1186.

33. Kim, J., et al., *Dispersion of cellulose crystallites by nonionic surfactants in a hydrophobic polymer matrix.* Polymer Engineering & Science, 2009. **49**(10): p. 2054-2061.

34. Brinatti, C., et al., *Structural and Energetic Studies on the Interaction of Cationic Surfactants and Cellulose Nanocrystals.* Langmuir, 2016. **32**(3): p. 689-98.

35. Ashori, A., *Nonwood Fibers—A Potential Source of Raw Material in Papermaking.* Polymer-Plastics Technology and Engineering 2006. **45**(10): p. 1133-1136.

36. Guthrie, A.H.a.J.T., *The chemistry and technology of cellulosic copolymers*. 1981, Berlin: Springer-Verlag.

37. Lavoine, N., et al., *Microfibrillated cellulose - its barrier properties and applications in cellulosic materials: a review.* Carbohydr Polym, 2012. **90**(2): p. 735-64.

38. Herrick, F.W.C., R.L.; Hamilton, J.K.; Sandberg, K.R., *Microfibrillated cellulose: morphology and accessibility.* J. Appl. Polym. Sci., 1983. **37**.

39. Turbak, A.F.S., F.W.; Sandberg, K.R., *Microfibrillated cellulose, a new cellulose product: properties, uses, and commercial potential.* J. Appl. Polym. Sci., 1983. **37**.

40. Ng, H.-M., et al., *Extraction of cellulose nanocrystals from plant sources for application as reinforcing agent in polymers.* Composites Part B: Engineering, 2015. **75**: p. 176-200.

41. Xu, X., et al., *Cellulose nanocrystals vs. cellulose nanofibrils: a comparative study on their microstructures and effects as polymer reinforcing agents.* ACS Appl Mater Interfaces, 2013. **5**(8): p. 2999-3009.

42. Karim Missoum, M.N.B.a.J.B., *Nanofibrillated Cellulose Surface Modification: A Review*. Materials 2013. **6**(5): p. 1746-1766.

43. Ruibin Wang, L.C., J.Y. Zhu, Rendang Yang, *Tailored and Integrated Production of Carboxylated Cellulose Nanocrystals (CNC) with Nanofibrils (CNF) through Maleic Acid Hydrolysis.* ChemNanoMat, 2017. **3**(5): p. 328-335.

44. Monika, P. Dhar, and V. Katiyar, *Thermal degradation kinetics of polylactic acid/acid fabricated cellulose nanocrystal based bionanocomposites.* Int J Biol Macromol, 2017. **104**(Pt A): p. 827-836.

45. Marielle Henriksson, L.A.B., Per Isaksson, Tom Lindstro¨m and Takashi Nishino|, *Cellulose Nanopaper Structures of High Toughness.* Biomacromolecules, 2008. **9**: p. 1579-1585.

46. Maureen A. Boyle, C.J.M., and John D. Neuner, *Epoxy Resins* in *ASM Handbook, Composites*. 2001, ASM International. p. 12.

47. Petrie, E.M., *Epoxy Adhesive Formulations*. 2006, New York: McGraw-HILL CHEMICAL ENGINEERING.

48. Bruce Burton, D.A., Howard Klein, Angela Garibay-Vasquez, Alan Pekarik and Chris Henkee *EPOXY FORMULATIONS USING JEFFAMINE® POLYETHERAMINES*. 2005.

49. Ratna, D., et al., *Novel epoxy compositions for vibration damping applications.* Polymers for Advanced Technologies, 2004. **15**(10): p. 583-586.

50. Patil, P.N., et al., *Free volumes and structural relaxations in diglycidyl ether of bisphenol-A based epoxy–polyether amine networks.* Soft Matter, 2013. **9**(13): p. 3589.

51. McKenna, A.L.a.G.B., *Effect of crosslink density on physical ageing of epoxy networks.* Polymer, 1988. **29**: p. 1812-1817.

52. Amir Asadi a, M.M.a., Robert J. Moon b,c, Kyriaki Kalaitzidou, <*Cellulose Nanocrystals as reinforcement in glass fiber epoxy sheet molding compound composites.pdf*>, in *SPE ANTEC*. 2016.

53. Asadi, A., et al., *Improving the interfacial and mechanical properties of short glass fiber/epoxy composites by coating the glass fibers with cellulose nanocrystals.* Express Polymer Letters, 2016. **10**(7): p. 587-597.

54. Asadi, A., et al., *Lightweight sheet molding compound (SMC) composites containing cellulose nanocrystals.* Composite Structures, 2017. **160**: p. 211-219.

55. Girouard, N., et al., *Exploiting colloidal interfaces to increase dispersion, performance, and pot-life in cellulose nanocrystal/waterborne epoxy composites.* Polymer, 2015. **68**: p. 111-121.

56. He, M., et al., *Microcrystalline cellulose as reactive reinforcing fillers for epoxidized soybean oil polymer composites.* Journal of Applied Polymer Science, 2015. **132**(36)

57. ISSAM I Qamhia, R.C.S., and Rani F. Elhajjar, *Static and Dynamic Characterization of Cellulose Nanofibril Scaffold-Based Composites.* BioResources, 2014. **9**(1): p. 381/392.

58. L. Cross, G.S., E. Mintz, Shanhong Xu, Natalie Girouard, Meisha Shofner, Carson Meredith, *Nanocellulose Reinforced Epoxy Elastomer*, in *36th Annual Meeting of the Adhesion*. 2013: Daytona Beach, FL.

59. Lu, J., P. Askeland, and L.T. Drzal, *Surface modification of microfibrillated cellulose for epoxy composite applications.* Polymer, 2008. **49**(5): p. 1285-1296.

60. Saba, N., et al., *Thermal and dynamic mechanical properties of cellulose nanofibers reinforced epoxy composites.* Int J Biol Macromol, 2017. **102**: p. 822-828.

61. Jabbar, A., et al., *Nanocellulose coated woven jute/green epoxy composites: Characterization of mechanical and dynamic mechanical behavior*. Composite Structures, 2017. **161**: p. 340-349.

62. Ma, I.A.W., et al., *Anticorrosion properties of epoxy/nanocellulose nanocomposite coating.* Bioresources, 2017. **12**(2): p. 2912-2929.

63. Masoodi, R., et al., *Mechanical characterization of cellulose nanofiber and bio-based epoxy composite.* Materials & Design (1980-2015), 2012. **36**: p. 570-576.

64. Emami, Z., et al., *Use of surfactants in cellulose nanowhisker/epoxy nanocomposites: effect on filler dispersion and system properties.* Cellulose, 2015. **22**(5): p. 3161-3176.

65. Chirayil, C.J., et al., *Rheological behaviour of nanocellulose reinforced unsaturated polyester nanocomposites.* International journal of biological macromolecules, 2014. **69**: p. 274-281.

66. Nair, S.S., et al., *Investigating the effect of lignin on the mechanical, thermal, and barrier properties of cellulose nanofibril reinforced epoxy composite.* Industrial crops and products, 2017. **100**: p. 208-217.

67. Abraham, E., et al., *Highly modified cellulose nanocrystals and formation of epoxy-nanocrystalline cellulose (CNC) nanocomposites.* ACS applied materials & interfaces, 2016. **8**(41): p. 28086-28095.

68. Barari, B., et al., *Mechanical, physical and tribological characterization of nano-cellulose fibers reinforced bio-epoxy composites: an attempt to fabricate and scale the 'Green' composite.* Carbohydrate Polymers, 2016. **147**: p. 282-293.

69. Kargarzadeh, H., et al., *Cellulose nanocrystal reinforced liquid natural rubber toughened unsaturated polyester: Effects of filler content and surface treatment on its morphological, thermal, mechanical, and viscoelastic properties.* Polymer, 2015. **71**: p. 51-59.

70. Lu, T., et al., *Effect of surface modification of bamboo cellulose fibers on mechanical properties of cellulose/epoxy composites.* Composites Part B: Engineering, 2013. **51**: p. 28-34.

71. Chang, H., et al., *Individually Dispersed Wood-Based Cellulose Nanocrystals.* ACS Appl Mater Interfaces, 2016. **8**(9): p. 5768-71.

72. Ma, J. and R.M. Larsen, *Comparative study on dispersion and interfacial properties of single-walled carbon nanotube/polymer composites using Hansen solubility parameters.* ACS Appl Mater Interfaces, 2013. **5**(4): p. 1287-93.

73. Marcio R. Loos, L.A.F.C., Sérgio H. Pezzin, *The effect of acetone addition on the properties of epoxy*. Polímeros, 2008. **18**(1): p. 76-80.

74. Wu, S.-G.H.a.C.-S., *DSC AND FTIR ANALYSES OF THE CURING BEHAVIOR OF EPOXY/DICY/SOLVENT SYSTEMS ON HERMETIC SPECIMENS.* Journal of Thermal Analysis and Calorimetry, 2000. **59**: p. 711-719.

75. Sun, J., et al., *The Effect of Residual Solvent N,N'-Dimethylformamide on the Curing Reaction and Mechanical Properties of Epoxy and Lignin Epoxy Composites.* Macromolecular Chemistry and Physics, 2016. **217**(9): p. 1065-1073.

76. Choo, K., et al., *Preparation and Characterization of Polyvinyl Alcohol-Chitosan Composite Films Reinforced with Cellulose Nanofiber.* Materials (Basel), 2016. **9**(8).

77. Zhang, R., et al., *High-performance sulfosuccinic acid cross-linked PVA composite pervaporation membrane for desalination.* Environ Technol, 2017: p. 1-9.

78. Lewis, L., et al., *Hydrothermal Gelation of Aqueous Cellulose Nanocrystal Suspensions.* Biomacromolecules, 2016. **17**(8): p. 2747-54.

79. Lee, S.-Y., et al., *Nanocellulose reinforced PVA composite films: Effects of acid treatment and filler loading.* Fibers and Polymers, 2009. **10**(1): p. 77-82.

80. Maria S. Peresin, Y.H., Justin O. Zoppe, Joel J. Pawlak, and Orlando J. Rojas, *Nanofiber Composites of Polyvinyl Alcohol and Cellulose Nanocrystals: Manufacture and Characterization.* Biomacromolecules, 2010. **11**: p. 674-681.

81. Ikram, S., et al., *Chitosan-Based Polymer Electrolyte Membranes for Fuel Cell Applications.* 2017: p. 381-398.

82. Kim, Y.S. and K.-S. Lee, *Fuel Cell Membrane Characterizations.* Polymer Reviews, 2015. **55**(2): p. 330-370.

83. Ma, J. and Y. Sahai, *Chitosan biopolymer for fuel cell applications.* Carbohydr Polym, 2013. **92**(2): p. 955-75.

84. Seo, S.H. and C.S. Lee, *A study on the overall efficiency of direct methanol fuel cell by methanol crossover current.* Applied Energy, 2010. **87**(8): p. 2597-2604.

85. Ye, Y.-S., J. Rick, and B.-J. Hwang, *Water Soluble Polymers as Proton Exchange Membranes for Fuel Cells.* Polymers, 2012. **4**(4): p. 913-963.

86. Zakil, F.A., S.K. Kamarudin, and S. Basri, *Modified Nafion membranes for direct alcohol fuel cells: An overview*. Renewable and Sustainable Energy Reviews, 2016. **65**: p. 841-852.

87. Hamideh Vaghari, H.J.-M., Aydin Berenjian and Navideh Anarjan, *Recent advances in application of chitosan in fuel cells.* Sustainable Chemical, 2013. **1**(16).

88. Brodd, M.W.a.R.J., *What Are Batteries, Fuel Cells, and Supercapacitors?* American Chemistry Society, 2004. **104**(10): p. 4245-4270.

89. Ahmed, M. and I. Dincer, *A review on methanol crossover in direct methanol fuel cells: challenges and achievements.* International Journal of Energy Research, 2011. **35**(14): p. 1213-1228.

90. Ran, J., et al., *Ion exchange membranes: New developments and applications.* Journal of Membrane Science, 2017. **522**: p. 267-291.

91. Zaidi, J. and T. Matsuura, *Polymer membranes for fuel cells*. 2008: Springer.

92. Li, N.N., et al., *Advanced membrane technology and applications*. 2011: John Wiley & Sons.

93. Lin, H.L. and S.H. Wang, *Nafion/poly(vinyl alcohol) nano-fiber composite and Nafion/poly(vinyl alcohol) blend membranes for direct methanol fuel cells.* Journal of Membrane Science, 2014. **452**: p. 253-262.

94. Cele, N.P., S. Sinha Ray, and L. Sikhwivhilu, *Nafion Titania Nanotubes Nanocomposite Electrolytes for High-Temperature Direct Methanol Fuel Cells.* Journal of Nanomaterials, 2012. **2012**: p. 1-7.

95. Kim, D., et al., *Nano-silica layered composite membranes prepared by PECVD for direct methanol fuel cells.* Electrochemistry Communications, 2004. **6**(10): p. 1069-1074.

96. Liu, Y.-L., et al., *Preparation and applications of Nafion-functionalized multiwalled carbon nanotubes for proton exchange membrane fuel cells.* Journal of Materials Chemistry, 2010. **20**(21): p. 4409.

97. Shabani, I., et al., *Nanofiber-based polyelectrolytes as novel membranes for fuel cell applications.* Journal of Membrane Science, 2011. **368**(1-2): p. 233-240.

98. Shirdast, A., A. Sharif, and M. Abdollahi, *Effect of the incorporation of sulfonated chitosan/sulfonated graphene oxide on the proton conductivity of chitosan membranes.* Journal of Power Sources, 2016. **306**: p. 541-551.

99. Liang, X., et al., *From metal-organic framework (MOF) to MOF–polymer composite membrane: enhancement of low-humidity proton conductivity.* Chem. Sci., 2013. **4**(3): p. 983-992.

100. Ogawa, T., et al., *The proton conduction mechanism in a material consisting of packed acids.* Chem. Sci., 2014. **5**(12): p. 4878-4887.

101. Bayer, T., et al., *High Temperature Proton Conduction in Nanocellulose Membranes: Paper Fuel Cells.* Chemistry of Materials, 2016. **28**(13): p. 4805-4814.

102. Agmon, N., *The grotthuss mechanism.* Chemical Physics Letters, 1995. **244**(5-6): p. 456-462.

103. Kreuer, K.D., A. Rabenau, and W. Weppner, *Vehicle mechanism, a new model for the interpretation of the conductivity of fast proton conductors.* Angewandte Chemie International Edition in English, 1982. **21**(3): p. 208-209.

104. Hasani-Sadrabadi, M.M., et al., *Cellulose nanowhiskers to regulate the microstructure of perfluorosulfonate ionomers for high-performance fuel cells.* Journal of Materials Chemistry A, 2014. **2**(29): p. 11334.

105. Yuan Lu, A.A.A., Juchuan Li, Halil L. Tekinalp, Jagjit Nanda and Soydan Ozcan, *A Cellulose nanocrystal-based composite electrolyte with superior dimensional*

stability for alkaline fuel cell membranes. Journal of Materials Chemistry A, 2015(25).

106. Rhim, J., et al., *Crosslinked poly(vinyl alcohol) membranes containing sulfonic acid group: proton and methanol transport through membranes.* Journal of Membrane Science, 2004. **238**(1-2): p. 143-151.

107. Duangkaew, P. and J. Wootthikanokkhan, *Methanol permeability and proton conductivity of direct methanol fuel cell membranes based on sulfonated poly(vinyl alcohol)–layered silicate nanocomposites.* Journal of Applied Polymer Science, 2008. **109**(1): p. 452-458.

108. Jing Zhang, L.L., Chengyu Ma, Yuyu Liu and Jinli Qiao, *Poly(vinyl alcohol)/sulfosuccinic acid (PVA/SSA) as proton-conducting membranes for fuel cells: Effect of cross-linking and plasticizer addition.* The Electrochemical Society, 2013. **53**(30): p. 29-34.

109. Jin Ah Seo, J.C.K., Jong Kwan Koh, Sung Hoon Ahn and Jong Hak Kim, *Preparation and characterization of crosslinked cellulose-sulfosuccinic acid membranes as proton conducting electrolytes.* Ionics, 2009. **15**: p. 555-560.

110. Morancho, J.M., et al., *Thermal analysis of enhanced poly(vinyl alcohol)-based proton-conducting membranes crosslinked with sulfonation agents for direct methanol fuel cells.* Journal of Applied Polymer Science, 2012. **124**(S1): p. E57-E65.

111. Kang, M.-S., et al., *Highly charged proton exchange membranes prepared by using water-soluble polymer blends for fuel cells.* Journal of Membrane Science, 2005. **247**(1-2): p. 127-135.

112. González, M.G., J.C. Cabanelas, and J. Baselga, *Applications of FTIR on epoxy resins-identification, monitoring the curing process, phase separation and water uptake*, in *Infrared Spectroscopy-Materials Science, Engineering and Technology*. 2012, InTech.

113. Bruckner, J.R., et al., *Enhancing Self-Assembly in Cellulose Nanocrystal Suspensions Using High-Permittivity Solvents.* Langmuir, 2016. **32**(38): p. 9854-62.

114. Wang, G., et al., *A comparative study of nanoscale glass filler reinforced epoxy composites: Electrospun nanofiber vs nanoparticle.* Composites Science and Technology, 2016. **129**: p. 19-29.

115. Chen, Q., et al., *Nanoscale and effective mechanical behavior and fracture of silica nanocomposites.* Composites Science and Technology, 2008. **68**(15): p. 3137-3144.

116. Li, M.-C., et al., *Cationic surface modification of cellulose nanocrystals: Toward tailoring dispersion and interface in carboxymethyl cellulose films.* Polymer, 2016. **107**: p. 200-210.

117. Mandal, A. and D. Chakrabarty, *Studies on the mechanical, thermal, morphological and barrier properties of nanocomposites based on poly(vinyl alcohol) and nanocellulose from sugarcane bagasse.* Journal of Industrial and Engineering Chemistry, 2014. **20**(2): p. 462-473.

118. Wei, J., et al., *N,N-Dimethylformamide (DMF) Usage in Epoxy/Graphene Nanocomposites: Problems Associated with Reaggregation.* Polymers, 2017. **9**(6): p. 193.

119. Hong, S.-G. and C.-S. Wu, *DSC and FTIR analysis of the curing behaviors of epoxy/DICY/solvent open systems.* Thermochimica Acta, 1998. **316**(2): p. 167-175.

120. Choi, S., et al., *Effect of water addition on the cure kinetics of an epoxy-amine thermoset.* Journal of Polymer Science Part A: Polymer Chemistry, 2011. **49**(21): p. 4650-4659.

121. Seferis, F.U.B.J.C., *Effect of reinforcement and solvent content on moisture absorption in epoxy composite materials.* Composites Part A: Applied Science and Manufacturing, 2000. **31**: p. 741-748.

122. Cano, L., D.H. Builes, and A. Tercjak, *Morphological and mechanical study of nanostructured epoxy systems modified with amphiphilic poly(ethylene oxide-b-propylene oxide-b-ethylene oxide)triblock copolymer.* Polymer, 2014. **55**(3): p. 738-745.

123. Palanisamy, A., et al., *Water Sorption and Solvent Sorption of Epoxy/Block-Copolymer and Epoxy/Thermoplastic Blends*, in *Handbook of Epoxy Blends*, p. 1097-1111.

124. Sun, P., et al., *Mobility, Miscibility, and Microdomain Structure in Nanostructured Thermoset Blends of Epoxy Resin and Amphiphilic Poly(ethylene oxide)-block-poly(propylene oxide)-block-poly(ethylene oxide) Triblock Copolymers Characterized by Solid-State NMR.* Macromolecules, 2005. **38**(13): p. 5654-5667.

125. Dumanli, A.G., et al., *Digital Color in Cellulose Nanocrystal Films.* ACS Applied Materials & Interfaces, 2014. **6**(15): p. 12302-12306.

126. Lee, W.J., et al., *Strong and Stiff: High-Performance Cellulose Nanocrystal/Poly(vinyl alcohol) Composite Fibers.* ACS Applied Materials & Interfaces, 2016. **8**(46): p. 31500-31504.

127. Tian, C., et al., *Polymerization Topochemistry of Cellulose Nanocrystals: A Function of Surface Dehydration Control.* Langmuir, 2014. **30**(48): p. 14670-14679.

128. Boroglu, M.S., et al., *Synthesis and proton conductivity studies of 5-aminotetrazole-doped sulfonated polymer electrolyte membranes.* Polymer Composites, 2011. **32**(10): p. 1625-1632.

129. Gasa, J.V., R.A. Weiss, and M.T. Shaw, *Ionic crosslinking of ionomer polymer electrolyte membranes using barium cations.* Journal of Membrane Science, 2007. **304**(1-2): p. 173-180.

130. Zhou, J., et al., *Crosslinked, epoxy-based anion conductive membranes for alkaline membrane fuel cells.* Journal of Membrane Science, 2010. **350**(1-2): p. 286-292.

131. Dashtimoghadam, E., M.M. Hasani-Sadrabadi, and H. Moaddel, *Structural modification of chitosan biopolymer as a novel polyelectrolyte membrane for green power generation.* Polymers for Advanced Technologies, 2009. **21**(10): p. 726-734.

132. Beydaghi, H., M. Javanbakht, and A. Badiei, *Cross-linked poly(vinyl alcohol)/sulfonated nanoporous silica hybrid membranes for proton exchange membrane fuel cell.* Journal of Nanostructure in Chemistry, 2014. **4**(2).